Multicomponent adsorption dynamics in the recovery of acetic and lactic acids using stratified fixed-beds

by

Haripriya Naidu

B.Tech., Gandhi Institute of Technology and Management, 2012
M.Tech., National Institute of Technology Warangal, 2014

AN ABSTRACT OF A DISSERTATION

submitted in partial fulfillment of the requirements for the degree

DOCTOR OF PHILOSOPHY

Department of Civil Engineering
Carl R. Ice College of Engineering

KANSAS STATE UNIVERSITY
Manhattan, Kansas

2020

Abstract

Industrial acetic acid production based on anaerobic fermentation technology is not economically viable at present due to the low efficiency and high cost of product recovery by adsorption or extraction at neutral pH conditions. With the recent advances in fermentation technology to produce organic acids at low pH conditions, a detailed study on the adsorption equilibria, kinetics, and dynamics at these conditions is necessary for the design of an efficient recovery scheme.

Adsorption equilibria and kinetics of acetic acid at low pH conditions on granular activated carbon (GAC) and weak base resins were studied using batch experiments. A simple nonlinear estimation method and approximations to analytical solutions of adsorption kinetic equations were developed to determine isotherm constants and kinetic parameters respectively. Weak base resins show higher adsorption capacities for the uptake of acetic acid compared to GAC. Multicomponent sorption equilibria of acetic and lactic acids were determined using the Ideal Adsorbed Solution Theory (IAST) model, and extended Langmuir and modified extended Langmuir models. The adsorption of acetic acid is shown to be controlled by both external mass transfer and intraparticle diffusion resistances in GAC and by intraparticle diffusion resistance alone in the weak base resins. The estimated transport coefficients are shown to predict batch adsorption kinetic data well.

Adsorption dynamics studies were conducted using single and multicomponent solutions of acetic and lactic acids in fixed-bed adsorbers of different configurations. These studies were conducted to examine potential enhancements to bed capacity utilization and thereby the overall efficiency of the recovery process. Five different configurations, namely, a conventional cylindrical adsorber (CCA), and a tapered bed adsorber with single adsorbent particle size, a

stratified cylindrical adsorber with particle sizes increasing in the direction of flow (SCA), a reverse stratified cylindrical adsorber (RSCA), and a reverse stratified convergent tapered adsorber (RSTA) were studied in this research. A general rate model that considers axial dispersion, external mass transfer, pore diffusion, and nonlinear isotherm was developed to predict sorption dynamics in single and multicomponent systems. Model predictions were in good agreement with experimental data.

The adsorption dynamics and breakthrough curves for acetic acid were similar in cylindrical and tapered beds when a single adsorbent particle size was used. The solute front becomes dispersive in the SCA and sharpens in the RSTA. Among the different configurations examined, RSTA gave the maximum bed capacity utilization which is 18.4% higher than that obtained using SCA. Multicomponent sorption dynamics of acetic and lactic acids on weak base resins were conducted in RSTA at pH 2.8 and 4.8. At pH 2.8, acetic acid eluted first, while at pH 4.8 lactic acid eluted first. Sensitivity analysis has shown that to achieve 90% bed capacity utilization, two column lengths or double the quantity of adsorbent will be required in the case of SCA when compared to RSTA. The model presented will be useful in the selection of optimum operating conditions to obtain maximum bed capacity utilization, and thereby enhance the economics of the recovery of organic acids from fermentations.

Multicomponent adsorption dynamics in the recovery of acetic and lactic acids using stratified fixed-beds

by

Haripriya Naidu

B.Tech., Gandhi Institute of Technology and Management, 2012
M.Tech., National Institute of Technology Warangal, 2014

A DISSERTATION

submitted in partial fulfillment of the requirements for the degree

DOCTOR OF PHILOSOPHY

Department of Civil Engineering
Carl R. Ice College of Engineering

KANSAS STATE UNIVERSITY
Manhattan, Kansas

2020

Approved by:

Major Professor
Dr. Alexander P Mathews

Copyright

Abstract

Industrial acetic acid production based on anaerobic fermentation technology is not economically viable at present due to the low efficiency and high cost of product recovery by adsorption or extraction at neutral pH conditions. With the recent advances in fermentation technology to produce organic acids at low pH conditions, a detailed study on the adsorption equilibria, kinetics, and dynamics at these conditions is necessary for the design of an efficient recovery scheme.

Adsorption equilibria and kinetics of acetic acid at low pH conditions on granular activated carbon (GAC) and weak base resins were studied using batch experiments. A simple nonlinear estimation method and approximations to analytical solutions of adsorption kinetic equations were developed to determine isotherm constants and kinetic parameters respectively. Weak base resins show higher adsorption capacities for the uptake of acetic acid compared to GAC. Multicomponent sorption equilibria of acetic and lactic acids were determined using the Ideal Adsorbed Solution Theory (IAST) model, and extended Langmuir and modified extended Langmuir models. The adsorption of acetic acid is shown to be controlled by both external mass transfer and intraparticle diffusion resistances in GAC and by intraparticle diffusion resistance alone in the weak base resins. The estimated transport coefficients are shown to predict batch adsorption kinetic data well.

Adsorption dynamics studies were conducted using single and multicomponent solutions of acetic and lactic acids in fixed-bed adsorbers of different configurations. These studies were conducted to examine potential enhancements to bed capacity utilization and thereby the overall efficiency of the recovery process. Five different configurations, namely, a conventional cylindrical adsorber (CCA), and a tapered bed adsorber with single adsorbent particle size, a

stratified cylindrical adsorber with particle sizes increasing in the direction of flow (SCA), a reverse stratified cylindrical adsorber (RSCA), and a reverse stratified convergent tapered adsorber (RSTA) were studied in this research. A general rate model that considers axial dispersion, external mass transfer, pore diffusion, and nonlinear isotherm was developed to predict sorption dynamics in single and multicomponent systems. Model predictions were in good agreement with experimental data.

The adsorption dynamics and breakthrough curves for acetic acid were similar in cylindrical and tapered beds when a single adsorbent particle size was used. The solute front becomes dispersive in the SCA and sharpens in the RSTA. Among the different configurations examined, RSTA gave the maximum bed capacity utilization which is 18.4% higher than that obtained using SCA. Multicomponent sorption dynamics of acetic and lactic acids on weak base resins were conducted in RSTA at pH 2.8 and 4.8. At pH 2.8, acetic acid eluted first, while at pH 4.8 lactic acid eluted first. Sensitivity analysis has shown that to achieve 90% bed capacity utilization, two column lengths or double the quantity of adsorbent will be required in the case of SCA when compared to RSTA. The model presented will be useful in the selection of optimum operating conditions to obtain maximum bed capacity utilization, and thereby enhance the economics of the recovery of organic acids from fermentations.

Table of Contents

List of Figures

List of Tables

Nomenclature

a	Langmuir isotherm parameter, (g/g)(L/g)
a	Linear-Freundlich isotherm parameter, (g/g)(L/g)
a	Sips isotherm parameter, (g/g)(L/g)$^{\gamma}$
a	concentration of exchangeable ions, meg/q (Equation (2.74))
a	kinetic parameter in Elovich equation, (sec)$^{-1}$
a_p	area per unit volume of adsorbent particle, cm^{-1}
A	cross-sectional area of the column, cm^2
A	specific area of adsorbent, cm^2/g
A_p	external surface area of adsorbent particle, cm^2
b	Langmuir isotherm parameter, L/g
b	Linear-Freundlich isotherm parameter, (L/g)$^{\beta}$
b	Sips isotherm parameter, (L/g)$^{\gamma}$
Bi	Biot number, $r_p k_f/\varepsilon_p D_p$
c	concentration of solute in the liquid phase, g/L
c_0	initial concentration of solute in the liquid phase, g/L
c_∞	equilibrium concentration of solute in the liquid phase, g/L
c_e	concentration of solute in the liquid phase at equilibrium, g/L
c_p	concentration in the pore phase of the adsorbent, g/L
c_s	concentration in of solute at the surface of the particle, g/L
$c_i^0(\pi)$	equilibrium concentration of solute corresponding to solution temperature and pressure, g/L
C	total concentration of solutes in liquid phase, g/L (Equation (2.29))

C	kinetic parameter in intraparticle diffusion rate equation, g/g (Equation (2.78))
C	dimensionless concentration in the liquid phase, c/c_0
C_{HA}	concentration of acid molecule HA in equilibrium with solid phase of resin
C_p	dimensionless concentration in the pore phase of the adsorbent, c_p/c_0
d_p	diameter of the adsorbent particle, cm
D_c	intraparticle diffusion coefficient, cm^2/sec
D_{eff}	effective diffusion coefficient, cm^2/sec
D_L	axial dispersion coefficient, cm^2/sec
D_m	molecular diffusion coefficient of solute in a solvent, cm^2/sec
D_p	pore diffusion coefficient of solute in the sorbent, cm^2/sec
D_s	solid phase diffusion coefficient of solute in the sorbent, cm^2/sec
D_s	surface diffusion coefficient of solute in the sorbent, cm^2/sec
H	Langmuir isotherm parameter, (g/g)(L/g)
k_1	pseudo-first-order rate constant, $(sec)^{-1}$
k_1	reaction constant, $(sec)^{-1}$ (Equation (2.74))
k_2	pseudo-second-order rate constant, $(g/g)(sec)^{-1}$
k_2	reaction constant, $(sec)^{-1}$ (Equation (2.74))
k_d	intraparticle diffusion rate constant, $(g/g)(sec)^{-1/2}$
k_f	external mass transfer coefficient, cm/sec
K_1	reaction equilibrium constant (Equation (2.1))
K	Langmuir isotherm parameter, L/g
K_{eff}	effective mass transfer coefficient, $(sec)^{-1}$
K_F	Freundlich isotherm parameter, $(g/g)(L/g)^n$

K_G	external mass transfer coefficient, cm/sec
$K_m a_p$	effective mass transfer coefficient, $(sec)^{-1}$
L	bed length, cm
L_{MTZ}	length of the mass transfer zone, cm
m	amount of adsorbent added in the batch reactor, g
m_t/m_∞	fractional uptake of the solute by the sorbent
$m_t/m_{\infty,e}$	experimental fractional uptake of the solute by the sorbent
$m_t/m_{\infty,p}$	predicted fractional uptake of the solute by the sorbent
M_B	molecular weight of solvent, g/mol
n	number of experimental data points in the determination of adsorption equilibrium
n	Freundlich isotherm parameter (Equation (2.20))
p	amount of exchanged ions, meq/g
Pe	Peclet number, vL/D_L
q	concentration of solute in the solid phase, g/g
q_0	equilibrium concentration of solute in the solid phase of the adsorbent at solute concentration of c_0, g/g
q_0'	initial concentration of solute in the solid phase of the adsorbent at solute concentration of c_0, g/g
$\bar{q}$	average concentration of solute in the solid phase, g/g
q_e	adsorption capacity at equilibrium, g/g
$q_{e,e}$	experimental equilibrium concentration of solute in the solid phase of adsorbent, g/g
$q_{e,mean}$	mean equilibrium concentration of solute in the solid phase of adsorbent, g/g
$q_{e,p}$	predicted equilibrium concentration of solute in the solid phase of adsorbent, g/g
q_m	maximum monolayer adsorption capacity, g/g

q_p	concentration of solute in the solid phase of the adsorbent, g/g
q_s	concentration of solute at the surface of the adsorbent, g/g
q_T	total amount of solute in the adsorbed phase, g/g
Q	sum of concentration of solute in pore and adsorbed phase, g/g
Q_o	sum of concentration of solute in pore and adsorbed phase at $t = 0$, g/g
Q_f	volumetric flow rate, cm^3/sec
Q_p	dimensionless concentration of solute in the solid phase of the adsorbent, q_p/c_0
r	radial distance along the particle, cm
r_c	radius of the adsorbent particle, cm
r_p	radius of the adsorbent particle, cm
R	dimensionless radius of the particle, r/r_p
R	gas constant, (L atm)/(mol K)
Re	Reynolds number, $d_p v\rho/\mu$
Sc	Schmidt number, $\mu/\rho D_m$
St	Stanton number, $3Lk_f/vr_p$
t	time, sec
t_b	time at breakthrough i.e., c/c_0 of 0.05 in the breakthrough curve, sec
t_{center}	time at center of breakthrough i.e., c/c_0 of 0.5 in the breakthrough curve, sec
t_{exit}	time at c/c_0 of 0.5 in the breakthrough curve, sec
t_{MTZ}	time taken for mass transfer zone to travel its own length, sec
t_s	time at saturation i.e., c/c_0 of 0.95 in the breakthrough curve, sec
T	operating temperature, ^0C

u	vector variable in the coefficient form PDE interface in COMSOL Multiphysics® software
U	superficial velocity, cm/sec
U_{sh}	shock front velocity, cm/sec
v	interstitial velocity, $Q_f/\varepsilon_b A$, cm/sec
V	volume of solution in batch reactor, L
V_A	molar volume of solute molecule at its normal boiling point, cm^3/mol
V_p	volume of adsorbent particle, cm^2
W	weight of adsorbent added to the batch reactor, g
x	axial position along the bed length, cm
x	mole fraction of solute in the adsorbed phase at equilibrium
X	dimensionless distance along the bed length, x/L
y	mole fraction of solute in liquid phase
α	kinetic parameter in Elovich equation, $(g/g)^{-1}$
α	fraction of solute ultimately adsorbed by the sorbent
ε_b	bed porosity
ε_p	particle porosity
η	interaction term in multicomponent Langmuir isotherm
η_B	viscosity of solvent, g/cm.sec
ρ	density of water, g/L
ρ_b	bulk density of the adsorbent, g/L
ρ_p	density of the adsorbent, g/L
φ	association parameter specific to the solvent

τ	dimensionless time, tv/L
π	spreading pressure, dynes/cm
γ	activity coefficient
μ	viscosity of water, g/cm.sec

Acknowledgements

I would like to express my gratitude to my major advisor, Dr. Alexander Mathews, for his support and guidance throughout my doctoral program. I am thankful to him for giving me this opportunity to pursue doctoral studies under his guidance. His extreme patience, encouragement, enthusiasm, and willingness to clarify my doubts at any time motivates me. I would also like to thank my friend, Dr. Sathyanarayanan Veeravalli, for being kind and mentoring me in every step.

I am thankful to my committee members, Dr. Keith Hohn, Dr. Prathap Parameswaran, and Dr. Mingjun Wei for their kind words and support. My special thanks to Dr. Jeongdae Im for his guidance and kindness.

I would like to thank my teachers, Dr. Indumathi Nambi, Dr. Chandrasekhar Matli, Dr. Jaykumar KV, Dr. Muralimohan Challa, and many more for their guidance and mentorship. I would like to thank my husband, Dr. Karthik Pandalaneni, for his guidance, encouragement, and love. I would like to thank my family members and friends who have supported me all these years.

Dedication

To my teachers.

Chapter 1
Introduction

1.1 Background

The global demand for resources is increasing due to world population growth and increasing per capita resource consumption rate. There is an emerging need to reduce dependence on nonrenewable resources and shift towards a circular economy. A biobased economy can be achieved by using renewable resources such as biomass and biomass wastes to produce energy, fuels, and chemicals. Aerobic and anaerobic bioconversion processes are increasingly being used to produce fuels and chemicals. These bioconversion processes are also carbon neutral and reduce CO_2 emissions in the long term thereby mitigating climate change impacts (Lange, 2007).

Approximately 10% of crude oil imported to the United States is used by the petrochemical industry to produce chemicals and their derived products (Anonymous, 2010a). Synthetic chemical production methods typically may need high operating temperatures and/or pressures. Petrochemical industries account for ~30% of the industrial energy demand and 20% of the industrial greenhouse gas emissions worldwide (Biddy et al., 2016). On the other hand, bioconversion production methods operate at relatively lower temperatures, pressures, can accommodate impure feedstocks, and produce less wastes including toxic materials (Erickson et al., 2012). Thus, producing chemicals through bioconversion processes using renewable feedstock will promote sustainability and energy independence. Renewable chemicals represented 9% of the worldwide chemical sales in 2012 and by 2025, this is estimated to be > 22% (Anonymous, 2018a; Philp et al., 2013). By 2100, more than 95% of the polymers and chemicals are envisioned to be derived from renewable resources (Devaney, 2016).

1.2 Development of bioconversion processes to produce chemicals

Although bioconversion processes to produce chemicals and fuels were developed decades ago, the low price and abundant supply of oil led to the rapid growth of petrochemical industry. In 1970s when the oil price began to rapidly increase, bioethanol production started to be investigated as an economically viable alternative. Further, phasing out of methyl tertiary-butyl ether (MTBE), a toxic gasoline oxygenate, and implementation of Renewable Fuel Standard (RFS) program boosted the production of bioethanol in the US. In 2016, around 15.9 billion gallons of bioethanol was produced in the US (Lane, 2017). However, limitations such as price volatility of product and feedstock, and tariffs on fuel imports in countries such as China and Brazil have led to the economic instability of bioethanol industry. These limitations led to the shutdown of two of the three largest bioethanol plants of DowDuPont (Neveda, IA) and Abengoa (Hugoton, KS) companies in the US (Hirtzer, 2017; McCoy, 2017). In order to become economically viable, while some bioethanol companies are ramping up the capacity, several of them are focusing on diversifying their product slate. Government initiatives such as the 2014 Farm Bill provided loan assistance and incentives under the biorefinery assistance program, which was open only to biofuel industries, to biorefineries producing chemicals (Lucas, 2014). The incentives include mandatory requirement for the federal agencies to purchase biobased products and a voluntary biobased labelling program to increase the acceptability of customers to purchase biobased products. Moreover, the production of chemicals through bioconversion methods is more attractive than that of fuels. This is because of the simple conversion steps in their production and higher selling price of chemicals (Lane and Stone, 2017). The similar effective hydrogen to carbon ratio of sugars and chemicals indicate a simpler production of chemicals compared to fuels through bioconversion methods (Wu et al., 2018). Among various

chemicals, the production of platform chemicals such as acetic and lactic acids using renewable resources has been gaining a lot of attention in recent years. This is attributed to their high demand and a wide array of uses for these chemicals in several industries.

1.2.1 Uses of acetic acid

Acetic acid, also known as ethanoic acid, is a monocarboxylic acid with the chemical formula CH_3COOH. It is a colorless liquid with a distinctive pungent odor and is widely used as a solvent for organic and inorganic substances (Davidson, 1931). The presence of a carboxylic acid group makes it a weak monoprotic acid and it has a p*K*a of 4.76 at 25 ^{o}C. It is a key building block in the production of a variety of chemicals such as vinyl acetate monomer, terephthalic acid, acetic anhydride, and esters. In 2014, 12.1 million tons of acetic acid was produced globally and it was projected to reach 16.3 million tons by 2018 (Lazonby, 2016). There is a growing demand to produce renewable polyethylene terephthalate (PET) plastic. Several industries such as Coca-Cola, Ford Motors, H.J. Heinz, Nike Inc., and Procter & gamble are working to develop renewable PET for the manufacture of bottles, automobile fabrics, footwear, and apparels (Anonymous, 2018a). Figure 1.1 shows a pie chart of the percentages of acetic acid, produced globally in 2016, used to produce various chemicals. It also shows a list of products made from these chemicals.

Acetic acid also has a large potential market in the production of environmentally benign road and aircraft deicing chemicals such as calcium magnesium acetate (CMA) and potassium acetate. The most widely used deicing chemical around the world is rock salt (sodium chloride). It accelerates the corrosion of reinforced steel, concrete, and other highway infrastructure assets. It is also harmful to the environment (Murray and Ernst, 1976). In the Western States alone, deicing using rock salt has led to $1.5 billion in annual costs for repairs of deteriorated bridges,

pavements, and vehicles (Voynick, 2003). However, several factors such as the relatively low cost of salt and policy to maintain bare pavements and safe roads during winter snow events has led to its extensive use (Wenta and Sorsa, 2018).

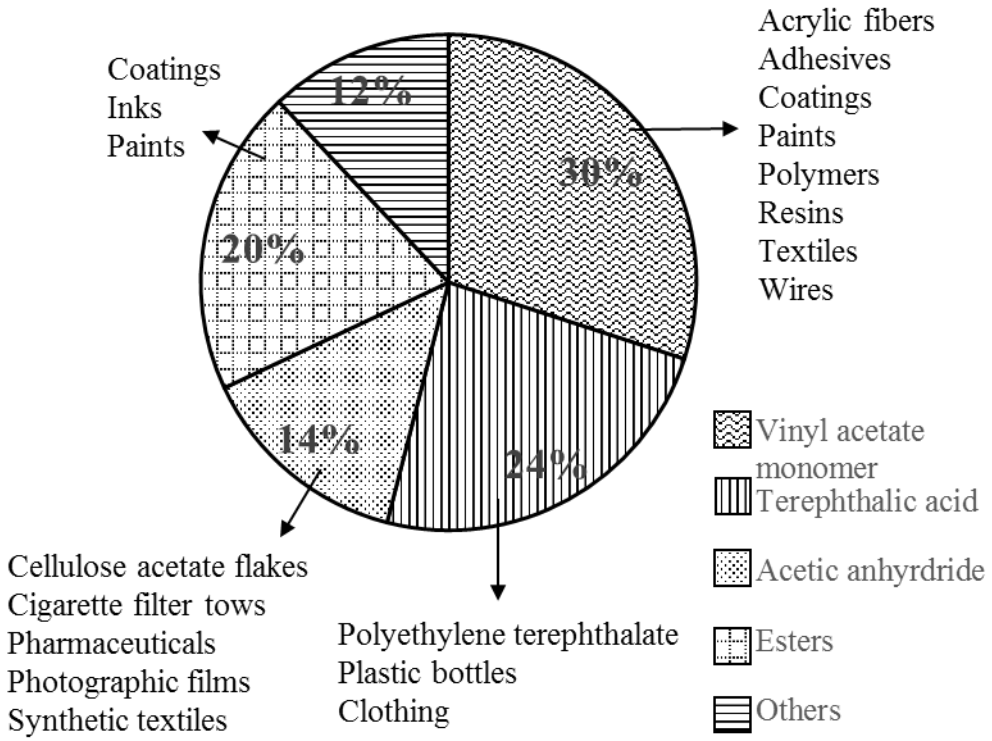

Figure 1.1: Percentages of total acetic acid, produced globally in 2016, consumed for the production of various chemicals (Anonymous, 2016a, 2016b, 2017)

In 2017, the total rock salt consumption for roadway deicing was 22 million metric tons (Bolen, 2017). Dunn and Schenk (1980) performed an extensive evaluation of chemical compounds in order to find a suitable road-deicing chemical to replace sodium chloride. Their study proved that CMA is an effective deicing chemical due to its low molecular weight and ability to lower the freezing point of water. CMA also inhibits corrosion, improves soil structure, and does not interfere with the turnover of lakes and is environmentally benign. However, the high cost of CMA has limited its application mainly to environmentally sensitive areas such as national parks and new road infrastructure. In addition, CMA has potential for use in a variety of environmental

applications such as the removal of sulfur and carbon dioxide from gas streams (Wise et al., 1991). While the industrial demand for acetic acid is about 15 million tons per year, the demand for its potential use as deicer is quite large at ~25 million tons per year in North America (Lilek, 2017; Pal and Nayak, 2017).

1.2.2 Uses of lactic acid

Lactic acid, also known as 2-hydroxypropanoic acid, is an alpha-hydroxy acid with the chemical formula $CH_3CH(OH)COOH$. It is an odorless and colorless to yellowish viscous liquid. The presence of a carboxylic acid group makes it a weak monoprotic acid and it has a p*K*a of 3.86 at 25 ^{o}C. Due to the presence of an asymmetric carbon in its chemical structure, lactic acid is present as two optical isomers, namely, L- and D- lactic acid. Lactic acid and its derivative compounds have a wide range of applications in chemical, food, metal, pharmaceutical, polymer, and semiconductor industries. Lactic acid and its salts such as sodium and potassium lactates have preservative and antimicrobial properties. The ethyl and butyl esters of lactic acid are used as biodegradable cleaning solvents and are widely used in the metal and semiconductor industries.

The United States Department of Energy listed lactic acid as one of the potential building block chemicals for the future (Komesu et al., 2017). The US was the largest consumer of lactic acid in 2018 with major demand stemming from its use in the production of polylactic acid (PLA) polymer (Anonymous, 2018b). The PLA polymer is biodegradable and is considered as an alternative for synthetic plastics produced using fossil fuels. The PLA polymer, marketed under the Ingeo® brand, has over 100 million pounds in annual sales volume (Erickson et al., 2012). In 2018, the price of Ingeo® PLA was ~1.88 $/kg. Whereas, the price of synthetic polyethylene terephthalate was ~1.44 $/kg (Anonymous, 2018c). The narrow price gap between

PLA and synthetic plastics and the growing awareness among consumers to reduce carbon footprint has led to the increase in demand for PLA. The global lactic acid demand is expected to reach 1.9 million tons by 2020 (Komesu et al., 2017).

1.3 Challenges in the production of organic acids through bioconversion methods

Almost 90% of the worldwide demand for acetic acid is met through the synthetic production methods such as methanol carbonylation by the Monsanto and Cativa processes, acetaldehyde oxidation, and butane liquid-phase oxidation processes (Jang et al., 2012; Nayak and Pal, 2013; Vidra and Németh, 2017). Bioconversion production methods accounts for the remaining 10% and are the sole route to producing food-grade vinegar (3-12% (w/v) acetic acid). In 2015, CMA produced using synthetic acetic acid was priced at ~ $1896 per ton (WV PO, 2015). This is almost 30 times higher than the price of rock salt. Several authors have reported that bioconversion processes to produce acetic acid can lower the cost of CMA. Through more efficient bioconversion production methods, CMA can be produced at a price of $200-500 per ton (Marynowski et al., 1985; Veeravalli and Mathews, 2019; Yang et al., 1992). Lactic acid is synthetically produced through the reaction of acetaldehyde and hydrogen cyanide to produce lactonitrile. It is then hydrolyzed to lactic acid using concentrated acids. This synthetic production method results in a racemic mixture while bioconversion methods are capable to produce optically pure lactic acid. Around 90% of the lactic acid produced worldwide is from microbial fermentation technology (Jang et al., 2012; Komesu et al., 2017). Based on the market and applications, lactic acid price varies around 1.3-2.3 $/kg (Biddy et al., 2016).

Several commercially successful bioproducts such as bioplastics have shown that sustainability is not the standalone factor for market success. Bioproducts need to be competitive in price and performance with respect to their synthetic counterparts. In addition, the market in

which they are introduced is also important (Erickson et al., 2012). For example, PLA polymer had a competitive advantage over its synthetic counterparts in select markets such as food packaging, food grade plastics, drink bottles, and plastic bags. This is due to its biodegradability and displacement of petrochemicals for these applications.

The economic viability of a large-scale microbial fermentation process for acetic acid and lactic acid production depends primarily on the cost of feedstock and downstream processing technologies (Chen and Nielsen, 2016; Van Dien, 2013). The use of low cost and non-edible biomass feedstocks such as agricultural wastes and sugar and starch-rich waste streams of industries such as breweries, food and beverage industries etcetera, to produce these organic acids will reduce the overall production cost and aid in effective waste management (Lee et al., 2014).

Most acidogenic bacteria such as the lactic acid bacteria (LAB) and acetic acid bacteria (AAB) cannot survive in acidic or extremely alkaline environments (Lee et al., 2014). The production of undissociated organic acids acts as inhibitor for microbial growth by decreasing the pH of the fermentation broth. The undissociated acid molecules will diffuse through the membrane and decrease the intracellular pH (Aljundi et al., 2005). In order to maintain the process viable, organic acid fermentation processes are typically operated at pH > p*K*a of the acid by the addition of bases such as sodium hydroxide and calcium hydroxide. (Tung and King, 1994). The end uses for organic acids usually require the acids in the undissociated form. But the bioconversion production methods typically result in the salts of organic acids which have high water solubility and very low vapor pressure (Eggeman and Verser, 2005). The final concentration of organic acids in the fermentation broth is typically much less than 10%. In order for a downstream process to be economically viable, typical organic acid concentration must be

at least 5%, and this is above the tolerance limit for many microbial species (Chen and Nielsen, 2016). In addition, fermentation processes often produce a mixture of organic acids instead of a single organic acid (Li et al., 2010; Veeravalli and Mathews, 2018; Zacharof et al., 2016). There are some exceptions in industrial-scale organic acid production, where nontraditional microbes such as *Saccharomyces cerevisiae* and *Rhizopus oryzae* have been used to produce a specific organic acid such as lactic or succinic acids at concentrations > 10% and at pH < p*K*a of the acid (Chen and Nielsen, 2016; Van Dien, 2013). However, there will be additional expenses for engineering and maintaining microbial strains when compared to the natural producers to obtain organic acids at high titer and under low pH conditions. The downstream processing costs for the recovery of bioproducts from such low concentrations and neutral pH fermentation broths represent up to 60% of the total production cost (Angenent et al., 2004; Zhang et al., 2014). Thus, the economic feasibility of bioconversion methods to produce chemicals is largely dependent on the efficiency of the recovery technique adopted.

1.4 Methods to enhance recovery and separation of organic acids

Organic acids such as acetic, citric, lactic, and succinic acids are recovered through precipitation using calcium hydroxide. Large-scale industries such as Cargill have been using this method for the production of lactic acid (Rush, 2012). In the traditional method, the fermentation process is carried out at pH of 5.0-7.0 by the addition of calcium hydroxide, thus all the organic acid that is produced is in the form of calcium salt. After the fermentation is completed, the broth is evaporated. Then, an acidulant, typically sulfuric acid, is added to the concentrated broth to free the organic acid. This step produces gypsum as the waste stream. However, this method is not energy efficient and produces lot of waste materials. In the recovery of lactic acid, 0.96 kg of gypsum is produced per kg of lactic acid recovered (Eggeman and

Verser, 2005). In order to enhance the recovery and economic viability of bioconversion production methods, the downstream separation methods need to produce products with high purity, with low energy requirements, while avoiding the production of waste materials.

Ion exchange or adsorption on polymeric resins or activated carbon can be a viable process for the recovery of organic acids from dilute aqueous solutions. Adsorption technology has the lowest energy requirement compared to other techniques such as distillation and liquid-liquid extraction (Abdehagh et al., 2013). When the fermentation process is operated at pH > pK_{a_1} of the acid, it is essential to identify a suitable sorbent which has adsorption capacity for these acids at pH > pK_{a_1} of the acid and can be regenerated with high recovery. However, weak base resins have high uptake capacities for organic acids at low pH values (pH < pK_{a_1} of the acid) and their uptake capacities decrease with increasing pH. Some weak base resins have high uptake capacities over a wide pH range. But, the recovery of acids is difficult with these resins as they require stronger bases for regeneration. Evangelista (1994) and González et al. (2006) have proposed acidification of the fermentation broth using a fixed-bed adsorber containing cation exchange resin to recover organic acids. The cation exchange resin exchanges hydrogen ions with the salt ions and thereby decreases the pH of the fermentation broth. However, this will lead to higher capital and operational costs as it increases the number of fixed-bed adsorber units, and the chemical and adsorbent inventory. The other alternative is to conduct the fermentation at pH < pK_{a_1} of the acid where sorption efficiency is high. Recently in order to address the problems of downstream separation efficiency and economic feasibility, a novel low pH fermentation process to produce carboxylic acids from biomass wastes that operates at pH of ~ 4 was developed by Veeravalli and Mathews (2018). Acetic and lactic acids are produced at high conversion rates using xylose as substrate. This proposed research will evaluate the extraction of these acids from

synthetic solution of acetic and lactic acids and develop phenomenological models to describe the adsorption dynamics in fixed-beds.

A second focus of this work is on the sharpening of the solute front in adsorption column to enhance bed capacity utilization. A high overall rate of adsorption is desirable in the adsorber to utilize the adsorbent capacity most efficiently to reduce frequent cycling and regeneration costs. In many applications, layered beds with adsorbent particles with different equilibrium or kinetic properties have been used to improve bed capacity utilization. Mathews and coworkers (Mathews, 1997; Mathews, 2005; Pota and Mathews, 2000) have described a novel adsorber design that utilizes a convergent tapered configuration with adsorbent particles layered according to size or density. The reactor configuration and particle size variation are such that the influent fluid contacts an adsorbent bed with decreasing particle size and decreasing velocity in the direction of flow leading to decreased mass transfer resistance along the bed length. This results in a solute front that sharpens as it travels through the column. Comparative studies have shown that breakthrough time can be increased by 46% to 75% for the sorption of a variety of solutes such as phenol and trichloroethylene from aqueous phase onto activated carbon using tapered beds with adsorbent layered according to kinetic properties (Pota and Mathews, 2000; Mathews, 2005).

1.5 Research objective

Many studies have been conducted on defining the sorption equilibria and dynamics for the uptake of organic acids on adsorbents from individual acids. However, in order to effectively design for recovery with high purity and selectivity from a multicomponent acid solution, an accurate representation of multicomponent sorption equilibria and dynamics must be obtained.

The main objective of this research is to study the adsorption dynamics of acetic acid and lactic acid in single and multicomponent solutions in stratified fixed-bed adsorbers.

The specific objectives intended for this research are:

1. Develop equilibrium data for single component and multicomponent adsorption for acetic and lactic acids on adsorbents such as granular activated carbon (GAC) and weak base resins
2. Determine the kinetics of acetic acid adsorption on GAC and weak base resins
3. Study fixed-bed adsorption dynamics and solute front movement for the adsorption of acetic and lactic acids on GAC and weak base resins in conventional and layered adsorbers of cylindrical and tapered geometries
4. Develop mathematical models to describe batch kinetics and fixed-bed adsorption dynamics for multicomponent adsorption of acetic and lactic acids from dilute aqueous solutions and implement model solutions using COMSOL Multiphysics® software

The thesis has been organized into seven chapters. Chapter 2 is devoted to the review of literature on adsorption and recovery of acetic and lactic acids using GAC and weak base resins. This chapter also provides a review on process modeling of organic acids adsorption and multicomponent adsorption dynamics in fixed-bed adsorbers. Chapter 3 describes the materials and experimental protocols used for this research. The chapters 4, 5, and 6 will present the results from experimental and fixed-bed adsorption dynamic modeling studies. Chapter 4 includes the single component and multicomponent adsorption equilibria and adsorption kinetics of acetic and lactic acids on weak base resins and activated carbon. Chapter 5 includes adsorption dynamics of organic acids on weak base resins and activated carbon in different fixed-bed adsorber configurations. Chapter 6 includes the multicomponent adsorption dynamics

in fixed-bed adsorber on weak base resins. The results and contributions from this research are summarized in chapter 7.

REFERENCES

Abdehagh, N., Tezel, F.H., Thibault, J., 2013. Adsorbent screening for biobutanol separation by adsorption: Kinetics, isotherms and competitive effect of other compounds. Adsorption 19, 1263–1272. https://doi.org/10.1007/s10450-013-9566-8

Aljundi, I.H., Belovich, J.M., Talu, O., 2005. Adsorption of lactic acid from fermentation broth and aqueous solutions on Zeolite molecular sieves. Chem. Eng. Sci. 60, 5004–5009. https://doi.org/10.1016/j.ces.2005.04.034

Angenent, L.T., Karim, K., Al-Dahhan, M.H., Wrenn, B.A., Domíguez-Espinosa, R., 2004. Production of bioenergy and biochemicals from industrial and agricultural wastewater. Trends Biotechnol. 22, 477–485. https://doi.org/10.1016/j.tibtech.2004.07.001

Anonymous, 2010. Biobased chemicals and products: A new driver of US economic development and green jobs.

Anonymous, 2016a. Acetic acid - chemical economics handbook (CEH) | IHS Markit [WWW Document]. URL https://ihsmarkit.com/products/acetic-acid-chemical-economics-handbook.html (accessed 11.27.18).

Anonymous, 2016b. Acetic anhydride - chemical economics handbook (CEH) | IHS Markit [WWW Document]. URL https://ihsmarkit.com/products/acetic-anhydride-chemical-economics-handbook.html (accessed 11.27.18).

Anonymous, 2017. Vinyl acetate - chemical economics handbook (CEH) | IHS Markit [WWW Document]. URL https://ihsmarkit.com/products/vinyl-acetate-chemical-economics-handbook.html (accessed 11.27.18).

Anonymous, 2018a. Advancing the biobased economy: renewable chemical biorefinery commercialization, progress, and market opportunities, 2016 and beyond [WWW Document]. http://www.biofuelsdigest.com. URL https://www.bio.org/advancing-biobased-economy-renewable-chemical-biorefinery-commercialization-progress-and-market (accessed 7.19.18).

Anonymous, 2018b. Lactic acid, its salts and esters - chemical economics handbook (CEH) | IHS Markit [WWW Document]. URL https://ihsmarkit.com/products/lactic-acid-its-salts-chemical-economics-handbook.html (accessed 11.27.18).

Anonymous, 2018c. Polylactic acid: A sustainable bioplastics packaging option [WWW Document]. URL https://packaging360.in/insights/polylactic-acid---a-sustainable-bioplastics-packaging-option (accessed 9.5.19).

Biddy, M.J., Scarlata, C., Kinchin, C., 2016. Chemicals from biomass: A market assessment of bioproducts with near-term potential (No. NREL/TP--5100-65509, 1244312). https://doi.org/10.2172/1244312

Bolen, W.P., 2017. Mineral commodity summaries. U.S. Geological Survey.

Chen, Y., Nielsen, J., 2016. Biobased organic acids production by metabolically engineered microorganisms. Curr. Opin. Biotechnol., Food biotechnology • Plant biotechnology 37, 165–172. https://doi.org/10.1016/j.copbio.2015.11.004

Davidson, A.W., 1931. An introduction to the chemistry of acetic acid solutions. Chem. Rev. 8, 175–190. https://doi.org/10.1021/cr60030a002

Devaney, L., 2016. Imagine the future [WWW Document]. tasteofscience. URL https://www.tasteofscience.com/articles/609/imagine-the-future.html (accessed 7.20.18).

Dunn, S.A., Schenk, R.U., 1980. Alternatives to sodium chloride for highway deicing. Transp. Res. Rec. 776, 12–15.

Eggeman, T., Verser, D., 2005. Recovery of organic acids from fermentation broths, in: twenty-sixth symposium on biotechnology for fuels and chemicals, ABAB Symposium. Humana Press, pp. 605–618. https://doi.org/10.1007/978-1-59259-991-2_52

Erickson, B., Nelson, J.E., Winters, P., 2012. Perspective on opportunities in industrial biotechnology in renewable chemicals. Biotechnol. J. 7, 176–185. https://doi.org/10.1002/biot.201100069

Evangelista, R.L., 1994. Recovery and Purification of Lactic Acid from Fermentation Broth by Adsorption. Iowa State University.

González, M.I., Álvarez, S., Riera, F.A., Álvarez, R., 2006. Purification of lactic acid from fermentation broths by ion-exchange resins. Ind. Eng. Chem. Res. 45, 3243–3247. https://doi.org/10.1021/ie051263a

Hirtzer, M., 2017. U.S. corn ethanol producers aim to out-pump competitors. Reuters.

Jang, Y.-S., Kim, B., Shin, J.H., Choi, Y.J., Choi, S., Song, C.W., Lee, J., Park, H.G., Lee, S.Y., 2012. Bio-based production of C2–C6 platform chemicals. Biotechnol. Bioeng. 109, 2437–2459. https://doi.org/10.1002/bit.24599

Komesu, A., Oliveira, J.A.R. de, Martins, L.H. da S., Maciel, M.R.W., Filho, R.M., 2017. Lactic acid production to purification: A review :: BioResources. BioResources 12, 4364–4383.

Lane, D., Stone, J., 2017. Opportunities to transition ethanol facilities to biochemical refineries : biofuels digest. URL http://www.biofuelsdigest.com/bdigest/2017/04/20/opportunities-to-transition-ethanol-facilities-to-biochemical-refineries/ (accessed 7.20.18).

Lane, J., 2017. US ethanol production sets record as 2016 ends : Biofuels Digest. URL http://www.biofuelsdigest.com/bdigest/2017/01/08/us-ethanol-production-sets-record-as-2016-ends/ (accessed 9.18.18).

Lange, J.P., 2007. Lignocellulose conversion: An introduction to chemistry, process and economics. Biofuels Bioprod. Biorefining 1, 39–48. https://doi.org/10.1002/bbb.7

Lazonby, J., 2016. Ethanoic acid (Acetic acid) [WWW Document]. URL http://www.essentialchemicalindustry.org/chemicals/ethanoic-acid.html (accessed 6.6.19).

Lee, W.S., Chua, A.S.M., Yeoh, H.K., Ngoh, G.C., 2014. A review of the production and applications of waste-derived volatile fatty acids. Chem. Eng. J. 235, 83–99. https://doi.org/10.1016/j.cej.2013.09.002

Li, Q., Wang, D., Wu, Y., Li, W., Zhang, Y., Xing, J., Su, Z., 2010. One step recovery of succinic acid from fermentation broths by crystallization. Sep. Purif. Technol. 72, 294–300. https://doi.org/10.1016/j.seppur.2010.02.021

Lilek, J., 2017. Roadway deicing in the United States: How a few industrial minerals supply a vital transportation service (Factsheet). American Geosciences Institute.

Lucas, F., 2014. H.R.2642 - 113th Congress (2013-2014): Agricultural Act of 2014 [WWW Document]. URL https://www.congress.gov/bill/113th-congress/house-bill/2642 (accessed 7.19.18).

Marynowski, C.W., Jones, J.L., Tuse, D., Boughton, R.L., 1985. Fermentation as an advantageous route for the production of an acetate salt for roadway de-icing. Ind. Eng. Chem. Prod. Res. Dev. 24, 457–465. https://doi.org/10.1021/i300019a025

Mathews, A.P., 1997. Tapered bed apparatus for fluid-solid mass transfer operations. US5626763A.

Mathews, A.P., 2005. Effect of adsorbent particle layering on performance of conventional and tapered fixed-bed adsorbers. J. Environ. Eng. 131, 1488–1494. https://doi.org/10.1061/(ASCE)0733-9372(2005)131:11(1488)

McCoy, M., 2017. DuPont seeks to sell its cellulosic ethanol plant | November 13, 2017 Issue - Vol. 95 Issue 45 | Chemical & Engineering News [WWW Document]. URL https://cen.acs.org/articles/95/i45/DuPont-seeks-sell-cellulosic-ethanol.html (accessed 7.20.18).

Murray, D.M., Ernst, U.F.W., 1976. An economic analysis of the environmental impact of highway deicing, Environmental Protection Technology. U.S. Environmental Protection Agency.

Nayak, J., Pal, P., 2013. Transforming waste cheese-whey into acetic acid through a continuous membrane-integrated hybrid process. Ind. Eng. Chem. Res. 52, 2977–2984. https://doi.org/10.1021/ie3033729

Pal, P., Nayak, J., 2017. Acetic acid production and purification: Critical review towards process intensification. Sep. Purif. Rev. 46, 44–61. https://doi.org/10.1080/15422119.2016.1185017

Philp, J.C., Ritchie, R.J., Allan, J.E.M., 2013. Biobased chemicals: The convergence of green chemistry with industrial biotechnology. Trends Biotechnol. 31, 219–222. https://doi.org/10.1016/j.tibtech.2012.12.007

Pota, A.A., Mathews, A.P., 2000. Adsorption dynamics in a stratified convergent tapered bed. Chem. Eng. Sci. 55, 1399–1409. https://doi.org/10.1016/S0009-2509(99)00032-9

Rush, B., 2012. Turning a novel yeast into a platform host for industrial production of fuels and chemicals. Metab. Eng. IX.

Tung, L.A., King, C.J., 1994. Sorption and extraction of lactic and succinic acids at pH > pKa$_1$. I. Factors governing equilibria. Ind. Eng. Chem. Res. 33, 3217–3223. https://doi.org/10.1021/ie00036a041

Van Dien, S., 2013. From the first drop to the first truckload: Commercialization of microbial processes for renewable chemicals. Curr. Opin. Biotechnol., Chemical biotechnology • Pharmaceutical biotechnology 24, 1061–1068. https://doi.org/10.1016/j.copbio.2013.03.002

Veeravalli, S.S., Mathews, A.P., 2018. Continuous fermentation of xylose to short chain fatty acids by *Lactobacillus buchneri* under low pH conditions. Chem. Eng. J. 337, 764–771. https://doi.org/10.1016/j.cej.2017.12.100

Veeravalli, S.S., Mathews, A.P., 2019. A novel low pH fermentation process for the production of acetate and propylene glycol from carbohydrate wastes. Enzyme Microb. Technol. 120, 8–15. https://doi.org/10.1016/j.enzmictec.2018.09.006

Vidra, A., Németh, Á., 2017. Bio-produced acetic acid: A review. Period. Polytech. Chem. Eng. 62, 245–256. https://doi.org/10.3311/PPch.11004

Voynick, S., 2003. The salting of the West – who cares? [WWW Document]. URL http://www.hcn.org/wotr/14487 (accessed 4.24.17).

Wenta, R., Sorsa, K., 2018. 2017 Road Salt Report. Public Health Madison & Dane County.

Wise, D.L., Levendis, Y.A., Metghalchi, M., 1991. Calcium magnesium acetate: An emerging bulk chemical for environmental applications. Elsevier.

Wu, W., Long, M.R., Zhang, X., Reed, J.L., Maravelias, C.T., 2018. A framework for the identification of promising bio-based chemicals. Biotechnol. Bioeng. 115, 2328–2340. https://doi.org/10.1002/bit.26779

WV PO, Deicing vendor response to West Virginia Purchasing Division [WWW Document], 2015. URL https://www.state.wv.us/admin/purchase/Bids/FY2016/B_0803_DOT1600000035_02.pdf (accessed 9.20.18).

Yang, S.T., Zhu, H., Lewis, V.P., Tang, I.C., 1992. Calcium magnesium acetate (CMA) production from whey permeate: Process and economic analysis. Resour. Conserv. Recycl., Calcium Magnesium Acetate: An emerging bulk chemical for environmental applications 7, 181–200. https://doi.org/10.1016/0921-3449(92)90016-U

Zacharof, M.P., Mandale, S.J., Williams, P.M., Lovitt, R.W., 2016. Nanofiltration of treated digested agricultural wastewater for recovery of carboxylic acids. J. Clean. Prod. 112, 4749–4761. https://doi.org/10.1016/j.jclepro.2015.07.004

Zhang, K., Zhang, L., Yang, S.T., 2014. Fumaric acid recovery and purification from fermentation broth by activated carbon adsorption followed with desorption by acetone. Ind. Eng. Chem. Res. 53, 12802–12808. https://doi.org/10.1021/ie501559f

Chapter 2
Literature Review

2.1 Introduction

This chapter is devoted to the review of literature on the objectives of this study. Firstly, the industrial scale production of acetic and lactic acids through bioconversion methods is discussed. Then, the existing separation techniques in the literature are detailed. This is followed by a section on adsorption and recovery of these acids using resins and activated carbon. Factors such as the basicity of the resin, p*K*a of the resin, pH of the solution, nature of fermentation broth, and presence of other acids (i.e., multicomponent acid solutions) are needed to be considered in the design of fixed-bed adsorbers using weak base resins. This chapter will explain the effects of these factors on the selection of resins for the recovery of acetic and lactic acids from fermentation broth. Further, a section of this chapter focuses on the solute front movement and bed capacity utilization in different fixed-bed configurations. In order to develop mathematical models to describe the adsorption dynamics in fixed-bed adsorbers, determination of equilibria, kinetics, and fixed-bed adsorption dynamics is necessary. The later section of this chapter focuses on the adsorption equilibrium in single and multicomponent solutions, kinetic models, and fixed-bed adsorption dynamic models.

2.2 Industrial scale production of acetic acid and lactic acid through bioconversion processes

At present, biochemical methods supply only about 10% of the worldwide demand of acetic acid. Low cost of natural gas and projections of its increased availability for the foreseeable future, challenges the economic viability of acetic acid production through bioconversion methods (Biddy et al., 2016). In addition, the downstream processing costs for the recovery of acetic acid from fermentation broths close to neutral pH represent up to 60% of the

total production costs (Erickson et al., 2012; Jang et al., 2012). In the bioproduction of acetic acid at industrial scale, substrates such as ethanol, cellulosic agricultural products, and agricultural residues are used as feedstock. Acetous fermentation process is the sole route to produce food-grade vinegar. It is a two-stage process comprising ethanol production and subsequent aerobic oxidation to produce acetic acid. This process uses acetic acid bacteria (AAB) such as *Acetobacter*, *Gluconacetobacter*, and *Gluconobacter*. However, this method is largely dependent on the cost of raw materials that are used to produce ethanol, which leads to its higher price compared to synthetically produced acetic acid (Jang et al., 2012). *Acetobacter* strains can produce up to 203 g/L of acetic acid using ethanol as a substrate at productivity of 1.6 g/(L h) and with a molar yield greater than 98% (Straathof, 2014). This fermentation process does not need pH control but requires oxygen to maintain aerobic conditions, which results in additional costs. Anaerobic acetogens of the genera *Clostridium* and *Acetobacterium* produce acetic acid from fermentation of sugars. *Clostridium thermoaceticum* (also known as *Moorella thermoacetica*) is extensively studied and is considered to have industrial applications for biobased production of acetic acid (Vidra and Németh, 2017). *Moorella thermoacetica* produces 100 g/L of acetic acid using glucose as a substrate, with productivity of 0.8 g/(L h) and 0.8 g/g yield at neutral pH (Straathof, 2014). Several anaerobic acetogens of the genera *Clostridium* and *Propionibacterium* also produce acetic acid as a product or coproduct from sugars such as glucose (Baumann and Westermann, 2016). Many of the industrial production plants are based on the fermentation of ethanol and simple sugars. The number of production plants using nonedible plant biomass as feedstock is scanty. A list of industries along with the process details that produce acetic acid through bioconversion methods is presented in Table 2.1.

Table 2.1: List of companies producing acetic acid through bioconversion methods

Company	Process details	Reference
Afyren, France	Non-food biomass is fermented under anaerobic conditions at pH 4-7 to produce a mixture of volatile fatty acids (VFAs). The VFAs are recovered by extraction	https://afyren.com/en/ (Nouaille and Pessiot, 2017)
Braskem, Brazil	Acetic acid is coproduced with isoprene through anaerobic fermentation of a carbon source at pH 6.5 using a genetically engineered microorganism	(Koch et al., 2015)
Godavari Biorefineries Ltd., India	Molasses based ethanol is used as the feedstock to produce acetic acid	(Guzman, 2018)
SEKAB, Sweden	Cellulosic bioethanol is used as feedstock to produce acetic acid, acetaldehyde, and ethyl acetate. The current capacity for acetic acid production is 24,000 tons/yr	http://www.sekab.com/
Wacker Chemie AG, Germany	Straw and other sugar-based biomass is fermented to ethanol, and subsequently converted to acetic acid via gas phase oxidation. The plant had a capacity of 500 tons/yr in 2009.	(Anonymous, 2010b)
ZeaChem Inc., USA	Cellulosic sugars are used as feedstock to produce acetic acid and other short chain VFAs, which are subsequently converted to alcohols via thermochemical processing. The capacity of ethanol biorefinery is 250,000 gallons/year and the acetic acid production capacity is ~100,000 L/year	http://www.zeachem.com/technology/ (Baumann and Westermann, 2016)

While the share of acetic acid that is produced through bioconversion methods is only 10%, lactic acid has an opposite trend. Almost 90% of the worldwide production of lactic acid is based on bioconversion routes (Jang et al., 2012; Komesu et al., 2017a). The technology readiness level (TRL) for the production of lactic acid from biomass is considered to be 9, meaning that the production processes are operational at full range (Biddy et al., 2016). Lactic acid producing bacteria are divided into four main groups, namely, lactic acid bacteria (LAB), *Bacillus* strains, *Escherichia coli*, and *Corynebacterium glutamicum* (Abdel-Rahman et al., 2013). Production of lactic acid from hexose and pentose sugars using homofermentative LAB is well established in industrial scale plants. Theoretical yields of 1 g/g of lactic acid using hexose and pentose sugars have been achieved (Abdel-Rahman et al., 2013; Straathof, 2014). However,

several drawbacks such as the ability of LAB to consume only simple sugars, requirement of nutrient rich media, product inhibition, production of racemic mixture, and risk of bacteriophage infection has led to extensive research on screening for superior strains. Nontraditional microorganisms belonging to algae, cyanobacteria, fungi, and yeast have been engineered to produce lactic acid (Abdel-Rahman et al., 2013; Rush, 2012). A metabolically engineered *E. coli* strain produced 138 g/L of D-lactic acid with an overall yield of 0.86 g/g and productivity of 3.5 g/(L h) using glucose as substrate (Jang et al., 2012). A *Bacillus coagulans* strain showed similar productivity of 3.69 g/(L h) with a yield of 0.95 g/g while operating at pH 6 using lignocellulosic biomass as feedstock (Murali et al., 2017). Many of the industrial production plants use edible crop products such as corn, sugarcane, beets, and cassava as feedstock for lactic acid production. Some companies are now considering using second-generation biomass such as waste biomass, sugar-, and starch-rich industrial waste streams as an alternative feedstock to improve sustainability and decrease the costs. A list of industries along with the process details that produce lactic acid through bioconversion methods is presented in Table 2.2.

2.3 Separation and recovery processes

Precipitation is widely used for the recovery of organic acids from dilute fermentation broth. Technical grade lactic acid (22-44%) can be obtained using this method (Komesu et al., 2017b). However, this method generates low value calcium sulfate as waste. In addition, the separation of organic acid mixtures is not feasible through this method. This necessitates the further development of recovery processes.

Various recovery and separation techniques such as distillation, extraction, esterification, and membrane separation have been studied to improve downstream separation efficiencies.

Table 2.2: List of companies producing lactic acid through bioconversion methods

Company	Process details	References
BBCA Biochemical Co., Ltd., China	L-lactic acid is produced from fermentation of corn. The company is projecting its production capacity to 30 million tons/year by 2030.	http://www.bbcagroup.com/
Cellulac, UK	D(-) lactic acid is produced from fermentation of deproteinized lactose whey	http://cellulac.com/sf/
Total Corbion PLA, Netherlands	Sugarcane is used as feedstock to produce PLA polymer. In 2018, the plant capacity was 75,000 tons/year.	https://www.total-corbion.com/ (O'Dowd, 2017)
Galactic, Brussels	Lactic acid is produced from algae, obtained as a waste from biodiesel production process	(Coppée, 2012)
Henan Jindan Lactic Acid Technology Co., Ltd., China	Corn is used as a feedstock to produce lactic acid and lactates. The plant capacity is 100,000 tons/year, which is the second biggest in the world and biggest in Asia.	http://jindanlactic.diytrade.com/
GC Innovation America, USA	Produces D- and L- lactic acids using various types of feedstocks	https://www.gcinnovationamerica.com/
NatureWorks, USA	Feedstocks such as corn, cassava, sugarcane, and beets are used to produce PLA polymer. In 2010, the plant capacity was 140,000 tons/year.	https://www.natureworksllc.com/
Synbra Technology bv, Netherlands	Plant capacity was 5000 tons/year	(Biddy et al., 2016)
thyssenkrupp AG, Germany	Feedstocks such as corn, cassava, sugarcane, beets, and cellulosic materials are used to produce PLA polymer. The plant capacity is reported as 3000 tons/year	https://www.thyssenkrupp.com/en/ (Biddy et al., 2016)

Many of these techniques were aimed at improving the recovery rate of lactic acid due to its high value and demand. Due to the close boiling points of water and many organic acids, particularly that of low molecular weight, the traditional distillation methods are ineffective. Hence, reactive and molecular distillation processes have been proposed as efficient alternatives

(Komesu et al., 2017b). In reactive distillation, two reversible reactions i.e., esterification and hydrolysis are carried out in a single unit. Thus, to obtain high yields optimum reaction conditions are to be maintained and catalysts such as acids and ion exchange resins are used. Several studies have been reported to achieve yields of > 80% when pure component solutes of concentration around 20% were used. On the other hand, molecular distillation requires expensive equipment, high temperature (55-95 ^{o}C), and vacuum conditions to separate organic acids from dilute aqueous solutions. These methods are considered as efficient purification techniques, but no studies have been reported on the industrial application of these techniques for the recovery of organic acids from fermentation broths.

A variety of extractants such as solvents, organophosphates, tertiary amines, and quaternary amines have been studied for the recovery of organic acids from dilute aqueous solutions. Among them, amine based extractants were found to be most suitable due to their specificity and high distribution coefficients. Yang et al., (1991) studied the extraction of organic acids from dilute aqueous solutions using tertiary and quaternary amines. Both these extractants proved to be efficient to recover organic acids. However, the regeneration of quaternary amines is quite difficult due to their high basicity. Hence, a tertiary amine, Alamine 336, was used in their follow up study for the extraction of acetic acid from fermentation broth (Yang et al., 1992). Synthetic lactose medium was used for fermentation process to produce acetic acid at a pH of 7.6 and concentration of 4%. A 50% mixture of tertiary amine extractant, Alamine 336, and a polar diluent 2-octanol were used for the extraction process. By back extraction with dolomitic lime, > 25% CMA was recovered. It was estimated that granular CMA can be produced at a cost of $215/ton using whey permeate as feedstock. However, the distribution coefficient or the extraction efficiency, for this extractant mixture decreases at pH > 4 and is zero

at pH > 7.5. Thus, low pH fermentation methods will improve the downstream separation efficiency and reduce the cost of the final product. This method cannot be used for *in situ* applications as the extractants are toxic to microorganisms. In addition, a high exchange area for extraction and stripping is needed.

Katikaneni and Cheryan (2002) compared esterification and extraction processes for the recovery of acetic acid from fermentation broth at pH 6.5 and concentration of 4.5%. The fermentation broth was subjected to acidification using electrodialysis. An equimolar mixture of Alamine 336 and 2-ethyl-1-hexanol at pH 3.5 resulted in an extraction efficiency of 85%. In comparison, the esterification process using an alcohol to acid ratio of 3:1 resulted in yields of < 20%. The low concentration of acetic acid in the broth resulted in poor yields. Several studies have been reported on the recovery of lactic acid using membrane processes. Due to their high selectivity, membranes are also used for *in situ* product recovery to reduce the need for further purification. However, the high cost of membranes, polarization, and fouling problems have limited their application.

Adsorption processes have been reported to have the least energy requirement compared to the other separation and recovery techniques that have been discussed (Abdehagh et al., 2013). Adsorption operations can be conducted *in situ* or *ex situ* for the recovery of organic acids from fermentation broths. In the *in-situ* application, adsorptive removal can also reduce the toxicity of organic acids to the microorganisms. The productivity of the fermentation processes were reported to increase by 1.3 and 4 times (Davison and Thompson, 1992; Garrett et al., 2015). In this research, adsorption process technology is studied from both experimental and phenomenological modeling standpoint for the effective separation of acetic and lactic acids.

2.4 Adsorption and recovery of organic acids using resins and activated carbon

Ion exchange and/or adsorption on polymeric resins and activated carbon can be a viable option for the recovery of organic acids produced by fermentation processes. Synthetic adsorbents are classified into strong-or weak-acid cation exchange resins and strong-or weak-base anion exchange resins (Evangelista, 1994; Harland, 1994). This classification is based on the functional or exchangeable ions attached to their polymeric matrix structures. Strong-and weak-acid cation exchange resins contain strong (e.g.–SO_3-H^+) and weak (e.g.–COOH) acids, respectively as functional groups. Similarly, strong- and weak-base anion exchange resins contain strong (e.g.–N-$(CH_3)_3$) and weak (e.g.–NH_3) bases, respectively as functional groups. Weak base resins are commonly used for the removal of free acids, and manufacturers such as Purolite® (Bala Cynwyd, PA) and Dupont® (Midland, MI) supply weak base resins specifically for the recovery of organic acids from dilute aqueous solutions. Many studies have been carried out on the use of weak base resins and activated carbon adsorbents for the recovery of organic acids from fermentation processes. A detailed list citing the use of weak base resins and activated carbons for the recovery of acetic acid and lactic acid from aqueous solutions is given in Table 2.3. This table also contains the information on resin characteristics such as the p*K*a value, functional group, and resin matrix.

2.4.1 Adsorption of organic acids on weak base resins

Adsorbent resins are insoluble in water, less toxic than extractants to microorganisms, and are typically stable maintaining sorption capacity over several adsorption and desorption cycles. Hence, they are considered suitable for use in extractive fermentation technology.

Table 2.3: Characteristics of weak base resins and activated carbon and their applications for recovery of acetic and lactic acids from aqueous solutions

Adsorbent	Characteristics	Process details
Amberlite IRA67	Functional group: Tertiary amine Type/Matrix: Acrylic/gel p*K*a :8-10	• Productivity of extractive fermentation process was 1.3 times compared to the controlled fed-batch process to produce lactic acid • Resin stability was tested over 108 days of fermentation and resin capacities for lactic and acetic acid were on average 112.2 mg/g and 19.6 mg/g, respectively (Garrett et al., 2015)
Amberlite IRA96	Functional group: Tertiary amine Type/Matrix: Styrene-DVB/microporous p*K*a :8-10	• Comparative evaluation of equilibria and kinetics for the adsorption of lactic acid at pH 4.85 on Amberlite resins namely IRA67, IRA96, IRA900, and IRA400 was performed • Amberlite IRA96 showed an uptake capacity of ~0.38 g/g (Moldes et al., 2003)
Amberlite IRA35	Functional group: Tertiary amine Type/Matrix: Acrylic/gel p*K*a :8.32	• At pH of 5-6, Reillex 425 has no uptake capacity while Dowex MWA-1 and Amberlite IRA35 had 0.17-0.28 g/g and 0.29-0.35 g/g, respectively • Selectivity for lactic acid over glucose followed the trend: Dowex MWA-1 > Amberlite IRA35 > Reillex 425; Higher swelling and water uptake by Amberlite IRA35 led to a decrease in the selectivity (Dai and King, 1996)
Dowex MWA-1	Functional group: Tertiary amine Type/Matrix: Styrene-DVB/microporous p*K*a :6.7/8.8	• Using Dowex MWA-1 and recovery with 1.5 bed volumes of 5% ammonium hydroxide resulted in complete recovery and lactic acid was concentrated by ~2 times (Evangelista, 1994)
Reillex 425	Functional group: Pyridine Type/Matrix: Poly (4 vinylpyridine) (PVP) p*K*a :3.92/4.9/5.2	• Overall yield of the extractive fermentation process reached the stoichiometric limit of 1 g/g glucose (Davison and Thompson, 1992) • Production of lactic acid was enhanced by 4 times compared to the normal fermentation process
Activated carbon		• Activated carbon was used to remove acetic acid from pretreated corn stover hydrolysate • Five stages of adsorption was needed for effective removal of acetic acid • Activated carbon showed high selectivity to acetic acid over glucose (Berson et al., 2005)

In extractive fermentation, the products are removed from aqueous phase into the solid resin phase, and this reduces the potential inhibitory effects from high product acid concentrations. Organic acids are weak acids and they do not ionize or protolyze completely in aqueous solutions. King and coworkers carried out extensive research on the development of separation processes for the recovery of organic acids such as acetic, lactic, and succinic acids from dilute aqueous solutions using weak base resins (Byers, 1996).When a fermentation process is operated at pH > pK_{a_1} of the acid, it is essential to identify a suitable sorbent which has adsorption capacity for the acid at that pH and can be regenerated with high recovery. The schematic of driving forces for the recovery of organic acids from aqueous solution is shown in Figure 2.1. Lactic acid has a p*K*a of 3.86 and when a weak base resin with p*K*a of 8.86 is employed for sorption of lactic acid, there are five pH units of driving force available for separation using sorption. When a basic regenerant such as sodium hydroxide with pH 10.86 is used for regeneration process, then there are only two pH units available as driving force for desorption. This leads to poor regeneration efficiencies and low recovery. Thus, it is essential to choose a weak base resin and regenerant such that there is enough driving forces for adsorption with high uptake capacities and regeneration with complete recovery (Lisa Ann Tung, 1993).

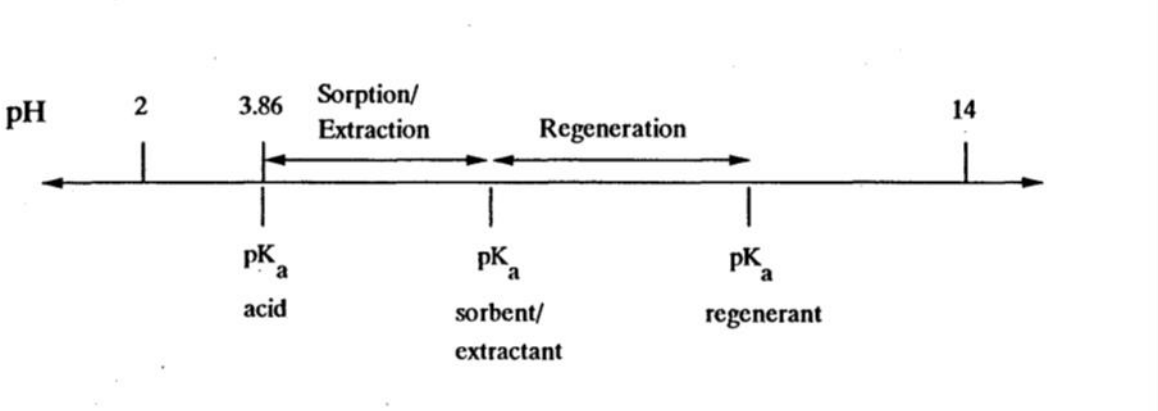

Figure 2.1: Driving forces for sorption and regeneration process in recovery of organic acids using sorbents or extractants (Lisa Ann Tung, 1993)

2.4.1.1 Chemical structure of weak base resins

Most commonly used weak base resins are prepared from vinyl polymers of styrene-divinylbenzene (DVB) or methyl acrylate-DVB (Harland, 1994) (Figure 2.2).

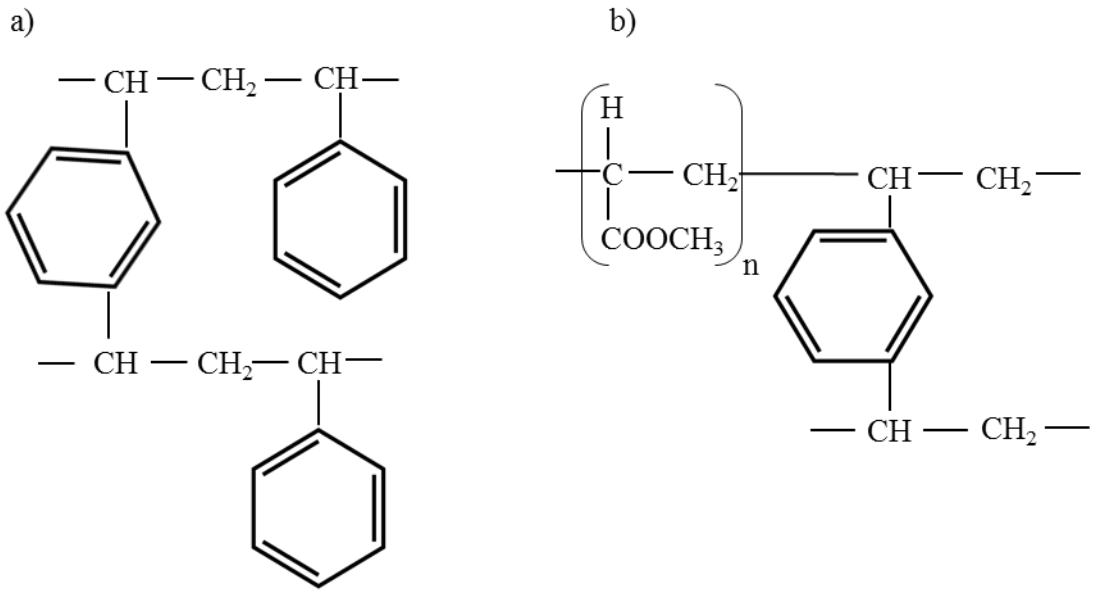

Figure 2.2: Chemical structure of (a) styrene-DVB, and (b) methacrylic acid-DVB copolymers (Harland, 1994)

These copolymers do not contain any exchange sites and are further treated to impart ion exchange functional groups. In case of styrene-based anion exchange resins, chloromethylated styrene-DVB copolymer is considered as a parent molecule from which different types of anion exchange resins are prepared. The reaction between the chloromethylated copolymers with trimethyl amine gives type I strong base resin polymer and reaction with dimethyl ethanol amine gives type II strong base resin polymer (Figure 2.3(a), (b)). When methylamine or dimethyl amine is reacted with the chloromethylated copolymer, weak base polymers of secondary or tertiary amines are produced (Figure 2.3(c)). On the other hand, acrylic anion exchange resins are produced from methyl acrylate-DVB copolymer. Acrylic weak base resin polymers with tertiary amine functional groups are produced by amination of the copolymer with dimethylaminproplyamine (DMAPA) (Figure 2.4(a)). Further reaction of this weak base polymer

with methyl chloride results in strongly basic resin polymer with quaternary ammonium group (Figure 2.4(b)).

Acrylic matrix resins are characterized by higher inorganic to organic content ratio compared to the styrene-DVB matrix (Matsuda et al., 1996). Due to this characteristic, acrylic resins are more hydrophilic than styrene-DVB resins. The hydrophilic matrix of acrylic resins enhances interactions of the resin functional groups to effectively sorb organic compounds from aqueous solutions. There is also a wider acceptance of acrylic based matrix resins for use in the removal of organic compounds due to their inherent nature that imparts better fouling resistance and high sorption capacities for high molecular weight compounds (Godshall, 2007).

2.4.1.2 Mechanisms in the adsorption of organic acids on weak base resins

The adsorption of organic acids on weak base anion exchange resins can be described using a simple model known as the ideal exchange model (Evangelista, 1994; Garcia and King, 1989).

According to this model, in a single component weak acid and weak base ion exchange resin system, one acid molecule (HA) from the bulk phase is exchanged with the water molecules attached to a functional group in the resin (R) as follows:

$$HA + (H_2O)_n - R <=> nH_2O + HA - R \quad (2.1)$$

The equilibrium in this reaction is defined by a constant K_1,

$$K_1 = \frac{\{HA-R\}*\{H_2O\}^n}{\{HA\}*\{(H_2O)_n-R\}} \quad (2.2)$$

The equilibrium parameter, K, in the Langmuir isotherm is related to the equilibrium constant, K_1 as:

$$K = \frac{K_1}{(H_2O)^n} = \frac{\{HA-R\}}{\{HA\}*\{(H_2O)_n-R\}} \quad (2.3)$$

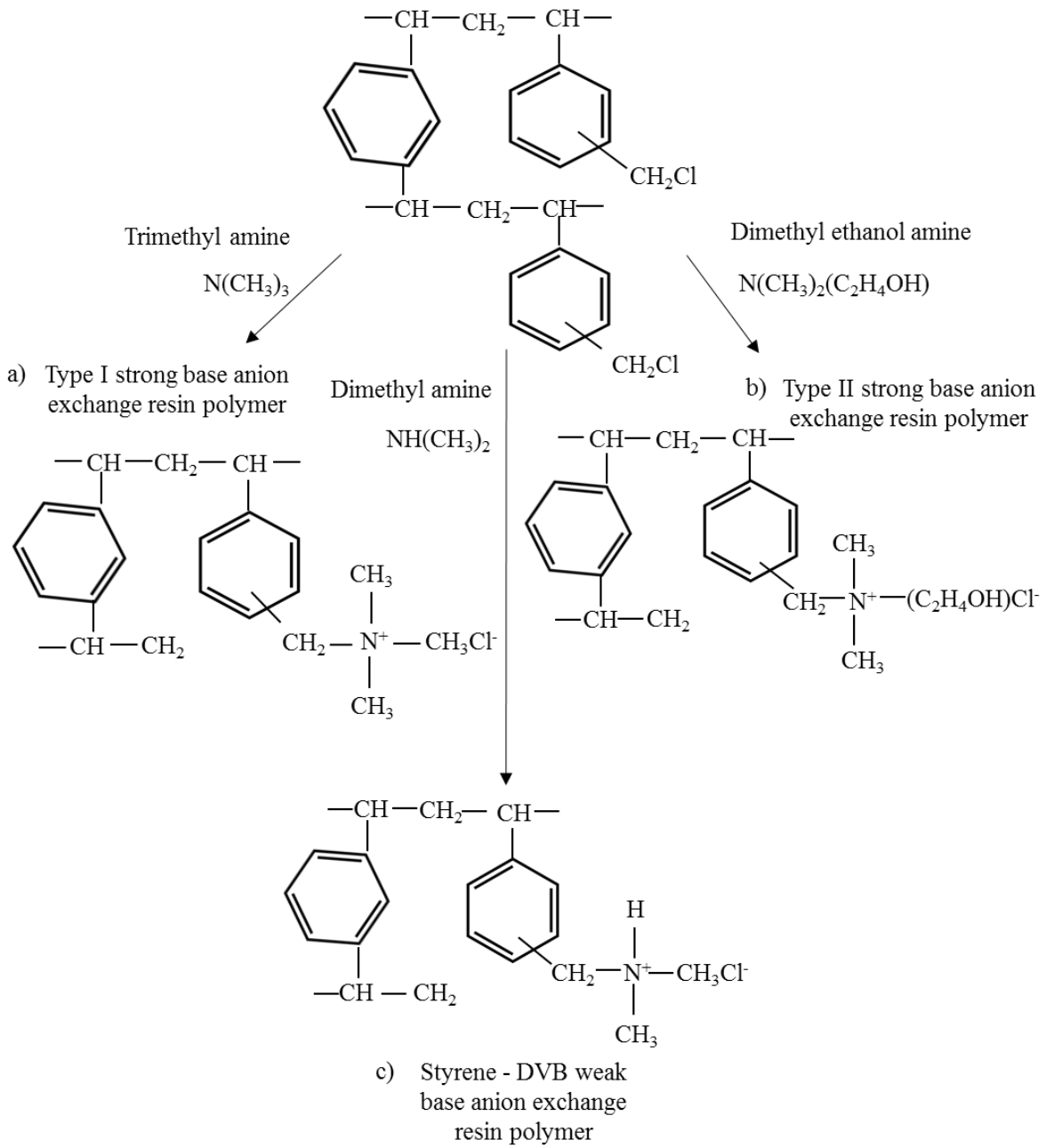

Figure 2.3: Process scheme for the synthesis of (a) type I, (b) type II strong base styrene-DVB anion exchange resin, and (c) weak base styrene-DVB anion exchange resin polymers (Harland, 1994)

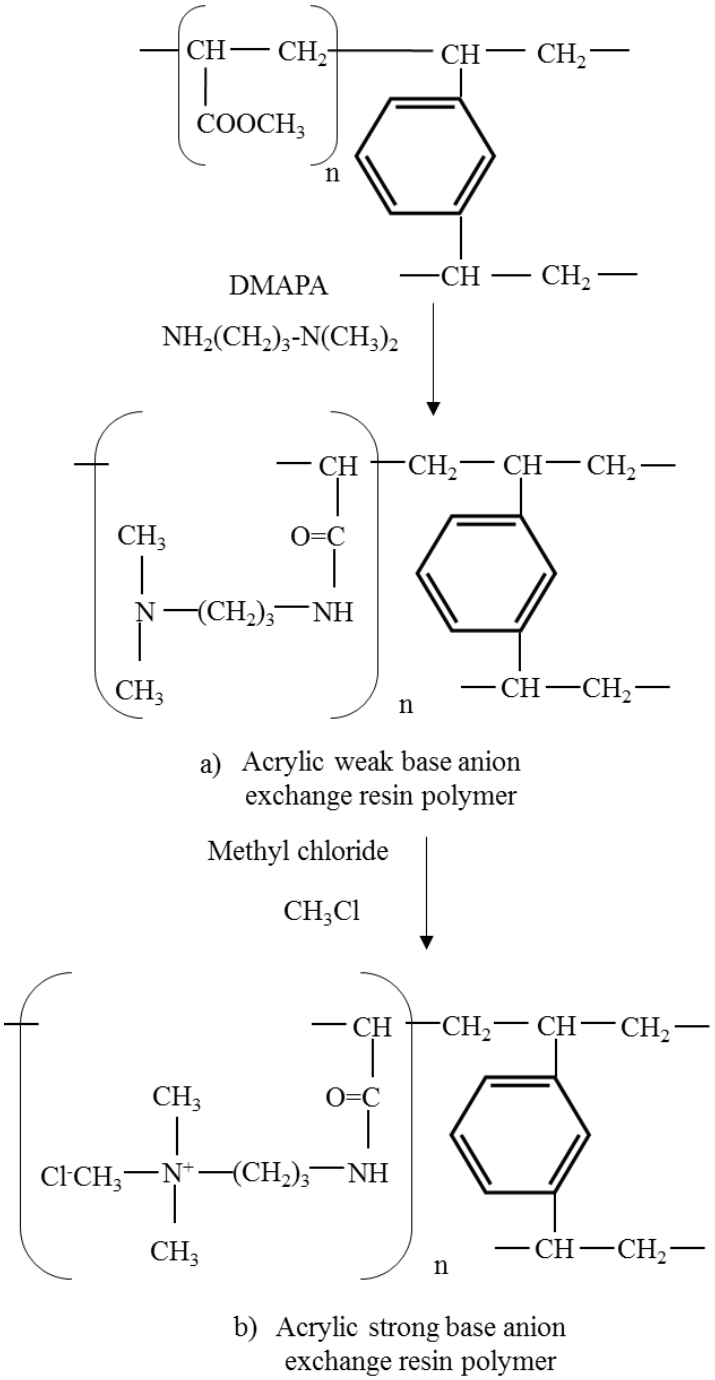

Figure 2.4: Process scheme for the synthesis of (a) weak base and (b) strong base acrylic anion exchange resin polymers (Harland, 1994)

Using the following assumptions: (1) each functional group associates with only one acid molecule, (2) all the functional groups in the resin are equally basic, accessible, and their total

number remains constant, and (3) the activity coefficient of all the components in the system remains constant, the following expression of Langmuir isotherm results:

$$\frac{q}{q_m} = \frac{KC_{HA}}{1+KC_{HA}} \tag{2.4}$$

where q is the concentration of acid molecule in the adsorbed phase (g/g), q_m is the maximum adsorption capacity (g/g), and C_{HA} is the concentration of acid molecule HA in the liquid phase in equilibrium with the solid phase of the resin (g/L). Substituting the expression for equilibrium parameter K, the ratio of equilibrium uptake capacity of the resin to the maximum uptake capacity is described by the following equation:

$$\frac{q}{q_m} = \frac{\{HA-R\}}{\{HA-R\}+\{(H_2O)_n-R\}} \tag{2.5}$$

The equilibrium parameter, K (L/g), is a measure of strength of complexation and basicity of the resin and is obtained from the slope of the sorption isotherm (Tung and King, 1994) (Figure 2.5). The higher the slope of the isotherm the higher is the basicity or the pKa of the resin. Weak base resins have higher uptake capacities for organic acids at low pH values (pH < pKa$_1$ of the acid) (discussed further in the section 2.4.1.3). But, their uptake capacities decrease with increasing pH values as shown in Figure 2.6. When strong basic resins with sorption capacity at pH greater than

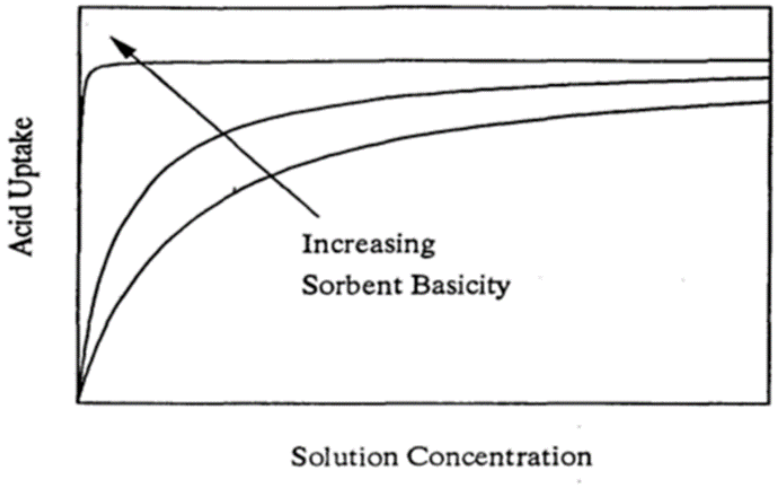

Figure 2.5: Effect of resin basicity on the acid uptake capacity of weak base resins (Tung and King, 1994)

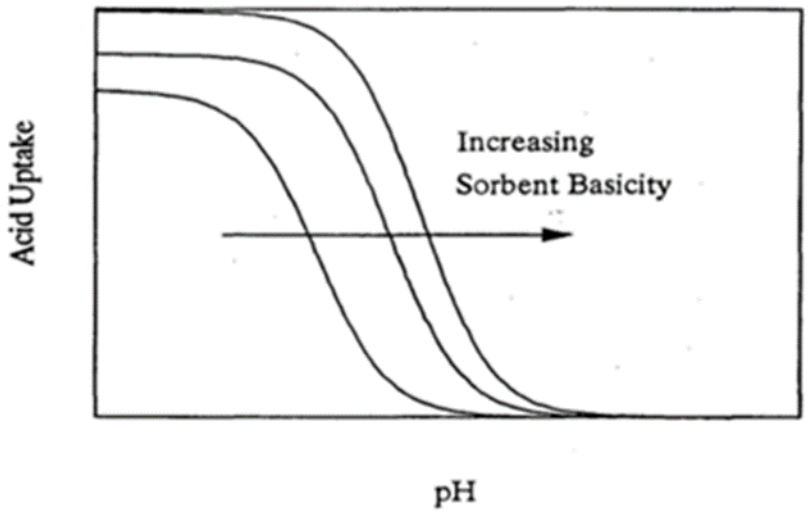

Figure 2.6: Effect of pH on the acid uptake capacity of weak base resins of different basicities (Tung and King, 1994)

p*K*a of the acid are used, the recovery process can be carried out in the fermenter or in the external loop without using chemicals for pH adjustment. But, stronger sorbents or resins with high basicity need stronger regeneration methods as well. Reisinger and King (1995) studied the sorption and recovery of acetic acid at pH > p*K*a using weak base resins of different basicities. The adsorption experiments were carried out at a pH of 6 and slaked dolomitic lime was used as the regenerating agent. The resins with high basicity needed the pH of the dolomitc lime to be above 11 and the resins with low basicity needed the pH to be at least 10. However, due to the insufficient driving forces, the recovery efficiencies were poor and there was no overall concentrating effect. Garrett et al., (2015) studied the adsorption performance and stability of Amberlite IRA67 for the *in situ* extraction of lactic acid at pH 5.5. Although the resin retained its adsorption capacity for 11 cycles of sorption and desorption over 108 days, the recovered acid was dilute in concentration at 3 g/L. Although weak base resins are suitable for the recovery of organic acids, the operating pH and basicity of the resin are needed to be considered for obtaining high recovery efficiencies.

2.4.1.3 Effect of p*K*a of the resin on the uptake capacity

The effect of the p*K*a of the weak base resins on acid uptake capacity has been illustrated using different reaction mechanisms in the literature. The main reactions are based on the dissociation reaction of organic acids in the aqueous solution and the reversible protonation of the functional group in weak base resins as (Helfferich and Hwang, 1985):

$$HA <=> H^+ + A^- \quad (2.6)$$

$$-R + H^+ <=> -RH^+ \quad (2.7)$$

Strong acid functional groups such as $–SO_3\text{-}H^+$ ionize even at low pH and weak acid functional groups such as the –COOH ionize only at high pH. Similarly, strong base functional groups such as $–N\text{-}(CH_3)_3$ remain ionized till a high pH, whereas weak base groups such as $–NH_3$ ionize only at low pH. Thus, the pH of the solution affects the degree of ionization of weak functional groups, and hence the exchange capacities of weak acid and weak base resins are pH dependent.

The p*K*a values of weak base resins are usually high (p*K*a 8-10), except for resins such as Reillex 425 which has a p*K*a of 4.9, and Riedel-de-Haen VI-15 which has a p*K*a of 6.9 (Evangelista, 1994). These resins stay protonated when pH of solution is less than their p*K*a (resin's p*K*a) and dissociate only when the pH of the solution is greater than its p*K*a. Thus, Equation (2.7) is considered essentially as an irreversible reaction as the resin can get protonated at a rapid rate when the solution pH < p*K*a of resin.

$$-R + H^+ => -RH^+ \quad (2.8)$$

During the uptake of acids, the protonation reaction of the weak base group is much faster than the diffusivity rate of the acid anion (A^-) and this creates a boundary in the resin particle. The resin particle is divided into an inner core, which is in the initial unprotonated form

and an outer core, which is in the protonated form. For dibasic acids such as sulfuric acid and succinic acid (H_2A), the HA^- also can protonate the weak base resin along with the H^+ ion. These reaction mechanisms are further simplified into the rate-controlling ion reaction where the protonation reaction controls the uptake of acid by the weak base resins.

$$-R + H^+ + A^- => -RH^+A^- \quad (2.9)$$

This reaction mechanism explains why in the adsorption of weak acids such as acetic acid and lactic acid, the undissociated acid is always the main proton carrier and rate-controlling ion. Thus, the pH of the solution effects the degree of ionization of weak base functional groups and the exchange capacities of weak base resins are pH dependent. Due to the presence of weak base functional groups such as tertiary amine and pyridine, the uptake capacity of weak base resins is maximum at low pH values and it decreases with increase in the pH of the solution (Reisinger and King, 1995). Also, because of the effect of the solution pH on the protonation of the resin, low basic resins such as Reillex 425 have a narrow pH range for the sorption of weak acids compared to the very high basic weak base resins (Tung and King, 1994) as shown in Figure 2.7. Present-day weak base resins contain common functional groups such as tertiary amine and pyridine with predetermined p*K*a values. Thus, it is important to consider the differences in the functional groups and utilize these resins at their best operating pH for the recovery of organic acids obtained from bioproduction methods.

2.4.1.4 Regeneration of weak base resins

In the typical bioprocess to produce acetic acid or lactic acid, the pH of the fermentation broth is maintained at close to neutral pH by the addition of alkali. This results in the formation of salt of the acid as the product. A strong base ion exchanger can recover the acid in the salt form. However, regeneration of the strong base resin requires a stronger desorbent. Moldes et al.,

(2003) compared the adsorption equilibria and kinetics of strong base and weak base resins for the recovery of lactic acid at a pH of 4.85.

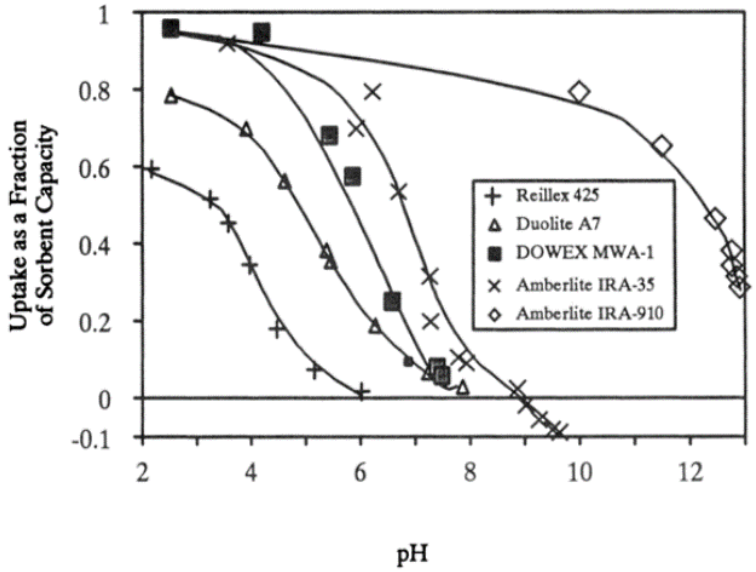

Figure 2.7: Effect of pH on the normalized uptake capacities of lactic acid on commonly used weak base resins (Tung and King, 1994)

Strong base resins contain quaternary ammonium cation as the functional group with Cl^- ion as the exchangeable ion. These resins can be converted between Cl^- and OH^- forms by washing them with HCl and NaOH respectively. When a strong base resin in Cl^- form is used for the recovery of organic acid present as a salt form (*NaA*), the recovery mechanism is represented as:

$$-R^+Cl^- + Na^+ + A^- <=> -R^+A^- + NaCl \quad (2.10)$$

$$-R^+A^- + H^+ + Cl^- <=> -R^+Cl^- + HA \quad (2.11)$$

When the strong base resin in OH^- form is used for the recovery of organic acid present as a salt form (*NaA*), the sorption and recovery is represented as:

$$-R^+OH^- + Na^+ + A^- <=> -R^+A^- + NaOH \quad (2.12)$$

$$-R^+A^- + H^+ + Cl^- <=> -R^+Cl^- + HA \quad (2.13)$$

$$-R^+Cl^- + Na^+ + OH^- <=> -R^+OH^- + NaCl \quad (2.14)$$

Thus, the application of strong base resins will result in increased costs, because of the requirement of higher number of stages, chemicals, and waste management. Also, based on adsorption equilibrium and kinetic studies, it has been proven that weak base resins are more favorable for the recovery of organic acids compared to strong base resins (Moldes et al., 2003).

Weak base resin adsorbents adsorb only the free organic acid, as they are effective at pH values where only the undissociated form of the acid is present. These resins are also easy to regenerate by using solvents such as alcohols (e.g., methanol and ethanol) or acetone. The product can be obtained in the acid form after evaporating the solvent. Other regeneration agents such as hot water and lime slurry have also been shown to be effective for the recovery of organic acids using weak base resins (Davison et al., 2004). Reisinger and King (1995) developed a process to produce CMA from fermentation methods. In this process, $Ca(OH)_2/Mg(OH)_2$ is used to regenerate the weak base resins. The mole ratios of calcium and magnesium used to prepare the regenerating chemical determines the chemical composition of CMA and the downstream processing steps. When 2.6 equivalents of dolomitic lime per equivalent of acetic acid was used, 90% of desorption was reported. However, the CMA obtained through this process is dilute in concentration and requires additional steps such as evaporation and spray drying. This regeneration scheme is given as:

$$-RH^+A^- + Ca(OH)_2 + Mg(OH)_2 <=> -R + CaMg(A) + H_2O \quad (2.15)$$

In a study on the recovery of adipic acid using weak base resins, solvents such as methanol, acetone, 2-propanol were tested as eluants (Kawabata et al., 1981). Adipic acid in aqueous solution at 1.5 wt% was adsorbed on a poly (4-vinyl pyridine) polymer and using methanol as an eluant, a final solution with 8-10 wt% concentration was obtained. Elution was simpler and required lower amount of eluant for poly (4-vinyl pyridine) resins compared to the

strong and weak base resins. However due to its low basicity, poly (4-vinylpyridine) resins have a narrow pH range for the uptake of organic acids compared to the strong base and weak base resins. Hence, weak base resins with tertiary amine functional groups are a better option for the recovery of organic acids as they have high uptake capacities over a wide pH range and can be easily regenerated with bases or solvents.

2.4.1.5 Recovery and separation of mixed acids

In a mixture of products, the selectivity of a sorbent to a compound can arise from different effects such as equilibrium, kinetic, molecular sieving, and desorption effects (Thomas and Crittenden, 1998). Gas and liquid mixtures are separated using adsorbents capable of introducing these effects. Processes such as those involving bulk separation of O_2-N_2, ethanol-water, and glucose-fructose are well known applications of these techniques. A mixture of carboxylic acids can be separated using weak base extractants or sorbents if their p*K*a values are different. Schügerl (2013) reported that formic acid (p*K*a 3.7) can be separated from acetic acid (p*K*a 4.76), and pyruvic acid (p*K*a 2.49) using a suitable extractant at an appropriate pH value. Monobasic and dibasic acids such as lactic and succinic acids can be separated by chromatographic fractionation in a fixed-bed containing basic resin, operating at a suitable pH (Husson and King, 1999). In addition to the separation of weak acids, weak base resins are also efficient in separating strong acids such as hydrochloric, sulfuric, and nitric acids from weak acids such as lactic acid (Gustafson et al., 1970). Resins with high basicity will have greater affinity to both strong and weak acids, whereas resins with low basicity will show selectivity towards strong acids than weak acids. A resin with p*K*a of 3.92 separated HCl from weak acids such as acetic, lactic, and citric acids efficiently for double the number of bed volumes compared to a resin with p*K*a ~ 6.7 (Gustafson et al., 1970). These separations of mixed acids depend on

the strength of the basic group of the sorbent. Thus, the basicity of the anion exchange resins becomes an important factor in the selection of a resin for separation and recovery of valuable products.

2.4.2 Adsorption of organic acids on GAC

Several studies have been reported on the use of GAC for the removal and recovery of organic acids from processes such as biomass hydrolysis, pulp production, and terephthalic acid production processes (Ahsan et al., 2013; Berson et al., 2005). GAC was also used to recover acetic acid from waste streams of industries such as petrochemical and fine chemical refineries (Ganguly and Goswami, 1996). Activated carbon was used for the recovery of lactic, acetic, and butyric acids present at initial concentrations of 11.66, 2.79, and 6.58 g/L in the fermentation broth of food waste. Percentage removals of 15.99, 49.67, and 64.92 were obtained for the adsorption of lactic, acetic, and butyric acids respectively at adsorbent dosages of 5 g per 50 ml (Yousuf et al., 2016). According to Traube's rule, the sorption affinity of carboxylic acids on activated carbon increases with increase in the length of the acid's carbon chain. A study on sorption of acetic, propionic, and butyric acids on activated carbon has shown that the adsorption capacities are in the order of butyric acid > propionic acid > acetic acid (da Silva and Miranda, 2013). Similar to weak base resins, activated carbon exhibits a high sorption capacity at low pH values and its sorption capacity decreases with an increase in the pH. At an initial pH of 2, activated carbon gave a maximum adsorption capacity of 0.31 g/g of acetic acid. The acid removal percentage for activated carbon decreased by 40% with an increase in pH from 2 to 6 (Yousuf et al., 2016).

The adsorption of organic acids on weak base anion exchange resins is based on the acid-base interactions between the carboxylic group of the acid and amine group of the resin, whereas

in activated carbon, the hydrophobic interactions between the carbon chain and surface of the activated carbon is the major contribution to the adsorption mechanism. Due to the non-specific nature of such interactions, the uptake capacities of acetic and lactic acids on activated carbon are lower compared those for resins. Comparative studies between resins such as Amberlite IRA67 and Purolite A133S and activated carbon have shown that the resins have higher uptake capacities for organic acids from single and multicomponent solutions than activated carbon (da Silva and Miranda, 2013; Yousuf et al., 2016).

Since, the adsorption of organic acids on activated carbon is due to weak hydrophobic interactions of acids with the carbon surface, the regeneration process is simple. Alcohols such as ethanol and propanol with higher hydrophobicity act as efficient vehicles for desorption of organic acids from activated carbon. Though activated carbon is less costly compared to resins, the low specificity and selectivity hinders its application as a recovery agent in the fermentation-based production processes. However, due to its low selectivity for organic acids, activated carbon is a viable option for the recovery of organic acids from waste and process streams where there are less competitive effects.

2.5 Fixed-bed adsorbers for the recovery of organic acids

In bioconversion production processes, the application of *in situ* product recovery (ISPR) schemes is attractive. These schemes improve the productivity by enabling continuous operation and reducing the product inhibition. Adsorption is carried out either in batch or fixed-bed mode of operation. In the batch mode of operation, the direct addition of resins or activated carbon promote the substrate consumption and improve the productivity. However, the recovery of spent sorbents from the fermentation broth is cumbersome and the process cannot be operated in a continuous mode. In a study on recovery of acetic acid from aqueous solutions, batch adsorption

using activated carbon and a three-stage countercurrent desorption process was used. Desorption with ethanol resulted in the recovery of > 90% of the acid, and a mass yield of 37.3% was achieved (da Silva and Miranda, 2013). The overall yield can be improved by using continuous product recovery systems such as fixed-bed adsorbers instead of batch systems.

Adsorption using fixed-bed adsorbers is the most widely used technology in industrial scale processes due to its ability to process large quantities of feed (Zhou et al., 2013). A fixed-bed adsorber containing 4.1 g of Amberlite IRA67 was used to recover lactic acid present at an initial concentration of 48 g/L and at a pH of 4.85 from a simultaneous saccharification and fermentation (SSF) broth. A flowrate of 3.5 ml/min was used and breakthrough was observed almost instantaneously. Desorption using HCl resulted in effluent concentration lower than the feed concentration of the solute (Moldes et al., 2003). Thus, when fixed-bed adsorbers with low empty bed contact times are used, it is difficult to obtain high product recovery. González et al., (2006, 2007) developed a novel scheme for the production and recovery of lactic acid from fermentation of sweet whey ultrafiltration permeate carried out at pH 5.6. The fermentation broth was first clarified using ultrafiltration and was then acidified using a cation exchange resin. Subsequently, lactic acid was recovered using anion exchange resin in a fixed-bed adsorber. The adsorber containing 25 g of resin was operated at a feed flow rate of 14 bed volumes/h at 25^{o}C. This resulted in 25 bed volumes of > 99% pure lactic acid with respect to other components in the broth, and further concentration using reverse osmosis and vacuum evaporation resulted in 50% (w/w) lactic acid. The authors conducted an economic evaluation for an industrial scale process using the same process schematic for the production and recovery of lactic acid with two fermenters each of 100 m^3 volume. They have reported that the proposed process was economically viable in producing 50% lactic acid at 1.25 $/kg compared to the then market price

at 1.38-1.6 $/kg. Thus, fixed-bed adsorption is considered to be an efficient technology for product recovery in bioconversion production methods.

2.5.1 Importance of bed capacity utilization in the design of fixed-bed adsorbers

A high overall rate of adsorption is desirable in the adsorber to utilize the adsorbent capacity most efficiently and to reduce frequent cycling and regeneration costs. In a typical fixed-bed adsorber, the movement of the solute front along the bed length is determined by the adsorption equilibrium, adsorption kinetics, bed geometry, and sorbent properties. In the absence of mass transfer resistances and axial dispersion effects, a solute with favorable isotherm moves along the fixed-bed as a shock front with a vertical concentration profile. As shown in Figure 2.8, at breakthrough, a sharp front exits the column leading to complete bed saturation and a maximum bed capacity utilization (Mathews, 2005). However, in practice, the presence of mass transfer resistances and axial dispersion effects will lead to spreading of the shock front and decrease the bed capacity utilization. In a conventional cylindrical adsorber with a single adsorbent particle size (Figure 2.9(a)), a constant pattern solute front (Figure 2.9(b)) will develop and it travels along the bed length with a constant velocity. For a solute with a favorable isotherm and symmetric solute front, the fractional bed capacity utilization is given by:

$$fractional\ bed\ capacity\ utilization = 1 - 0.5\frac{L_{MTZ}}{L} \tag{2.16}$$

where L is the bed length and L_{MTZ} is the length of the mass transfer zone. As a rule of thumb, the lower the L_{MTZ} the higher the bed capacity utilization. Moreover, in liquid phase applications the mass transfer zone is quite diffuse resulting in poor bed capacity utilization. When a diffuse solute front exits the column at breakthrough, a significant portion of the sorbent in the fixed-bed will be left unutilized.

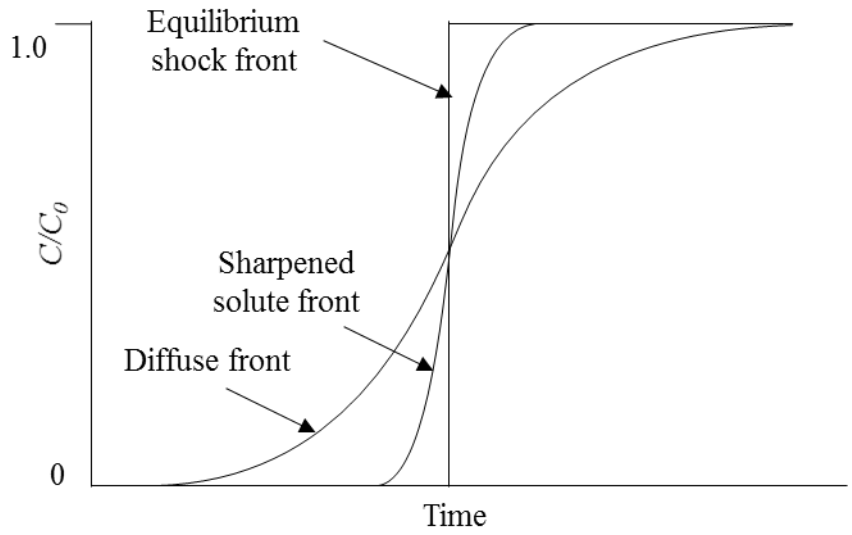

Figure 2.8: Effect of solute front shape on breakthrough curves for a solute with favorable adsorption isotherm (Mathews, 2005)

Several studies have been conducted on the recovery of a variety of products from bioconversion processes using fixed-bed adsorbers. GAC was used in a fixed-bed adsorber to separate and recover fumaric acid from fermentation broth containing 5 g/L fumaric acid, 3.1 g/L glucose, and 1.8 g/L malic acid at pH 2.0. Subsequent desorption with acetone resulted in a recovery yield of 93% for fumaric acid (Zhang et al., 2014). The experimental data reported in their study show that the fixed-bed adsorber did not attain saturation. However, based on the time of exit for the breakthrough curve and given bed height, the fractional bed capacity utilization was estimated to be only ~53%.

There are several methods to increase the bed capacity utilization. Lin et al. (2017a) studied the recovery of levulinic acid from aqueous solutions using a fixed-bed adsorber with a single adsorbent particle size at different operating conditions. They have reported that the bed capacity utilization decreased when there was either an increase in the inlet flow rate or decrease in the diameter of the column. They have also reported that by increasing the bed length in three separate fixed-bed experiments, L/L_{MTZ} values of 1.45, 1.72, and 4.23 were obtained, and the bed capacity utilization was increased only by 13% overall.

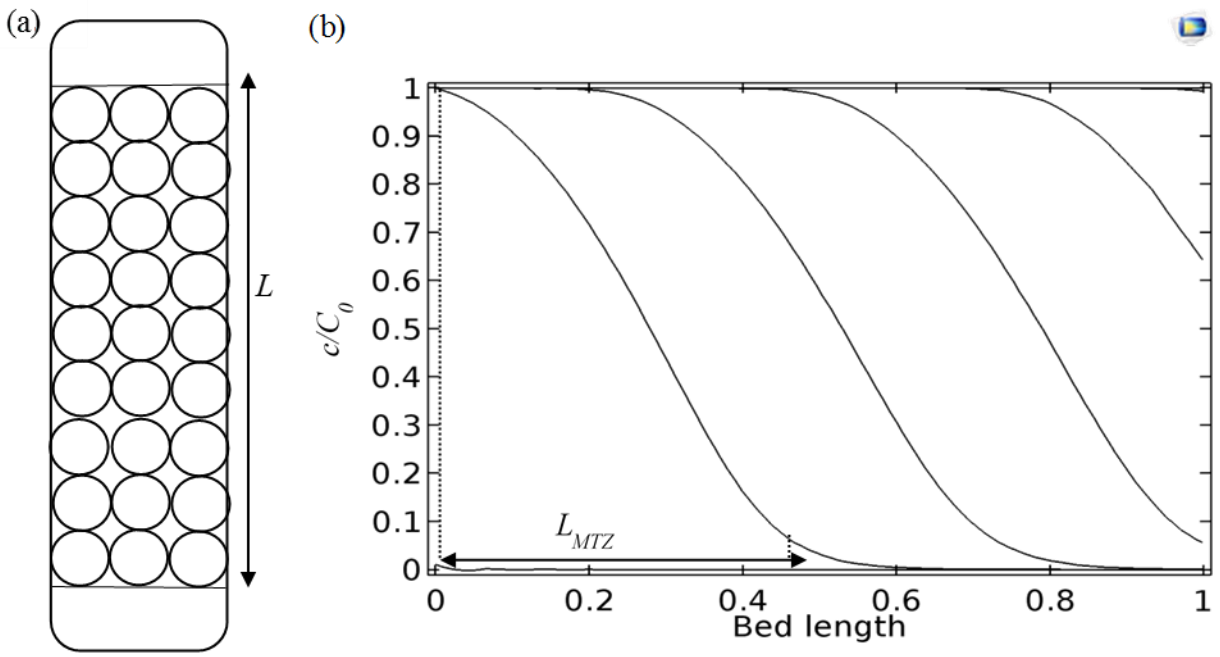

Figure 2.9: (a) Cylindrical adsorber with single adsorbent particle size, and (b) length of mass transfer zone, L_{MTZ}, and concentration profile along the bed length (L)

Equation (2.16) shows that an increase in L/L_{MTZ} beyond a factor of three does not result in any significant improvement in the bed capacity utilization. Another method to improve bed capacity utilization is to use smaller adsorbent particle sizes. In a study on recovery of 1-butanol from acetone-butanol-ethanol(ABE) fermentation broth, the effect of particle size on adsorption rate was studied (Saravanan et al., 2010). Zeolite and alumina/silica based extrudates of 30-80, 16-24, and 12-24 mesh sizes were used for biobutanol recovery. The breakthrough curves obtained in their study showed that the bed capacity utilization is highest for the bed with the smallest particle size. However, the dramatic increase in pressure drop as particle size is decreased, limits this approach.

2.5.2 Application of layered beds for improving the bed capacity utilization

In some applications, layered beds with adsorbent particles with different equilibrium or kinetic properties have been used to improve bed capacity utilization. In gas phase applications

such as hydrogen separation from multicomponent gas mixtures, adsorbents with low uptake capacities are placed at the inlet and those with higher uptake capacities follow along the bed length. This arrangement aids in sharpening the solute front and thus increase the bed capacity utilization (Jang et al., 2011; Park et al., 1998). However, in liquid phase applications there have been no studies reported on the use of layered beds with different equilibrium sorption capacities. This is due to the difficulty of regeneration and particle mixing during the backwash process. Mathews and coworkers have described a novel adsorber design that utilizes a convergent tapered configuration with adsorbent particles layered according to size or density (Figure 2.10(a)) (Mathews, 2005, 1997; Pota and Mathews, 2000). The reactor configuration and particle size variation are such that the influent fluid contacts an adsorbent bed with decreasing particle size and decreasing velocity in the direction of flow leading to decreased mass transfer resistance along the bed length. This results in a solute front that sharpens as it travels through the column (Figure 2.10(b)). In this novel configuration, particle diameters and angle of the bed can be chosen such that the minimum fluidization velocity of the upper layers are lower than the succeeding layers that follow. This type of arrangement will let the particles remain reverse stratified during backwash. Comparative studies have shown that breakthrough time can be increased by 46% to 75% for the sorption of a variety of solutes such as phenol and trichloroethylene from aqueous phase onto activated carbon using tapered beds with adsorbent layered according to kinetic properties (Mathews, 2005; Pota and Mathews, 2000). Thus, the reverse stratified tapered bed adsorber provides higher bed capacity utilization compared to the other configurations.

2.6 Process modeling of organic acid adsorption on weak base resins

In a fixed-bed adsorber, the flow conditions and mass transfer rate affect the uptake capacity throughout the column length.

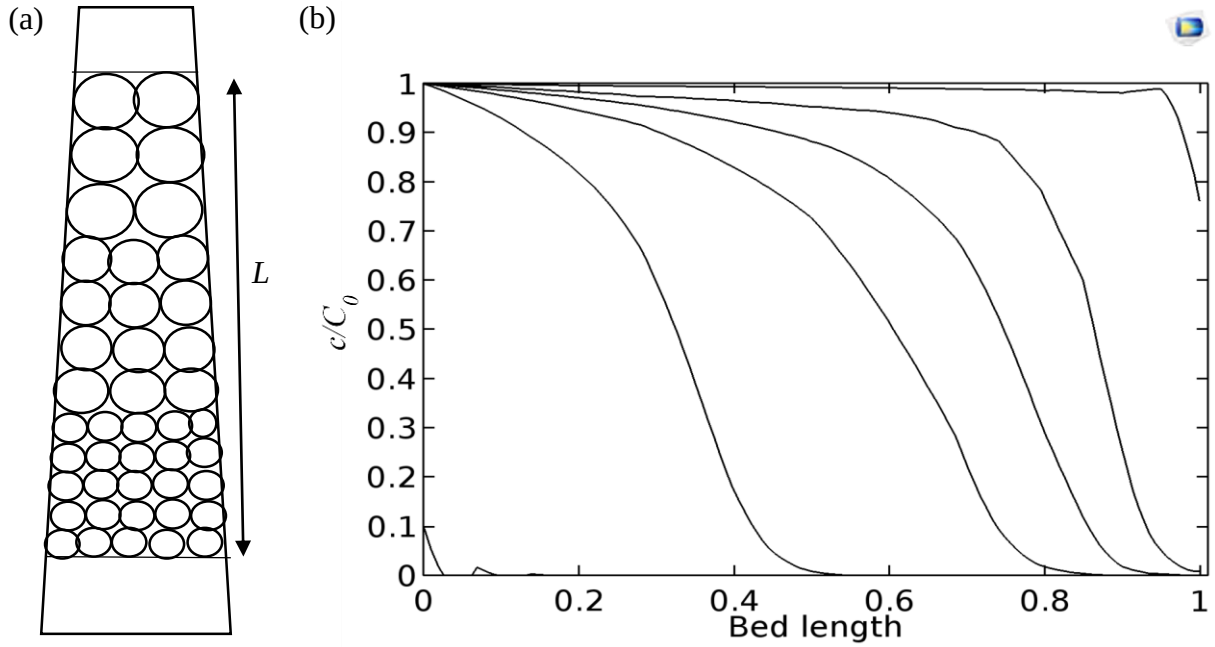

Figure 2.10: (a) Tapered adsorber with adsorbents layered according to size and (b) concentration profile along the bed length (L)

Mathematical model of a fixed-bed adsorber is useful for the design and optimization of adsorption process at different process conditions without the need for extensive experimentation. Moreover, a suitable mathematical model will also be useful to predict the concentration profile for various scenarios such as variable inlet concentration, change in particle diameter, and it can predict the concentration profile at any location along the bed length within the fixed-bed adsorber. The design and scale up of fixed-bed adsorbers need a systematic study of equilibria, kinetics, and sorption dynamics in the column.

2.6.1 Adsorption equilibrium

The accurate description of adsorption equilibrium data using appropriate isotherm equations is important for the estimation of kinetic parameters, effective simulation of adsorption dynamics in fixed-beds, and prediction of breakthrough curves. Batch experiments are usually conducted to develop isotherm models to fit the data and to establish the strength of affinity of the adsorbate to the adsorbent.

2.6.1.1 Single-component adsorption equilibrium

Adsorption equilibrium experimental data are usually fitted to Langmuir (1918), Freundlich (e.g. Foo and Hameed (2010)), linear-Freundlich (e.g. Mathews (2005); Redlich and Peterson (1959)), and Sips (1948) isotherm equations.

2.6.1.1.1 Langmuir isotherm

According to Langmuir's theory, the adsorption between gas molecules and solid or liquid surfaces depend upon the intensity of chemical forces. All the sites on a sorbent surface are assumed to have equal affinity for the adsorbate and true adsorption occurs only on a single molecular layer till the surface sites are saturated. Adsorption experiments with different gases on mica, glass, and platinum have shown that monolayer sorption occurs depending upon the pressure and the surface forces on the adsorbent (Langmuir, 1918). The Langmuir isotherm is given as follows (e.g. Bolster and Hornberger (2007)):

$$q_e = \frac{q_m K c_e}{1 + K c_e} \tag{2.17}$$

where q_e and c_e are the equilibrium sorption capacity (g/g) and solute concentration in bulk phase (g/L) respectively. The linearized forms of the isotherm equations are given as:

$$\frac{1}{q_e} = \frac{1}{q_m} + \frac{1}{q_m K c_e} \tag{2.18}$$

$$\frac{c_e}{q_e} = \frac{c_e}{q_m} + \frac{1}{q_m K} \quad (2.19)$$

2.6.1.1.2 Freundlich isotherm

This is an empirical model explained in terms of an adsorbent with heterogeneous surface with non-uniform distribution of adsorption affinities. The adsorption sites with high bonding energy are occupied first and the adsorption energy will decrease till the adsorbent reaches saturation (Foo and Hameed, 2010). This isotherm does not reduce to the Henry's law at low concentrations and lacks the fundamental thermodynamic basis. Because of the log-log transformation in the linearized form, it gives a good fit to the sorption data. The Freundlich isotherm is given as:

$$q_e = K_F {c_e}^n \quad (2.20)$$

where K_F is the Freundlich isotherm parameter (g/g)(L/g)^n. The linearized equation is given as:

$$log\ q_e\ =\ log\ K_F\ + n\ log\ c_e \quad (2.21)$$

The value of *n* ranges between 0 and 1. It is a measure of surface heterogeneity, becoming more heterogeneous as its value gets closer to zero.

2.6.1.1.3 Linear-Freundlich isotherm

Redlich and Peterson proposed an empirical isotherm for the adsorption of pentane on molecular sieves and is applied to other adsorbent-adsorbate systems as well (Redlich and Peterson, 1959). This isotherm reduces to the Freundlich isotherm at high concentrations and to the linear isotherm at low concentrations. It is called the linear-Freundlich isotherm by Mathews (2005). The isotherm is given as:

$$q_e = \frac{a c_e}{1 + b {c_e}^{\beta}} \quad (2.22)$$

where a (g/g)(L/g), b (L/g)$^{\beta}$, and β are linear-Freundlich isotherm parameters.

2.6.1.1.4 Sips isotherm

Sips developed a theoretical isotherm for the sorption of gases on heterogeneous catalytic surfaces. The active sites on these surfaces are characterized by a statistical distribution of sorption energies similar to a Gaussian distribution (Sips, 1948). At high concentrations, the isotherm reaches saturation and at low concentrations it reduces to the Freundlich isotherm. The isotherm is given as follows:

$$q_e = \frac{ac_e{}^{\gamma}}{1+bc_e{}^{\gamma}} \tag{2.23}$$

where a (g/g)(L/g)$^{\gamma}$, b (L/g)$^{\gamma}$, and γ are Sips isotherm parameters.

The traditional and most widely used approach for finding the best fitting isotherm is through linear regression of isotherm data to fit the linearized isotherm equations. Many studies reported in the literature have used linearized isotherm equations to fit the experimental data and determine the isotherm constants based on the value of coefficient of determination, r^2.

$$Coefficient\ of\ determination\ =\ 1-\frac{\sum_{i=1}^{n}(q_{e,e}-q_{e,p})^2}{\sum_{i=1}^{n}(q_{e,e}-q_{e,mean})^2} \tag{2.24}$$

where $q_{e,e}$ and $q_{e,p}$ are the experimental and predicted equilibrium concentration of solute in the solid phase of adsorbent (g/g) respectively. In such cases, the effect of linearizing the isotherms on the transformation of data and the consistency and accuracy of the obtained results are ignored. Though this method is simple, it is erroneous as the linearized isotherm equations evaluate the data on a transformed scale. Also, it is not possible to obtain the isotherm constants for a three-parameter isotherm through this method as the number of unknowns are higher than the known values we obtain from a linear fit. The inherent bias in determining adsorption isotherm constants from linearized equations has been pointed out by some researchers (Foo and Hameed, 2010; Wong et al., 2004). Foo and Hameed (2010) have stressed the importance of using proper estimating procedures to fit appropriate isotherm equations to equilibrium data

particularly in light of the growing interest in the use of adsorption as an effective purification technology in water treatment and wastewater renovation. These authors have shown that linear estimation methods generate different outcomes based on the way the isotherm equation is linearized. Wong et al. (2004) have reported that in the adsorption of acid dyes on chitosan, while the Langmuir isotherm in the linear form gave a good fit for the entire concentration range, the Freundlich isotherm gave different isotherm constants for each set of concentration range studied. However, the linear-Freundlich isotherm gave a better overall fit using the nonlinear regression method due to its ability to represent data in the low and high concentration ranges. This led to the conclusion that least squares minimization procedures to fit data with non-linearized isotherm equations leads to better outcomes than the use of linearized isotherm equations. An iterative procedure targeted to minimize the average relative error (ARE) between the experimental and predicted adsorbed phase concentration values can be implemented. The ARE is defined as:

$$Average\ relative\ error = \sum_{i=1}^{n} \left| \frac{q_{e,e} - q_{e,p}}{q_{e,e}} \right| * \frac{100}{n} \tag{2.25}$$

where *n* is the number of experimental data points. The isotherm constants are obtained by minimizing target error value using an iterative procedure and initial estimates of the isotherm constants.

2.6.1.2 Multicomponent adsorption equilibria

The multicomponent Langmuir isotherm model is simple and commonly used to predict multicomponent equilibrium data. It is also known as the extended Langmuir isotherm model. It depends on the parameters obtained from the single component system and is given as:

$$q_{ei} = \frac{q_{mi} K_i c_{ei}}{1 + \sum_j^k K_j c_{ej}} \tag{2.26}$$

Several studies on multicomponent sorption equilibria have been conducted using this model for fitting the experimental data instead of predicting the isotherms. Jiao et al., (2015) studied the adsorption dynamics of acetone, butanol, and ethanol on a polystyrene diethylbenzene resin in fixed-bed adsorbers. The single component isotherm data for the sorption of butanol on this resin proved to give high uptake capacity for butanol. However, the single component isotherms for the other components was not studied. Hence, in the multicomponent sorption study, the experimental data was fitted with the Equation (2.26) to obtain the isotherm parameters. Zhou et al., (2013) studied the multicomponent sorption dynamics of ethanol, glucose, glycerol, and acetic acid on a polystyrene-DVB resin. Single- and multi-component equilibrium studies were conducted. However, the isotherm constants obtained from the single component isotherm data were not utilized to predict the isotherm parameters for Equation (2.26). In these cases, the new isotherm constants obtained are different from the single component isotherm constants.

Another modification of this equation is the use of interaction term, η_i, to improve the fit for multicomponent adsorption equilibrium. This equation adjusts the single solute isotherm constants such that they give a good fit for the multicomponent systems.

$$q_{ei} = \frac{\left(q_{mi}K_i c_{ei}/\eta_i\right)}{1+\sum_j^k\left(K_j c_{ej}/\eta_j\right)} \tag{2.27}$$

Lee et al., (2004) developed a simulated moving bed process for the recovery of lactic acid from fermentation broth. In their study, the adsorption equilibria of lactic acid and acetic acid was determined using a dual-site Langmuir isotherm model.

$$q_{ei} = H_i c_{ei} + \frac{(a_i c_{ei})}{1+\sum_j^k(b_j c_{ej})} \tag{2.28}$$

where *H* (g/g)(L/g), *a* (g/g)(L/g), and *b* (L/g) are dual-site Langmuir isotherm parameters. Multiple frontal tests were conducted to determine the isotherm parameters for the single-

component adsorption of acetic and lactic acids on a PVP resin. The modified Langmuir isotherm, i.e., the dual-site Langmuir isotherm model provided a better prediction especially at low concentrations for the multicomponent experimental data compared to the extended Langmuir isotherm model. Song et al., (2017) studied the adsorption equilibria of lactic acid, acetic acid, and glucose on polystyrene-DVB resin. They have used the dual-site Langmuir isotherm model, given in Equation (2.28), to obtain the multicomponent equilibria. However, instead of using the single component isotherm constants to predict the multicomponent adsorption equilibria, they have fit the experimental data with the dual-site Langmuir isotherm equation. Thus, this model might not be good for predicting the multicomponent equilibria at concentrations outside the range used in their experiments. Also, at low concentrations, this isotherm will not reduce to linear isotherm. Thermodynamic consistency requires all isotherms to reduce to the linear isotherm or the Gibbs isotherm at low concentrations.

Myers and Prausnitz (1965) proposed the ideal adsorption solution theory (IAST) for gas mixtures in order to predict multicomponent equilibria using the single component isotherm data. This theory assumes that the adsorbed phase is ideal. The concentration of solute in the liquid phase in equilibrium with the solid phase, *c*, is given by the product of its mole fraction in the adsorbed phase, *x*, and the equilibrium concentration, c_i^0 (π), corresponding to the solution temperature and spreading pressure, π, for adsorption of pure component, *i*.

$$C * y_i = c_i^0(\pi) * x_i \tag{2.29}$$

The difference in surface tension between a clean surface and a surface covered with a solute *i* in a pure component solution is given by spreading pressure, π, as given below:

$$\frac{\pi_i * A}{R * T} = \int_0^{c_i^0} \mathrm{q}_i^0(c_i) * \frac{dc_i}{c_i} \tag{2.30}$$

where *A*, *R*, and *T* are the specific area of adsorbent (cm^2/g), gas constant (L atm)/(mol K), and temperature (*K*), respectively. Using the assumptions as: (1) the adsorbed phase forms an ideal solution, and (2) the available surface area is same for all solutes in a multicomponent system, the spreading pressure of each solute in a binary system with component *i*, *j* is given by:

$$\pi_i = \pi_j \tag{2.31}$$

If the single component isotherms can be represented by the Langmuir isotherm, above equation simplifies to,

$$q_{mi} * ln\left(1 + K_i\left(\frac{C*y_i}{x_i}\right)\right) = q_{mj} * ln\left(1 + K_j\left(\frac{C*y_j}{x_j}\right)\right) \tag{2.32}$$

Using the values of x_i and x_j, we can obtain the adsorbed phase concentration for each component q_i and q_j in the multicomponent solutions as shown below:

$$\frac{1}{q_T} = \frac{x_i}{q_i^0} + \frac{x_j}{q_j^0} \tag{2.33}$$

$$q_i = x_i * q_T \tag{2.34}$$

$$q_j = x_j * q_T \tag{2.35}$$

The accuracy of prediction of multicomponent sorption equilibria using IAST model depends on how well the single component data are fit to the isotherms, especially at low and high concentration ranges. Errors in single component isotherm prediction can cause a large error in multicomponent isotherm predictions (Walton and Sholl, 2015). Oudshoorn et al., (2009) studied the sorption equilibria for unary, binary, ternary, and higher-order mixtures of various components for the recovery of butanol from fermentation broth. They have compared the extended Langmuir isotherm, Equation (2.26), and IAST model for predicting multicomponent adsorption equilibria. IAST model gave good predictions at all the concentration ranges whereas the extended Langmuir isotherm predicted high deviations in the multicomponent equilibria at

low equilibrium concentrations. Eom et al., (2013) also conducted a similar study to evaluate the adsorption equilibria of butanol, ethanol, acetone, acetic acid, and butyric acid present in the fermentation broth. IAST model was found to be more accurate for predicting the multicomponent equilibria over the entire concentration range compared to the extended Langmuir isotherm. IAST can provide a more accurate representation of multicomponent equilibria data subject to the limitations of the assumptions therein and provide for a better description of sorption systems for fermentation product recovery and other applications involving multicomponent systems.

Several researchers have used Real Adsorption Solution Theory (RAST) model to predict multicomponent sorption equilibria when the adsorbed solutes exhibit nonideal behavior. The IAST equations are modified to include activity coefficient, γ

$$c * y_i = c_i^0(\pi) * \gamma_i * x_i \tag{2.36}$$

$$ln(\gamma_i) = f(T, \pi, \bar{x}) \tag{2.37}$$

$$\frac{1}{q_T} = \sum_{i=1}^{n} \frac{x_i}{q_i^0} + \sum_{i=1}^{n} x_i \left(\frac{\partial ln\gamma_i}{\partial \left(\frac{\pi_i * A}{R * T} \right)} \right) \tag{2.38}$$

The activity coefficient, γ, values are obtained from binary adsorption equilibria data using an iterative calculation procedure with models such as Wilson equation (e.g. Erto et al. (2012)), Nonrandom two-liquid (NRTL) (e.g. Sochard et al. (2010)), Margules equation (e.g. Zhang and Wang (2017)), or UNIversal QUAsi Chemical (UNIQUAC) (e.g. Sochard et al. (2010)) as starting values for γ. This model is then used to predict multicomponent adsorption equilibria of ternary and higher-order mixtures.

Sochard et al., (2010) used RAST model to determine the binary adsorption equilibria of VOCs namely methyl-ethyl-ketone (MEK) and isopropylanol on GAC, where increasing

concentration of MEK led to nonideality of the mixture. UNIQUAC and NRTL models were used to determine the activity coefficients of the adsorbed phase. The UNIQUAC model failed to adequately represent binary equilibria for different mixture compositions, whereas NRTL model gave good results. Erto et al., (2012) compared the RAST and Predictive Real Adsorbed Solution Theory (PRAST) models to determine the competitive adsorption equilibria of tetrachloroethylene and trichloroethylene (PCE and TCE) mixtures on GAC. In the PRAST model, the γ values at infinite dilution are determined from pure component isotherm data and used to predict binary adsorption equilibria. However, due to the dependence of γ on spreading pressure, the PRAST model was not able to predict the binary adsorption equilibria well. They have concluded that for accurate predictions of γ values, binary adsorption equilibria data is essential. Jadhav and Srivastava (2013) used IAST and RAST models to determine the binary adsorption equilibria of wastewater contaminants such as nitrobenzene, aniline, and phenol on GAC. At higher concentration levels in the solution, binary mixtures showed nonideal behavior and RAST model gave good prediction compared to IAST model. Zhang and Wang (2017) applied IAST, RAST, and segregated IAST (SIAST), that uses site energy distribution, and multisolute dual-site Langmuir models to predict bisolute adsorption equilibria of organic compounds on GAC. RAST model combined with an empirical four parameter model, to determine γ, was found to be more accurate in determining the bisolute sorption equilibria compared to other models.

The activity coefficient, γ, varies with temperature, adsorption capacity, and spreading pressure. Accurate information on bisolute adsorption equilibria is necessary to determine γ for different experimental conditions. The literature on multicomponent adsorption equilibria is much smaller compared to the reported number of pure component isotherms (Walton and Sholl,

2015). The reliable prediction of multicomponent adsorption equilibria for a diverse range of mixtures remains challenging. Hence it is necessary to develop multicomponent adsorption equilibria data and suitable models for the effective simulation of adsorption dynamics of mixtures in fixed-bed adsorbers,

2.6.2 Adsorption kinetics

The rate at which a solute molecule is transferred from the fluid phase to the solid sorbent is an important factor in the multicomponent sorption dynamics of organic acids from dilute aqueous solutions on weak base resins. The mechanistic processes involved include: (1) diffusion in the bulk phase to the boundary of the sorbent, (2) external mass transfer through the boundary layer or fluid film, (3) intraparticle diffusion of the adsorbate into the interior of the sorbent particle, and (4) adsorption (Figure 2.11). The adsorption rate is maximum in the initial time period, when the system is far from equilibrium, and the rate decreases asymptotically to zero as the system reaches equilibrium (Mathews and Weber, Jr., 1984). In most cases, the bulk phase concentration is uniform due to mixing, and the adsorption step is rapid compared to the diffusion steps.

Most widely used kinetic models are classified into reaction rate models and diffusion models based on the representation of the overall transport process of adsorbate from the bulk phase to the adsorption site on the adsorbent. The reaction rate models consider the overall transport process of adsorbate in the adsorption process as a single step and hence the equations for these models are mathematically simple. In the diffusion based models, the transport of the adsorbate through external mass transfer layer and intraparticle diffusion are represented by a set of partial differential equations (PDEs), and these may be solved analytically or numerically depending on the nature of the system and the equilibrium isotherm i.e., linear or nonlinear.

Several diffusion based kinetic models such as homogeneous solid phase diffusion model, surface diffusion model, and pore diffusion models have been used to describe adsorption kinetics in various solute-sorbent systems.

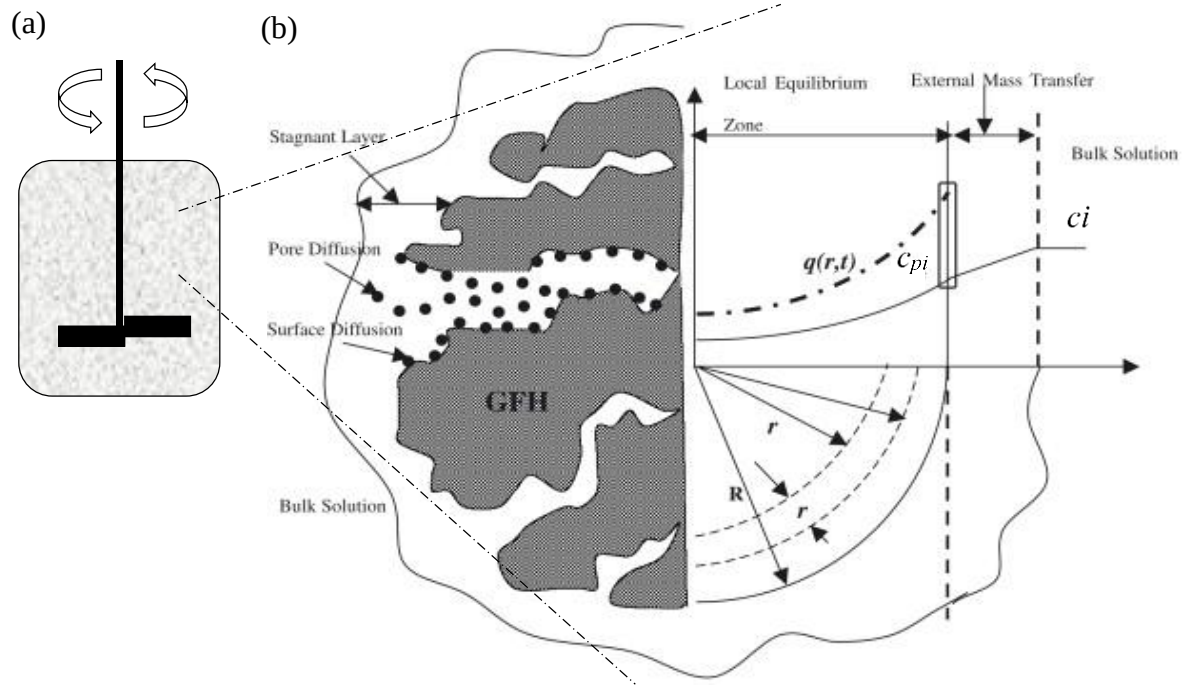

Figure 2.11: (a) Batch adsorber and (b) schematic of organic acid transport from bulk solution into weak base resin (Badruzzaman et al., 2004)

2.6.2.1 Homogeneous solid phase diffusion model

The homogeneous solid phase diffusion model considers that adsorption occurs on the outer surface of the particle and the adsorbate diffuses into the particle in the adsorbed state. Rosen (1952) provided the exact and approximate solutions to the PDEs of this model for a fixed-bed adsorber for solutes with linear isotherm. In this model, the rate of adsorption is controlled by the combined effect of external mass transfer through the film and internal solid phase diffusion. Mathews and Weber (1977, 1980) developed a finite difference approximation to this model for studying adsorption rate in batch reactors for solute and sorbent systems with

nonlinear isotherms and extended the model to study adsorption rate in multicomponent solutions.

For a typical adsorption system where both external and internal particle transport need to be considered, and the liquid phase concentration decreases as a function of time, the following PDEs need to be solved. The mass balance for the bulk phase is given by:

$$-W\frac{d\bar{q}}{dt} = V\frac{dc}{dt} \tag{2.39}$$

where W is the weight of adsorbent added to the batch reactor (g) and V is the volume of solution in batch reactor (L). The solute transport within the solid phase of a particle with radius r_p is given by:

$$\frac{\partial q}{\partial t} = D_s\left(\frac{\partial^2 q}{\partial r^2} + \frac{2}{r}\frac{\partial q}{\partial r}\right) \tag{2.40}$$

where D_s is the solid phase diffusion coefficient of solute in the sorbent (cm^2/sec). The mass transfer from the fluid phase to the solid surface of the particle is expressed as rate change of average solute concentration of the particle as:

$$\frac{d\bar{q}}{dt} = \frac{k_f A_p}{V_p \rho_p}(c - c_s) \tag{2.41}$$

where k_f is the external mass transfer coefficient (cm/sec), A_p is the area per unit volume of adsorbent particle (cm^{-1}), V_p is the volume of adsorbent particle (cm^2), ρ_p is the density of the adsorbent (g/L), and c_s is the concentration of solute on the surface of adsorbent particle (g/L). The average solute concentration in the particle is obtained by:

$$\bar{q} = \frac{3}{R^3}\int_0^R q_i r^2 dr \tag{2.42}$$

The adsorption equilibrium at the external surface of the particle is given by:

$$q_s = f(c_s) \tag{2.43}$$

Following are the initial and boundary conditions for the above equations:

$$c(0) = c_0 \tag{2.44}$$

$$\bar{q}(r, 0) = 0 \tag{2.45}$$

$$q(R, t) = q_s(t) \tag{2.46}$$

$$\frac{\partial q}{\partial r}(0, t) = 0 \tag{2.47}$$

Mathews and Weber (1980) extended this model to describe kinetics of multicomponent adsorption. The multicomponent sorption equilibria was described using:

$$q_{si} = \frac{a_i\left(c_{si}/\eta_i\right)}{\sum_i^k\left(1+b_j\left(c_{sj}/\eta_j\right)^{\beta_j}\right)} \tag{2.48}$$

Adsorption kinetics of phenol, p-bromophenol, p-toulene sulfonate, and dodecyl benzene sulfonate on GAC was studied. This model gave good predictions for solutes with comparable diffusion rates and for other solutes, solute-solute interactions affected the diffusional flows. Mathews and Weber (1984, 1977) used the numerical method to estimate the external mass transfer coefficient and intraparticle diffusivity simultaneously through parameter estimation procedures. Mathews and Zayas (1989) and Mathews and Weber (1984) have shown that the intraparticle diffusivities estimated in this manner are invariant with sorbent particle diameter and the initial solute concentration used in batch sorption experiments. However, this procedure requires repeated iterative solutions of the PDEs for different parameter values for convergence such that the sum of the squares of the relative error between experimental and predicted data is minimum.

2.6.2.2 Pore diffusion model

The most commonly used weak base resins are either macroporous or gel based, and they are considered as microgels connected with a network of pores. The pore diffusion model considers that the adsorption kinetics is controlled by external mass transport through the film

and internal diffusion in the pore. The adsorbate diffuses into the pores in fluid phase and adsorbs in the internal surfaces of the adsorbent (Mathews and Weber, Jr., 1984). The pore diffusion model was used to determine the adsorption rate kinetics in many studies on adsorption of organic acids on weak base resins (Jiao et al., 2015; Lin et al., 2017; Song et al., 2017). The mathematical model for adsorption kinetics in a batch reactor with multicomponent solution using the pore diffusion model is given by the equations listed below. The mass balance in the bulk phase for a single component *i* in a multicomponent solution of *k* components is given by equation:

$$V\frac{\partial c_i}{\partial t} + \frac{3Wk_{fi}}{\rho_p r_p}\left(c_i - c_{pi,r=r_p}\right) = 0 \tag{2.49}$$

where c_p is the concentration of solute in pore phase (g/L). The initial condition for this equation is given as:

$$c_i(0) = c_{0_i} \tag{2.50}$$

The mass balance for the concentration of solute *i* in the solid phase of the particle with radius r_p is given by:

$$\varepsilon_p\frac{\partial c_{pi}}{\partial t} + \rho_p\frac{\partial q_{pi}}{\partial t} = \varepsilon_p D_{pi}\frac{1}{r^2}\frac{\partial}{\partial r}\left(r^2\frac{\partial c_{pi}}{\partial r}\right) \tag{2.51}$$

where D_p is the pore diffusion coefficient (cm^2/sec). The initial and boundary conditions for this equation are given by:

$$c_{pi}(r,0) = 0 \tag{2.52}$$

$$q_{pi}(r,0) = 0 \tag{2.53}$$

$$\frac{\partial c_{pi}}{\partial r}(0,t) = 0 \tag{2.54}$$

$$\frac{\partial q_{pi}}{\partial r}(0,t) = 0 \tag{2.55}$$

$$\varepsilon_p D_{pi} \frac{\partial c_{pi}}{\partial r}\left(r_p, t\right) = k_{fi}\left(c_i - c_{pi,r=r_p}\right) \tag{2.56}$$

The isotherm equation is used to represent the amount adsorbed in the solid phase in equilibrium with the pore fluid. The Langmuir isotherm equation for a solute *i* in a multicomponent solution with *k* solutes is given by,

$$q_{pi} = \frac{q_{mi} K_i c_{pi}}{1+\sum_j^k K_j c_{pj}} \tag{2.57}$$

Jiao et al., (2015) used this model to study the multicomponent sorption dynamics of acetone, butanol, and ethanol on a polystyrene resin in fixed-bed adsorber. The external mass transfer coefficient, k_f, was determined using the Wilson and Geankoplis (1966) correlation:

$$k_{fi} = \frac{1.09}{\varepsilon_b}\frac{D_{mi}}{d_p}\left(\frac{v d_p}{D_{mi}}\right)^{1/3} \tag{2.58}$$

The pore diffusion coefficient was determined using the Mackie-Meares (1955) correlation:

$$D_{pi} = \frac{\varepsilon_p}{\left(2-\varepsilon_p\right)^2} D_{mi} \tag{2.59}$$

Using the values obtained from the correlations, the model gave good predictions for the experimental data. Lin et al., (2017b) used this model to study the adsorption kinetics of levulinic acid on a hyper-cross-linked microporous resin. Pore diffusion was found to be rate controlling in the adsorption process and thus this model was modified in order to exclude the effect of external mass transfer coefficient. The pore diffusion coefficient was obtained by fitting the experimental data to the model equations. The model provided a good fit to the experimental data. The authors reported that the pore diffusion coefficient obtained from fitting was ~0.35 times that of the free liquid diffusion coefficient of levulinic acid. Song et al., (2017) used this model to study the adsorption dynamics of lactic acid, acetic acid, and glucose on a hyper-cross-linked polystyrene-DVB resin. The external mass transfer coefficient and pore diffusion coefficient were determined using the Wilson-Geankoplis (1966) and the Mackie-Meares (1955)

correlations respectively. This model gave predictions in good agreement with the experimental data.

2.6.2.3 Pore and surface diffusion model

Ma et al., (2004) classified the adsorbates in to low- and high-affinity adsorbates based on their adsorption capacities. In case of low-affinity adsorbates, intraparticle diffusion is dominated by pore diffusion alone. However, in high-affinity adsorbates due to their high uptake capacities, the surface concentration can be higher than the pore concentration by several orders of magnitude. Although the surface diffusion coefficient is smaller than the pore diffusion coefficient by one or two orders of magnitude, the surface diffusion flux will be greater than the pore diffusion flux. In such cases, a pore diffusion model would estimate the intraparticle diffusion coefficient to be higher than the free liquid diffusion coefficient and dependent on solute concentration. Yoshida et al., (1994) explained that in case of protein adsorption on ion exchange resins, parallel pore and surface diffusion mechanisms control the adsorption rate. On the other hand, in the adsorption based on affinity chromatography, surface diffusion was considered negligible due to the strong interaction between the ligand and the adsorbate. Several researchers have developed the numerical formulations for parallel pore and surface diffusion model to determine the adsorption dynamics in fixed-bed adsorbers (Koh et al., 1998; Ma Z. et al., 2004).

Yoshida et al., (1994) developed a finite difference scheme to determine the pore and surface diffusion coefficients for batch adsorption kinetic study. In this model, first the effective diffusion coefficient, D_{eff}, based on the homogeneous Fickian diffusion mechanism is determined.

$$\frac{\partial Q}{\partial t} = \frac{D_{eff}}{r^2}\frac{\partial}{\partial r}\left(r^2\frac{\partial Q}{\partial r}\right) \tag{2.60}$$

Yoshida et al. (1994), defined Q as the sum of the concentration of adsorbate in the pore solution and that adsorbed in the internal pore walls.

$$Q = q + \varepsilon_p c_p \tag{2.61}$$

The initial and boundary conditions are given by:

$$t = 0, Q = 0 \tag{2.62}$$

$$r = 0, \frac{\partial Q}{\partial r} = 0 \tag{2.63}$$

$$r = r_p, Q = Q_0 \tag{2.64}$$

The estimated effective diffusion coefficient was found to be dependent on initial solute concentration and the protein adsorption in their study was found to be controlled by pore and surface diffusion occurring in parallel.

For a model with pore and surface diffusion occurring in parallel, the equation for the particle phase is given by:

$$\varepsilon_p \frac{\partial c_p}{\partial t} + \frac{\partial q}{\partial t} = \frac{D_p}{r^2} \varepsilon_p \frac{\partial}{\partial r}\left(r^2 \frac{\partial c_p}{\partial r}\right) + \frac{D_s}{r^2} \varepsilon_p \frac{\partial}{\partial r}\left(r^2 \frac{\partial q}{\partial r}\right) \tag{2.65}$$

where D_s is the surface diffusion coefficient (cm^2/sec). The equilibrium between the bulk phase concentration and the adsorbed concentration is given by any isotherm.

$$q = f(c_p) \tag{2.66}$$

The initial and boundary conditions are given by:

$$t = 0, c_p = 0, q = 0 \tag{2.67}$$

$$r = 0, \frac{\partial c_p}{\partial r} = 0, \frac{\partial q}{\partial r} = 0 \tag{2.68}$$

$$r = r_p, c_p = c_0, q = q_0 \tag{2.69}$$

A numerical solution was developed to determine the pore and surface diffusion coefficients and the predicted model was compared against pure pore diffusion control and surface diffusion

control models. The parallel pore and surface diffusion model gave a better prediction for the experimental data.

2.6.2.4 Adsorption rate models

The complexities involved in modeling and solution of the PDEs has prompted the development and use of several simpler adsorption rate models. Simplistic models have been developed to describe the adsorption rate by a single equation with little consideration of the transport processes involved as noted in the diffusion models of the subsections 2.6.2.1, 2.6.2.2, 2.6.2.3.

The so-called pseudo-first-order rate equation attributed to Lagergren (Equation (2.70)) assumes that the adsorption rate is proportional to the number of available sites on the adsorbent and independent of the sorbate concentration. This equation has been used particularly by many researches in South Asia and Southeast Asia (Ho, 2004) to describe adsorption kinetics regardless of whether the rate is controlled by surface reaction or mass transfer. The use of this equation for typical mass transfer controlled systems is problematic when no attempt is made to correlate k_1 with solute transport properties. Ho and McKay (1999) describe a "pseudo-second-order" rate equation to model the adsorption rate of copper (Cu^{2+}) ions on peat (Equation (2.71)).

$$\frac{dq}{dt} = k_1(q_e - q) \tag{2.70}$$

$$\frac{dq}{dt} = k_2(q_e - q)^2 \tag{2.71}$$

where k_1 and k_2 are pseudo-first- $(sec)^{-1}$ and pseudo-second-order $(g/g)(sec)^{-1}$ rate model coefficients. This model assumes that reaction rate is independent of the sorbate concentration, and that the exchange reaction of one Cu^{2+} ion occurs with two sorption sites. The rate of adsorption as shown in by Equation (2.71) is proportional to the square of the sorption sites remaining. The validity of this equation for systems that are mass transfer controlled or where

adsorption is reversible is questionable. Several researchers (e.g., Abdullah et al. (2009), Moldes et al. (2003), Wu et al. (2009)) have used these equations to analyze adsorption rates in diffusion controlled systems due to the simplicity of determining the adsorption rate constants k_1 and k_2 form the linearized equations (Equations (2.72) and (2.73)).

$$log(q_e - q_t) = logq_e - \left(\frac{k_1 t}{2.303}\right) \tag{2.72}$$

$$\frac{t}{q_t} = \frac{1}{k_2 q_e^2} + \frac{t}{q_e} \tag{2.73}$$

The estimated rate constants from fitting the data with linear plots are not consistent and vary with initial concentration of the solute (Ho and McKay, 1999). The estimated rate constants have not been validated in the reported studies with predictive capabilities for batch systems under different experimental conditions or for fixed-bed sorption systems.

Simonin (2016) critically evaluated the abilities of the pseudo-first-order and the pseudo-second-order rate expressions to represent adsorption kinetics by examining several batch kinetic data in the literature where either the pseudo-first-order or the pseudo-second order equation was reported to give a good fit. It was found that neither of the equations gave a good fit in ~31% of the data sets, and the rate equations cannot give a good fit in cases where intraparticle diffusion is controlling. In addition, the goodness of fit for these equations is determined based on the value of r^2. In several studies, most experimental data are taken from the sampling time near equilibrium, and hence as t increases, t/q increases linearly with t. This results in a skewed straight line fit with r^2 close to one. In the case of the pseudo-first-order rate equation, the accuracy of the linear fit decreases as q gets close to q_e and $ln\ (q_e\text{-}q)$ becomes uncertain.

Thomas (1944) proposed a second order rate law to determine the kinetics of cation exchange in zeolites with specific application to water softening. This model considers that the exchange process in the particle is rate controlling when compared to the diffusion processes

either in the solution or in the zeolite particles. In a fixed-bed adsorber of zeolite when a solution containing cations at initial concentration of c_0 is passed, the net rate of exchange of ions into the zeolite is given by:

$$\frac{\partial p}{\partial t} = k_1(a-p)c - k_2 p(c_0 - c) \tag{2.74}$$

At equilibrium this equation reduces to the Langmuir isotherm equation. The mathematical solution to this model is applicable to any solid substance capable of exchanging ions with the solution.

Roginsky and Zeldovich (e.g. McLintock (1967)) proposed a simple rate equation, called the Elovich equation, which is frequently applied to determine adsorption kinetics. The Elovich equation is given by:

$$\frac{dq}{dt} = ae^{-\alpha q} \tag{2.75}$$

The parameters a $(sec)^{-1}$and α are determined using the integrated form as:

$$q = \frac{2.3}{\alpha} log(t + t_0) - \frac{2.3}{\alpha} log\, t_0 \tag{2.76}$$

where t_0 is given as:

$$t_0 = \frac{1}{a\alpha} \tag{2.77}$$

A value of t_0 is chosen and the experimental data is linearized to fit the Equation (2.76). The slope of the plot gives α and the value of a is obtained from Equation (2.77). This Elovich equation does not apply to the initial part of the uptake curve where external mass transfer is controlling. Several studies have imposed this equation on the entire uptake curve data to determine the rate parameters. McLintock (1967) explained that this method is correct only when the determined values of α and a can reproduce the experimental data. This validation has been

seldom conducted in the published research and the determined values do not always reproduce experimental data.

Another simple method for modeling adsorption rates is the "square root equation" approach wherein the adsorbed quantity is plotted against the square root of time to obtain a linear plot (e.g., Weber Jr and Morris (1963)). This simple correlation is given by the equation:

$$q = k_d\sqrt{t} + C \tag{2.78}$$

where k_d is the intraparticle diffusion rate constant (g/g)(sec)$^{-1/2}$. This empirical equation conceptually stems from the approximation for the initial time region to the analytical solution to the diffusion equations for intraparticle diffusion controlled adsorption with constant surface concentration (Crank, 1975; Ruthven, 1984).

$$\frac{m_t}{m_\infty} = 6\left(\frac{D_c t}{r_c^2}\right)^{\frac{1}{2}}\left[\frac{1}{\sqrt{\pi}} + 2\sum_{n=1}^{\infty} i\,erfc\left(\frac{nr_c}{\sqrt{D_c t}}\right)\right] - 3\frac{D_c t}{r_c^2} \tag{2.79}$$

where m_t/m_∞ is the fractional uptake of the solute by the sorbent and D_c is the intraparticle diffusion coefficient (cm^2/sec). This equation reduces to the following equation in the initial time region when $m_t/m_\infty \leq 0.3$.

$$\frac{m_t}{m_\infty} \approx \frac{6}{\sqrt{\pi}}\left(\frac{D_c t}{r_c^2}\right)^{\frac{1}{2}} \tag{2.80}$$

The constant C has been arbitrarily described by some authors to represent external mass transfer resistance, with larger values indicating higher boundary layer thickness (e.g., Ahmad and Rahman (2011), Shi et al. (2013)). A critical analysis of this approach has been provided by Schwaab et al. (2017), who indicate that this analysis is only valid under very restrictive conditions of adsorption in a semi-infinite solid and constant liquid phase concentration, or for batch adsorption where external mass transfer is rapid, and the sorption isotherm is linear.

2.6.2.5 Micropore diffusion control model-analytical solution

A simpler method that does not require the computation intensive numerical solution of PDEs is presented in this subsection. In the initial time period, the rate of solute uptake by the sorbent is controlled essentially by the external mass transfer resistance. For large values of power input or high intensity mixing, intraparticle diffusion becomes controlling.

At longer times, the concentration versus time profile becomes nonlinear due to the intraparticle diffusion resistance. In a batch reactor with isothermal single component sorption and micropore diffusion control, the transport of adsorbate in the solid phase of a spherical particle and constant intraparticle diffusivity is given by:

$$\frac{\partial q}{\partial t} = D_c \left(\frac{\partial^2 q}{\partial r^2} + \frac{2}{r} \frac{\partial q}{\partial r} \right) \tag{2.81}$$

In the case of an infinite bath system when the sorbate concentration in the bulk phase remains constant, the following initial and boundary conditions apply:

$$q(r, 0) = q_0' \tag{2.82}$$

$$q(r_c, t) = q_0 \tag{2.83}$$

$$\left(\frac{\partial q}{\partial r} \right)_{r=0} = 0 \tag{2.84}$$

The solution to the above equations in terms of uptake of solute by the sorbent is given as (Ruthven, 1984):

$$\frac{\bar{q} - q_0'}{q_0 - q_0'} = \frac{m_t}{m_\infty} = 1 - \frac{6}{\pi^2} \sum_{n=1}^{\infty} \frac{1}{n^2} exp^{\left(-\frac{n^2 \pi^2 D_c t}{r_c^2} \right)} \tag{2.85}$$

In the long time region, at an uptake of greater than ~ 70%, Equation (2.85) reduces to

$$1 - \frac{m_t}{m_\infty} \approx \frac{6}{\pi^2} exp^{\left(-\frac{\pi^2 D_c t}{r_c^2} \right)} \tag{2.86}$$

A plot of $ln\ (1-m_t/m_\infty)$ versus t will give a straight line with slope $-\pi^2 D_c / r_c^2$ and intercept $ln\ (6/\pi^2)$. In the case of a finite bath system where the surface concentration varies with time, the

above equations can be used if the fraction of sorbent ultimately adsorbed by the sorbent, α (Equation (2.87)) is approximately < 0.1.

$$\alpha = \frac{C_0 - C_\infty}{C_0} \tag{2.87}$$

For $\alpha > 0.1$, the intraparticle diffusivity can be determined from Equations (2.88) and (2.89) proposed by Crank (1975).

$$\frac{m_t}{m_\infty} = 1 - 6\sum_{n=1}^{\infty} \frac{exp\left(-\frac{p_n^2 D_c t}{r_c^2}\right)}{\frac{9\alpha}{(1-\alpha)} + (1-\alpha)p_n^2} \tag{2.88}$$

The value of p_n is given by the nonzero roots of the equation below:

$$tan\, p_n = \frac{3p_n}{3 + \left(\frac{1}{\alpha} - 1\right)p_n^2} \tag{2.89}$$

This method of estimating intraparticle diffusivity for finite bath systems is simpler and does not require numerical solution of the diffusion equations. Li and SenGupta (2000) used this model to study the intraparticle diffusion of ionic pentachlorophenol (PCP) in gel and macroporous anion exchange resins. In batch uptake studies and at high stirrer speeds, the uptake rate remained independent of the stirrer speed. This indicated that the external film diffusional resistance is negligible. The intraparticle diffusion coefficients obtained using this model were found to be independent of concentration and particle sizes. For particle sizes of 0.4 ± 0.04 mm and 0.6 ± 0.06 mm, the intraparticle diffusion coefficient were obtained in the range 9.3-9.5*10^{-11} cm^2/sec. The free liquid diffusivity for PCP obtained from the Wilke-Chang (1955) correlation was 4.7*10^{-6} cm^2/sec.

2.6.2.6 Determination of the rate limiting step

The accurate determination of rate parameters and the controlling mechanism is important for the effective application of adsorption processes for various applications (Mathews and Weber, Jr., 1977). In the literature, several dimensionless numbers such as the Biot number

and the Delta factor have been used to determine the rate limiting or the rate-controlling step (Jiao et al., 2015; Kumar et al., 2014). The Delta factor was used to determine the governing resistance in the adsorption of protein on ion exchange resins in preparative scale chromatography. The Delta factor is given by:

$$\delta = \frac{1}{5}\frac{k_f r_p C_0}{D_c q_0} \tag{2.90}$$

In the case of protein adsorption, due to their larger molecular sizes, ion exchange resins with relatively larger pore sizes (≥500 A^o) are used to increase accessibility of binding sites to proteins and to improve their uptake capacities and kinetics. Adsorption is controlled by external mass transfer for $\delta < 1$, intraparticle diffusion for $\delta > 1$, and by both for $\delta \sim 1$. The Biot number is widely used to establish the rate limiting step in the adsorption of organic compounds on activated carbon and resins (Jiao et al., 2015; Mathews, 2005). It is defined as the ratio of maximum flux from the external bulk phase diffusion to the maximum flux from the intraparticle diffusion. It is given by the following equation (Poulopoulos and Inglezakis, 2006; SenGupta, 2017):

$$Bi = \frac{k_f r_p C_0}{D_c q_0} \tag{2.91}$$

Adsorption is controlled by external mass transfer for $Bi < 0.5$, intraparticle diffusion for $Bi > 30$, and by both for $0.5 < Bi < 30$.

2.6.3 Fixed bed adsorption dynamics

A detailed study of adsorption dynamics in fixed-bed adsorbers is useful to plan the scope of pilot scale studies, interpret their results, scale-up, and estimate the cost for industrial scale units (Hand et al., 1983). Several diffusion-based kinetic models (refer to subsection 2.6.2.1, 2.6.2.2, 2.6.2.3) can be simply extended by including the mass transfer effects along the length of fixed-bed adsorber (Figure 2.12). Mathews and coworkers used the homogeneous solid phase

diffusion model to study the adsorption dynamics of solutes in fixed-bed adsorbers with different particle stratifications and bed geometries (Mathews, 2005; Pota and Mathews, 1999). Ma et al., (2004) developed a parallel pore and surface diffusion model to study multicomponent adsorption dynamics in fixed-bed systems. Of all these models, the linear driving force and general rate models have been widely used for studying adsorption dynamics in fixed-bed adsorbers in the product recovery from bioconversion methods.

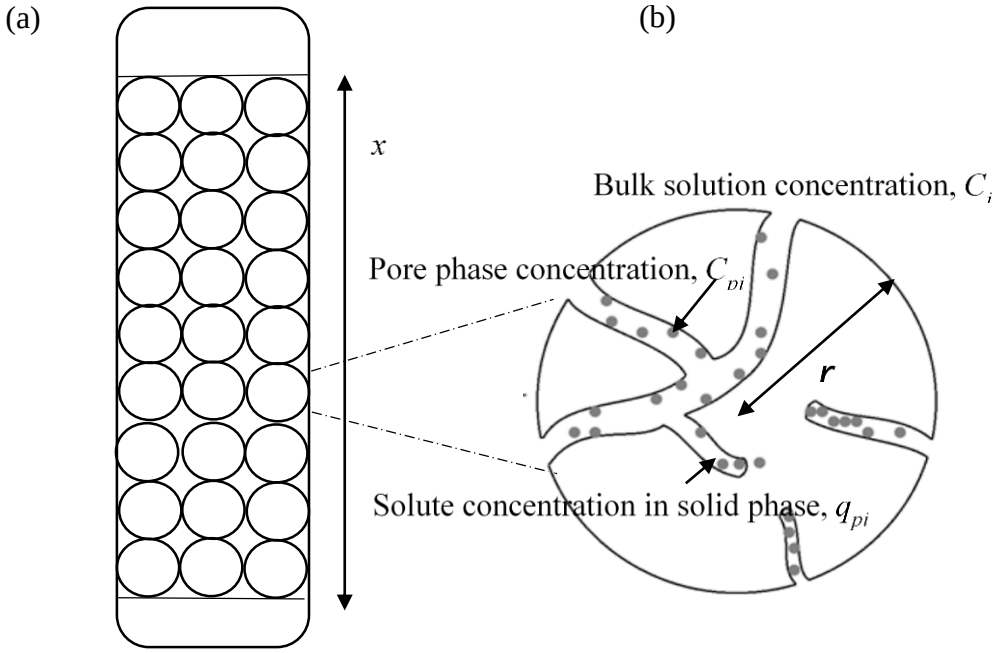

Figure 2.12: (a) Conventional cylindrical fixed-bed adsorber and (b) schematic of organic acid transport from bulk solution into weak base resin in a fixed-bed adsorber

2.6.3.1 Linear driving force model

The linear driving force (LDF) model is widely used for studying fixed-bed adsorption dynamics because it is simple, physically consistent, and can be solved either analytically or numerically (Sircar and Hufton, 2000). This model eliminates the mass balance in the solid phase increasing its flexibility for application in process design (Li and Yang, 1999). LDF model has

been used to fit and predict breakthrough curves in many gas and multicomponent liquid phase adsorption systems (Aguilera and Gutiérrez Ortiz, 2016; Zhou et al., 2013).

Linear driving force model relates the uptake rate in the particle phase to the difference between the average concentration of solute in the particle and the equilibrium concentration in the fluid phase. The mass balance for the solute *i* in the bulk phase with multicomponent solutes of *k* in the fixed-bed adsorber is given by:

$$-D_{Li}\frac{\partial^2 c_i}{\partial x^2} + v\frac{\partial c_i}{\partial x} + \frac{\partial c_i}{\partial t} + \rho_p\left(\frac{1-\varepsilon_b}{\varepsilon_b}\right)\frac{\partial q_i}{\partial t} = 0 \tag{2.92}$$

where D_L is the axial dispersion coefficient (cm^2/sec), v is the interstitial velocity (cm/sec), x is the distance along the bed length (cm), t is the time (sec), ρ_p is the density of the adsorbent (g/L), and ε_b is the bed porosity. The uptake rate of the solute in the particle phase is given by the rate of change in concentration of solute in the particle phase by:

$$\frac{\partial q_i}{\partial t} = K_{effi}(q_{ei} - q_i) \tag{2.93}$$

The equilibrium between the concentrations of solute *i* in the bulk phase and the particle phase is given by Langmuir isotherm as:

$$q_{ei} = \frac{q_{mi}K_i\, c_{ei}}{1 + \sum_j^k K_j\, c_{ej}} \tag{2.94}$$

The initial and boundary conditions are given by:

$$t = 0, c_i = 0, q_i = 0 \tag{2.95}$$

$$x = 0, D_{Li}\frac{\partial c_i}{\partial z} = v * (c_{z=0,i} - c_i) \tag{2.96}$$

$$x = L, \frac{\partial c_i}{\partial z} = 0 \tag{2.97}$$

In the literature, several methods have been used to determine the effective mass transfer coefficient, K_{eff}. In a study on multicomponent sorption dynamics of ethanol, glucose, glycerol, and acetic acid on a synthetic resin, K_{eff} was obtained from fitting the experimental data to the

model (Zhou et al., 2013). In another study on single component gas phase sorption dynamics, K_{eff} is named as K_G and it is obtained from a correlation given below (Aguilera and Gutiérrez Ortiz, 2016):

$$\frac{1}{K_G} = \frac{r_p q_o \rho_b}{3 k_f c_0 \varepsilon_b} + \frac{r_p^2 q_o \rho_b}{15 D_{eff} c_0 \varepsilon_b} \tag{2.98}$$

Lee et al., (2004) developed a standing wave design model considering a dual site Langmuir isotherm and a lumped mass transfer coefficient, similar to Equation (2.98), to simulate the adsorption dynamics of acetic and lactic acids. The experiments were conducted in an 8 column simulated moving bed with a synthetic solution of acetic and lactic acids at pH of 2.2 using Reillex HP resin. The external mass transfer and intraparticle diffusion coefficients were obtained using the Wilson and Geankoplis (1966) and Mackie and Meares (1955) correlations respectively. This study was shown to obtain lactic acid with 99.9% purity and a yield of > 93%.

In cases where the uptake rate is influenced by both external mass transfer and pore or surface diffusion, the effective mass transfer coefficient is given by $K_m a_p$ (Ruthven, 1984). This can be obtained from:

$$\frac{1}{K_m * a_p} = \frac{1}{k_f * a_p} + \frac{1}{(K a_p)_{pore}} \tag{2.99}$$

$$(K a_p)_{pore} = \frac{60 * D_p * \left(\frac{\partial q}{\partial c}\right)_{avg} * (1-\varepsilon_b) * \rho}{d_p^2} \tag{2.100}$$

$$\frac{1}{K_m * a_p} = \frac{1}{k_f * a_p} + \frac{1}{(K a_p)_{surface}} \tag{2.101}$$

$$(K a_p)_{surface} = \frac{60 * D_s * \left(\frac{\partial q}{\partial c}\right)_{avg} * (1-\varepsilon_b) * \rho}{d_p^2} \tag{2.102}$$

The mass transfer coefficient, k_f, is determined using the correlation below (Dwivedi and Upadhyay, 1977):

$$k_f = \frac{v}{Sc^{2/3}} * \left\{\frac{0.765}{Re^{0.82}} + \frac{0.365}{Re^{0.386}}\right\} \quad (2.103)$$

The mass transfer coefficient in this model is dependent on the particle diameter similar to a reaction rate model.

2.6.3.2 General rate model

The general rate model is commonly used to model fixed-bed adsorber dynamics in applications such as liquid chromatography and fermentation product recovery (e.g. Gluszcz et al. (2004), Gu et al. (2013). Jiao et al. (2015), Lin et al. (2017b), Song et al. (2017)). In this model, adsorption process and transport mechanism of a solute from liquid phase to the solid phase is described using axial dispersion, mass transfer resistance, and nonlinear equilibrium. This model includes two mass transfer resistances namely, external mass transfer resistance through the liquid film on the solid phase and internal mass transfer resistance governed by pore diffusion. The liquid phase mass balance equation for a solute *i* in a multicomponent solution of *k* components is given by the following equation:

$$-D_{Li}\frac{\partial^2 c_i}{\partial x^2} + v\frac{\partial c_i}{\partial x} + \frac{\partial c_i}{\partial t} + \left(\frac{1-\varepsilon_b}{\varepsilon_b}\right)\frac{3}{r_p}k_{fi}\left(c_i - c_{pi,r=rp}\right) = 0 \quad (2.104)$$

The initial condition is given by the following equation:

$$0 < x < L, t = 0: c_i = 0 \quad (2.105)$$

Due to the effect of axial dispersion in the inlet of the bed, the inlet boundary condition is given by a Danckwert-type boundary condition as follows:

$$x = 0, t > 0: D_{Li}\frac{\partial^2 c_i}{\partial x^2} = v(c_{ix=0} - c_{0i}) \quad (2.106)$$

The outlet boundary condition is given by a constant flux at the bed outlet as follows:

$$x = L, t > 0: \frac{\partial c_i}{\partial x}_{x=L} = 0 \quad (2.107)$$

The diffusion of solute molecules in the pore phase of the adsorbent through pore diffusion process is given by the following mass balance equation:

$$\varepsilon_p \frac{\partial c_{pi}}{\partial t} + \rho_p \frac{\partial q_{pi}}{\partial t} = \frac{1}{r^2}\frac{\partial}{\partial r}\left[r^2\left(\varepsilon_p D_{pi}\frac{\partial c_{pi}}{\partial r}\right)\right] \tag{2.108}$$

This equation is governed by initial and boundary conditions given below:

$$0 < r < r_p, t = 0: c_{pi} = 0, q_{pi} = 0 \tag{2.109}$$

$$r = 0, t > 0: \frac{\partial c_{pi}}{\partial r}_{r=0} = \frac{\partial q_{pi}}{\partial r}_{r=0} = 0 \tag{2.110}$$

$$r = r_p, t > 0: \varepsilon_p D_{pi}\frac{\partial c_{pi}}{\partial r}_{r=r_p} = k_{fi}\left(c_i - c_{pi,r=rp}\right) \tag{2.111}$$

The equilibrium relationship between the concentrations of solute *i* in the solid phase and the pore phase is given by the Langmuir isotherm as below:

$$q_{pi} = \frac{q_{mi}K_i\, c_{pi}}{1+\sum_j^k K_j c_{pj}} \tag{2.112}$$

Gu et al. (2013), used the general rate model for the simulation of sorption dynamics in liquid chromatographic columns. Song et al. (2017) compared three models i.e., linear driving force, transport dispersive, and general rate models for the prediction of adsorption dynamics in fixed-beds. Multicomponent solution of lactic acid, acetic acid, and glucose and a polystyrene divinylbenzene polymeric resin were used in their study. The multicomponent equilibrium data was fit to a modified Langmuir isotherm. The external mass transfer and internal pore diffusion coefficients were obtained from correlations. All the three models gave similar predictions as the multicomponent adsorption isotherms were close to linear and the general rate model gave a good prediction to the experimental data. Lin et al., (2017a) and Jiao et al., (2015) used this model to simulate the adsorption dynamics of single component and multicomponent adsorption dynamics respectively. Lin et al., (2017a) studied the adsorption dynamics of levulinic acid in a pure component solution on a hyper-crosslinked microporous resin at different experimental

conditions and the general rate model gave good predictions for all the scenarios studied. Jiao et al., (2015) studied the multicomponent sorption dynamics of acetone, butanol, and ethanol on a crosslinked polystyrene resin in a fixed-bed adsorber. In addition, the model was validated in their study by predicting the breakthrough curves for the adsorption of fermentation broth. The model provided an accurate description of adsorption dynamics for actual broth and the other components in the fermentation broth did not affect the adsorption efficiency. Gluszcz et al., (2004) fitted the breakthrough curves for the single component adsorption of citric and lactic acids on Amberlite IRA67 resin. The axial dispersion and mass transfer coefficients were obtained by fitting the data to the model equations. With an increase in temperature from 20 ^{o}C to 60 ^{o}C, the pore diffusion coefficient was found to increase by two times. This proved that the adsorption is controlled by intraparticle diffusion resistance. However, there have been no studies reported on general rate model formulations to describe adsorption dynamics in fixed-beds with particle stratification and tapered geometry.

REFERENCES

Abdehagh, N., Tezel, F.H., Thibault, J., 2013. Adsorbent screening for biobutanol separation by adsorption: Kinetics, isotherms, and competitive effect of other compounds. Adsorption 19, 1263–1272. https://doi.org/10.1007/s10450-013-9566-8

Abdel-Rahman, M.A., Tashiro, Y., Sonomoto, K., 2013. Recent advances in lactic acid production by microbial fermentation processes. Biotechnol. Adv. "Bioenergy and Biorefinery from Biomass" through innovative technology development 31, 877–902. https://doi.org/10.1016/j.biotechadv.2013.04.002

Abdullah, M.A., Chiang, L., Nadeem, M., 2009. Comparative evaluation of adsorption kinetics and isotherms of a natural product removal by Amberlite polymeric adsorbents. Chem. Eng. J. 146, 370–376. https://doi.org/10.1016/j.cej.2008.06.018

Aguilera, P.G., Gutiérrez Ortiz, F.J., 2016. Prediction of fixed-bed breakthrough curves for H_2S adsorption from biogas: Importance of axial dispersion for design. Chem. Eng. J. 289, 93–98. https://doi.org/10.1016/j.cej.2015.12.075

Ahmad, M.A., Rahman, N.K., 2011. Equilibrium, kinetics, and thermodynamic of Remazol Brilliant Orange 3R dye adsorption on coffee husk-based activated carbon. Chem. Eng. J. 170, 154–161. https://doi.org/10.1016/j.cej.2011.03.045

Ahsan, L., Jahan, M.S., Ni, Y., 2013. Recovery of acetic acid from the prehydrolysis liquor of kraft based dissolving pulp production process: Sodium hydroxide back extraction from the trioctylamine/octanol system. Ind. Eng. Chem. Res. 52, 9270–9275. https://doi.org/10.1021/ie401285v

Anonymous, 2010. Germany's Wacker to license bio-based acetic acid process [WWW Document]. Icis. URL https://www.icis.com/explore/resources/news/2010/03/25/9345966/germany-s-wacker-to-license-bio-based-acetic-acid-process (accessed 12.27.18).

Badruzzaman, M., Westerhoff, P., Knappe, D.R.U., 2004. Intraparticle diffusion and adsorption of arsenate onto granular ferric hydroxide (GFH). Water Res. 38, 4002–4012. https://doi.org/10.1016/j.watres.2004.07.007

Baumann, I., Westermann, P., 2016. Microbial production of short chain fatty acids from lignocellulosic biomass: Current processes and market. BioMed Res. Int. 2016, 1–15. https://doi.org/10.1155/2016/8469357

Berson, R.E., Young, J.S., Kamer, S.N., Hanley, T.R., 2005. Detoxification of actual pretreated corn stover hydrolysate using activated carbon powder. Appl. Biochem. Biotechnol. 124, 923–934. https://doi.org/10.1385/ABAB:124:1-3:0923

Biddy, M.J., Scarlata, C., Kinchin, C., 2016. Chemicals from biomass: a market assessment of bioproducts with near-term potential (No. NREL/TP--5100-65509, 1244312). https://doi.org/10.2172/1244312

Bolster, C.H., Hornberger, G.M., 2007. On the use of linearized Langmuir equations. Soil Sci. Soc. Am. J. 71, 1796–1806. https://doi.org/10.2136/sssaj2006.0304

Byers, C.H., 1996. Professor C. Judson King III. An informal minibiography. Ind. Eng. Chem. Res. 35, 991–992. https://doi.org/10.1021/ie960823q

Coppée, P.E., 2012. Galactic to develop third generation lactic acid from algae with "eclipse" project. Bio-based News. URL http://news.bio-based.eu/galactic-to-develop-third-generation-lactic-acid-from-algae-with-eclipse-project/ (accessed 12.28.18).

Crank, J., 1975. The Mathematics of Diffusion. Clarendon Press.

da Silva, A.H., Miranda, E.A., 2013. Adsorption/desorption of organic acids onto different adsorbents for their recovery from fermentation broths. J. Chem. Eng. Data 58, 1454–1463. https://doi.org/10.1021/je3008759

Dai, Y., King, C.J., 1996. Selectivity between lactic acid and glucose during recovery of lactic acid with basic extractants and polymeric sorbents. Ind. Eng. Chem. Res. 35, 1215–1224. https://doi.org/10.1021/ie9506274

Davison, B.H., Nghiem, N.P., Richardson, G.L., 2004. Succinic acid adsorption from fermentation broth and regeneration. Appl. Biochem. Biotechnol. 113–116, 653–669.

Davison, B.H., Thompson, J.E., 1992. Simultaneous fermentation and separation of lactic acid in a biparticle fluidized-bed bioreactor. Appl. Biochem. Biotechnol. 34–35, 431–439. https://doi.org/10.1007/BF02920566

Dwivedi, P.N., Upadhyay, S.N., 1977. Particle-fluid mass transfer in fixed and fluidized beds. Ind. Eng. Chem. Proc. Des. Dev. 16, 157–165. https://doi.org/10.1021/i260062a001

Eom, M.H., Kim, W., Lee, J., Cho, J.H., Seung, D., Park, S., Lee, J.H., 2013. Modeling of a biobutanol adsorption process for designing an extractive fermentor. Ind. Eng. Chem. Res. 52, 603–611. https://doi.org/10.1021/ie301249z

Erickson, B., Nelson, J.E., Winters, P., 2012. Perspective on opportunities in industrial biotechnology in renewable chemicals. Biotechnol. J. 7, 176–185. https://doi.org/10.1002/biot.201100069

Erto, A., Lancia, A., Musmarra, D., 2012. A Real Adsorbed Solution Theory model for competitive multicomponent liquid adsorption onto granular activated carbon. Microporous and Mesoporous Materials, Special Issue: Characterisation of Porous Solids IX 154, 45–50. https://doi.org/10.1016/j.micromeso.2011.10.041

Evangelista, R.L., 1994. Recovery and Purification of Lactic Acid from Fermentation Broth by Adsorption. Iowa State University.

Foo, K.Y., Hameed, B.H., 2010. Insights into the modeling of adsorption isotherm systems. Chem. Eng. J. 156, 2–10. https://doi.org/10.1016/j.cej.2009.09.013

Ganguly, S.K., Goswami, A.N., 1996. Surface diffusion kinetics in the adsorption of acetic acid on activated carbon. Sep. Sci. Technol. 31, 1267–1278. https://doi.org/10.1080/01496399608006950

Garcia, A.A., King, C.J., 1989. The use of basic polymer sorbents for the recovery of acetic acid from dilute aqueous solution. Ind. Eng. Chem. Res. 28, 204–212. https://doi.org/10.1021/ie00086a013

Garrett, B.G., Srinivas, K., Ahring, B.K., 2015. Performance and stability of Amberlite™ IRA-67 ion exchange resin for product extraction and pH control during homolactic fermentation of corn stover sugars. Biochem. Eng. J. 94, 1–8. https://doi.org/10.1016/j.bej.2014.11.004

Gluszcz, P., Jamroz, T., Sencio, B., Ledakowicz, S., 2004. Equilibrium and dynamic investigations of organic acids adsorption onto ion-exchange resins. Bioprocess Biosyst Eng 26, 185–190. https://doi.org/10.1007/s00449-003-0348-7

Godshall, M.A., 2007. Sugar and other sweeteners, in: Kent, J.A. (Ed.), Kent and Riegel's Handbook of Industrial Chemistry and Biotechnology. Springer US, pp. 1657–1693. https://doi.org/10.1007/978-0-387-27843-8_35

González, M.I., Álvarez, S., Riera, F.A., Álvarez, R., 2006. Purification of lactic acid from fermentation broths by ion-exchange resins. Ind. Eng. Chem. Res. 45, 3243–3247. https://doi.org/10.1021/ie051263a

González, M.I., Álvarez, S., Riera, F. A, Álvarez, R., 2007. Economic evaluation of an integrated process for lactic acid production from ultrafiltered whey. J. Food Eng. 80, 553–561. https://doi.org/10.1016/j.jfoodeng.2006.06.021

Gu, T., Iyer, G., Cheng, K.S.C., 2013. Parameter estimation and rate model simulation of partial breakthrough of bovine serum albumin on a column packed with large Q Sepharose anion-exchange particles. Sep. Purif. Technol. 116, 319–326. https://doi.org/10.1016/j.seppur.2013.06.004

Gustafson, R.L., Fillius, H.F., Kunin, R., 1970. Basicities of weak base ion exchange resins. Ind. Eng. Chem. Fund. 9, 221–229. https://doi.org/10.1021/i160034a006

Guzman, D. de, 2018. Godavari restarts bio-based acetic acid production. Green Chemicals Blog.

Hand, D., Crittenden, J., Thacker, W., 1983. User-oriented batch reactor solutions to the homogeneous surface diffusion model. J. Environ. Eng. 109, 82–101. https://doi.org/10.1061/(ASCE)0733-9372(1983)109:1(82)

Harland, C.E., 1994. Ion Exchange: Theory and Practice. Royal Society of Chemistry.

Helfferich, F.G., Hwang, Y.L., 1985. Kinetics of acid uptake by weak-base anion exchangers. Mechanism of proton transfer. Adsorption and ion exchange: recent developments 17–27.

Ho, Y.S., 2004. Citation review of Lagergren kinetic rate equation on adsorption reactions. Scientometrics 59, 171–177. https://doi.org/10.1023/B:SCIE.0000013305.99473.cf

Ho, Y.., McKay, G., 1999. Pseudo-second order model for sorption processes. Process Biochem. 34, 451–465. https://doi.org/10.1016/S0032-9592(98)00112-5

Husson, S.M., King, C.J., 1999. Multiple-acid equilibria in adsorption of carboxylic acids from dilute aqueous solution. Ind. Eng. Chem. Res. 38, 502–511. https://doi.org/10.1021/ie9804430

Jadhav, A.J., Srivastava, V.C., 2013. Adsorbed solution theory based modeling of binary adsorption of nitrobenzene, aniline and phenol onto granulated activated carbon. Chemical Engineering Journal 229, 450–459. https://doi.org/10.1016/j.cej.2013.06.021

Jang, S.C., Yang, S.I., Oh, S.G., Choi, D.K., 2011. Adsorption dynamics and effects of carbon to zeolite ratio of layered beds for multicomponent gas adsorption. Korean J. Chem. Eng. 28, 583–590. https://doi.org/10.1007/s11814-010-0399-9

Jang, Y.S., Kim, B., Shin, J.H., Choi, Y.J., Choi, S., Song, C.W., Lee, J., Park, H.G., Lee, S.Y., 2012. Bio-based production of C2–C6 platform chemicals. Biotechnol. Bioeng. 109, 2437–2459. https://doi.org/10.1002/bit.24599

Jiao, P., Wu, J., Zhou, J., Yang, P., Zhuang, W., Chen, Y., Zhu, C., Guo, T., Ying, H., 2015. Mathematical modeling of the competitive sorption dynamics of acetone–butanol–ethanol on KA-I resin in a fixed-bed column. Adsorption 21, 165–176. https://doi.org/10.1007/s10450-015-9659-7

Katikaneni, S.P.R., Cheryan, M., 2002. Purification of fermentation-derived acetic acid by liquid−liquid extraction and esterification. Industrial & Engineering Chemistry Research 41, 2745–2752. https://doi.org/10.1021/ie010825x

Kawabata, N., Yoshida, J., Tanigawa, Y., 1981. Removal and recovery of organic pollutants from aquatic environment. 4. Separation of carboxylic acids from aqueous solution using crosslinked poly(4-vinylpyridine). Ind. Eng. Chem. Prod. Res. Dev. 20, 386–390. https://doi.org/10.1021/i300002a030

Koch, D.J., Lopes, M.S.G., Gouvea, I.E., Zeidler, A.F.B., Dumaresq, A.S.R., Rodrigues, M.E.P., 2015. Modified microorganisms and methods of using same for anaerobic coproduction of isoprene and acetic acid. WO2015002977A1.

Koh, J.H., Wankat, P.C., Wang, N.H.L., 1998. Pore and surface diffusion and bulk-phase mass transfer in packed and fluidized beds. Ind. Eng. Chem. Res. 37, 228–239. https://doi.org/10.1021/ie970337i

Komesu, A., Oliveira, J.A.R. de, Martins, L.H. da S., Maciel, M.R.W., Filho, R.M., 2017a. Lactic acid production to purification: A review :: BioResources. BioResources 12, 4364–4383.

Komesu, A., Wolf Maciel, M.R., Rocha de Oliveira, J.A., da Silva Martins, L.H., Maciel Filho, R., 2017b. Purification of lactic acid produced by fermentation: focus on non-traditional distillation processes. Separation & Purification Reviews 46, 241–254. https://doi.org/10.1080/15422119.2016.1260034

Kumar, P., Lau, P.W., Kale, S., Johnson, S., Pareek, V., Utikar, R., Lali, A., 2014. Kafirin adsorption on ion-exchange resins: Isotherm and kinetic studies. J. Chromatogr. A 1356, 105–116. https://doi.org/10.1016/j.chroma.2014.06.035

Langmuir, I., 1918. The adsorption of gases on plane surfaces of glass, mica, and platinum. J. Am. Chem. Soc. 40, 1361–1403. https://doi.org/10.1021/ja02242a004

Lee, H.J., Xie, Y., Koo, Y.M., Wang, N.H.L., 2004. Separation of lactic acid from acetic acid using a four-zone SMB. Biotechnol. Prog. 20, 179–192. https://doi.org/10.1021/bp025663u

Li, P., SenGupta, A.K., 2000. Intraparticle diffusion during selective sorption of trace contaminants: the effect of gel versus macroporous morphology. Environ. Sci. Technol. 34, 5193–5200. https://doi.org/10.1021/es001299o

Li, Z., Yang, R.T., 1999. Concentration profile for linear driving force model for diffusion in a particle. AIChE J. 45, 196–200. https://doi.org/10.1002/aic.690450118

Lin, X., Huang, Q., Qi, G., Shi, S., Xiong, L., Huang, C., Chen, Xuefang, Li, H., Chen, Xinde, 2017a. Estimation of fixed-bed column parameters and mathematical modeling of breakthrough behaviors for adsorption of levulinic acid from aqueous solution using SY-01 resin. Separation and Purification Technology 174, 222–231. https://doi.org/10.1016/j.seppur.2016.10.016

Lin, X., Huang, Q., Qi, G., Xiong, L., Huang, C., Chen, Xuefang, Li, H., Chen, Xinde, 2017b. Adsorption behavior of levulinic acid onto microporous hyper-cross-linked polymers in aqueous solution: Equilibrium, thermodynamic, kinetic simulation and fixed-bed column studies. Chemosphere 171, 231–239. https://doi.org/10.1016/j.chemosphere.2016.12.084

Ma Z., Whitley R. D., Wang N.-H. L., 2004. Pore and surface diffusion in multicomponent adsorption and liquid chromatography systems. AIChE J. 42, 1244–1262. https://doi.org/10.1002/aic.690420507

Mackie, J.S., Meares, P., 1955. The diffusion of electrolytes in a cation-exchange resin membrane I. Theoretical. Proc. R. Soc. Lond. A 232, 498–509. https://doi.org/10.1098/rspa.1955.0234

Mathews, A.P., 1997. Tapered Bed Apparatus for Fluid-Solid Mass Transfer Operations. US5626763A.

Mathews, A.P., 2005. Effect of adsorbent particle layering on performance of conventional and tapered fixed-bed adsorbers. J. Environ. Eng. 131, 1488–1494. https://doi.org/10.1061/(ASCE)0733-9372(2005)131:11(1488)

Mathews, A.P., Weber Jr, W.J., 1977. Effects of external mass transfer and intraparticle diffusion on adsorption rates in slurry reactors. AIChE Symp. Ser. 73, 91–98.

Mathews, A.P., Weber Jr, W.J., 1980. Mathematical modeling of adsorption in multicomponent systems, in: Adsorption and Ion Exchange with Synthetic Zeolites, ACS Symposium Series. American Chemical Society, pp. 27–53. https://doi.org/10.1021/bk-1980-0135.ch002

Mathews, A.P., Weber Jr, W.J., 1984. Modeling and parameter evaluation for adsorption in slurry reactors. Chem. Eng. Commun. 25, 157–171. https://doi.org/10.1080/00986448408940104

Mathews, A.P., Zayas, I., 1989. Particle size and shape effects on adsorption rate parameters. J. Environ. Eng. 115, 41–55. https://doi.org/10.1061/(ASCE)0733-9372(1989)115:1(41)

Matsuda, N., Agui, W., Ogino, K., Kawashima, N., Watanabe, T., Sakai, H., Abe, M., 1996. Disinfection of viable *Pseudomonas stutzeri* in ultrapure water with ion exchange resins. Colloids Surf., B 7, 91–100. https://doi.org/10.1016/0927-7765(96)01285-4

McLintock, I.S., 1967. The Elovich equation in chemisorption kinetics. Nature 216, 1204–1205. https://doi.org/10.1038/2161204a0

Moldes, A.B., Alonso, J.L., Parajó, J.C., 2003. Recovery of lactic acid from simultaneous saccharification and fermentation media using anion exchange resins. Bioprocess Biosyst. Eng. 25, 357–363. https://doi.org/10.1007/s00449-002-0316-7

Murali, N., Srinivas, K., Ahring, B.K., 2017. Biochemical production and separation of carboxylic acids for biorefinery applications. Fermentation 3, 22. https://doi.org/10.3390/fermentation3020022

Myers, A.L., Prausnitz, J.M., 1965. Thermodynamics of mixed-gas adsorption. AIChE J. 11, 121–127. https://doi.org/10.1002/aic.690110125

Nouaille, R., Pessiot, J., 2017. Method for Producing Organic Molecules from Fermentable Biomass. US20170158572A1.

O'Dowd, E., 2017. Industry giants Total and Corbion begin their journey to "support the future of bioplastics". URL https://www.biobasedworldnews.com/industry-giants-total-and-corbion-begin-their-journey-to-support-the-future-of-bioplastics (accessed 12.28.18).

Oudshoorn, A., van der Wielen, L.A.M., Straathof, A.J.J., 2009. Adsorption equilibria of bio-based butanol solutions using zeolite. Biochem. Eng. J. 48, 99–103. https://doi.org/10.1016/j.bej.2009.08.014

Park, J.H., Kim, J.N., Cho, S.H., Kim, J.D., Yang, R.T., 1998. Adsorber dynamics and optimal design of layered beds for multicomponent gas adsorption. Chem. Eng. Sci. 53, 3951–3963. https://doi.org/10.1016/S0009-2509(98)00196-1

Pota, A. A., Mathews, A. P., 1999. Effects of particle stratification on fixed bed absorber performance. J. Environ. Eng. 125, 705–711. https://doi.org/10.1061/(ASCE)0733-9372(1999)125:8(705)

Pota, A.A., Mathews, A.P., 2000. Adsorption dynamics in a stratified convergent tapered bed. Chem. Eng. Sci. 55, 1399–1409. https://doi.org/10.1016/S0009-2509(99)00032-9

Poulopoulos, S.G., Inglezakis, V.J., 2006. Adsorption, Ion Exchange and Catalysis: Design of Operations and Environmental Applications. Elsevier.

Redlich, O., Peterson, D.L., 1959. A useful adsorption isotherm. J. Phys. Chem. 63, 1024–1024. https://doi.org/10.1021/j150576a611

Reisinger, H., King, C.J., 1995. Extraction and sorption of acetic acid at pH above p*K*a to form calcium magnesium acetate. Ind. Eng. Chem. Res. 34, 845–852. https://doi.org/10.1021/ie00042a016

Rosen, J.B., 1952. Kinetics of a fixed bed system for solid diffusion into spherical particles. The Journal of Chemical Physics 20, 387–394. https://doi.org/10.1063/1.1700431

Rush, B., 2012. Turning a novel yeast into a platform host for industrial production of fuels and chemicals. Metabolic Engineering IX.

Ruthven, D.M., 1984. Principles of Adsorption and Adsorption Processes. John Wiley & Sons.

Saravanan, V., Waijers, D.A., Ziari, M., Noordermeer, M.A., 2010. Recovery of 1-butanol from aqueous solutions using zeolite ZSM-5 with a high Si/Al ratio; suitability of a column process for industrial applications. Biochem. Eng. J. 49, 33–39. https://doi.org/10.1016/j.bej.2009.11.008

Schügerl, K., 2013. Solvent Extraction in Biotechnology: Recovery of Primary and Secondary Metabolites. Springer Science & Business Media.

Schwaab, M., Steffani, E., Barbosa-Coutinho, E., Severo Júnior, J.B., 2017. Critical analysis of adsorption/diffusion modelling as a function of time square root. Chem. Eng. Sci. 173, 179–186. https://doi.org/10.1016/j.ces.2017.07.037

SenGupta, A.K., 2017. Ion Exchange in Environmental Processes: Fundamentals, Applications and Sustainable Technology. John Wiley & Sons.

Shi, Y., Kong, X., Zhang, C., Chen, Y., Hua, Y., 2013. Adsorption of soy isoflavones by activated carbon: Kinetics, thermodynamics, and influence of soy oligosaccharides. Chem. Eng. J. 215–216, 113–121. https://doi.org/10.1016/j.cej.2012.10.100

Simonin, J.P., 2016. On the comparison of pseudo-first order and pseudo-second order rate laws in the modeling of adsorption kinetics. Chem. Eng. J. 300, 254–263. https://doi.org/10.1016/j.cej.2016.04.079

Sips, R., 1948. On the structure of a catalyst surface. The Journal of Chemical Physics 16, 490–495. https://doi.org/10.1063/1.1746922

Sircar, S., Hufton, J.R., 2000. Why does the linear driving force model for adsorption kinetics work? Adsorption 6, 137–147. https://doi.org/10.1023/A:1008965317983

Sochard, S., Fernandes, N., Reneaume, J.-M., 2010. Modeling of adsorption isotherm of a binary mixture with real adsorbed solution theory and nonrandom two-liquid model. AIChE Journal 56, 3109–3119. https://doi.org/10.1002/aic.12220

Song, M., Jiao, P., Qin, T., Jiang, K., Zhou, J., Zhuang, W., Chen, Y., Liu, D., Zhu, C., Chen, X., Ying, H., Wu, J., 2017. Recovery of lactic acid from the pretreated fermentation broth based on a novel hyper-cross-linked meso-micropore resin: Modeling. Bioresour. Technol. 241, 593–602. https://doi.org/10.1016/j.biortech.2017.05.179

Straathof, A.J.J., 2014. Transformation of biomass into commodity chemicals using enzymes or cells. Chem. Rev. 114, 1871–1908. https://doi.org/10.1021/cr400309c

Thomas, H.C., 1944. Heterogeneous ion exchange in a flowing system. J. Am. Chem. Soc. 66, 1664–1666. https://doi.org/10.1021/ja01238a017

Thomas, W.J., Crittenden, B., 1998. Design procedures, in: Adsorption Technology & Design. Butterworth-Heinemann, Oxford, pp. 135–186. https://doi.org/10.1016/B978-075061959-2/50007-0

Tung, L.A., 1993. Recovery of Carboxylic Acids at pH Greater Than p*K*a. University of California, Berkeley.

Tung, L.A., King, C.J., 1994. Sorption and extraction of lactic and succinic acids at pH > pK_{a_1}. I. Factors governing equilibria. Ind. Eng. Chem. Res. 33, 3217–3223. https://doi.org/10.1021/ie00036a041

Vidra, A., Németh, Á., 2017. Bio-produced acetic acid: A review. Periodica Polytechnica Chemical Engineering 62, 245–256. https://doi.org/10.3311/PPch.11004

Walton, K.S., Sholl, D.S., 2015. Predicting multicomponent adsorption: 50 years of the ideal adsorbed solution theory. AIChE Journal 61, 2757–2762. https://doi.org/10.1002/aic.14878

Weber Jr, W.J., Morris, J.C., 1963. Kinetics of adsorption on carbon from solution. J. Sanit. Eng. Div., Am. Soc. Civ. Eng. 89, 31–60.

Wilke, C.R., Chang, P., 1955. Correlation of diffusion coefficients in dilute solutions. AIChE J. 1, 264–270. https://doi.org/10.1002/aic.690010222

Wilson, E.J., Geankoplis, C.J., 1966. Liquid mass transfer at very low reynolds numbers in packed beds. Industrial & Engineering Chemistry Fundamentals 5, 9–14. https://doi.org/10.1021/i160017a002

Wong, Y.C., Szeto, Y.S., Cheung, W.H., McKay, G., 2004. Adsorption of acid dyes on chitosan—equilibrium isotherm analyses. Process Biochem. 39, 695–704. https://doi.org/10.1016/S0032-9592(03)00152-3

Wu, F.C., Tseng, R.L., Huang, S.C., Juang, R.S., 2009. Characteristics of pseudo-second-order kinetic model for liquid-phase adsorption: A mini-review. Chem. Eng. J. 151, 1–9. https://doi.org/10.1016/j.cej.2009.02.024

Yang, S.T., White, S.A., Hsu, S.T., 1991. Extraction of carboxylic acids with tertiary and quaternary amines: Effect of pH. Ind. Eng. Chem. Res. 30, 1335–1342. https://doi.org/10.1021/ie00054a040

Yang, S.T., Zhu, H., Lewis, V.P., Tang, I.-C., 1992. Calcium magnesium acetate (CMA) production from whey permeate: Process and economic analysis. Resources, Conservation and Recycling, Calcium Magnesium Acetate: An emerging bulk chemical for environmental applications 7, 181–200. https://doi.org/10.1016/0921-3449(92)90016-U

Yoshida, H., Yoshikawa, M., Kataoka, T., 1994. Parallel transport of BSA by surface and pore diffusion in strongly basic chitosan. AIChE J. 40, 2034–2044.

Yousuf, A., Bonk, F., Bastidas-Oyanedel, J.-R., Schmidt, J.E., 2016. Recovery of carboxylic acids produced during dark fermentation of food waste by adsorption on Amberlite IRA-67 and activated carbon. Bioresour. Technol. 217, 137–140. https://doi.org/10.1016/j.biortech.2016.02.035

Zhang, H., Wang, S., 2017. Modeling bisolute adsorption of aromatic compounds based on adsorbed solution theories. Environ. Sci. Technol. 51, 5552–5562. https://doi.org/10.1021/acs.est.6b05576

Zhang, K., Zhang, L., Yang, S.T., 2014. Fumaric acid recovery and purification from fermentation broth by activated carbon adsorption followed with desorption by acetone. Ind. Eng. Chem. Res. 53, 12802–12808. https://doi.org/10.1021/ie501559f

Zhou, J., Wu, Jinglan, Liu, Y., Zou, F., Wu, Jian, Li, K., Chen, Y., Xie, J., Ying, H., 2013. Modeling of breakthrough curves of single and quaternary mixtures of ethanol, glucose, glycerol and acetic acid adsorption onto a microporous hyper-cross-linked resin. Bioresour. Technol. 143, 360–368. https://doi.org/10.1016/j.biortech.2013.06.009

Chapter 3
Materials and Methods

3.1 Materials

Anion exchange resins Amberlite IRA67, Amberlite IRA96, Purolite A835, and Reillex 425 were obtained in their free base forms. These resins were sourced from Alfa Aesar (Ward Hill, MA), Sigma Aldrich (St. Louis, MO), Purolite (Philadelphia, PA), and Vertellus (Indianapolis, IN) respectively. GAC was obtained from CECA Inc. (Pyror, OK). It is a wood-based activated carbon with a particle porosity of 0.67, pore volume of 0.95 ml/g, and a uniform bed porosity of 0.412 (Mathews, 2005). The properties of the GAC and weak base anion exchange resins are listed in Table 3.1.

The resins were rinsed with deionized water until the water looked clear with no impurities and pretreated as specified by the manufacturer. Resins were vacuum filtered, dried at room temperature for 24 hours, and stored in airtight bottles. Purolite A835 resin was sieved into various size fractions to use in stratified fixed-bed adsorbers. Based on the largest weight fractions obtained from sieving, three particle sizes with geometric mean diameters of 0.771, 0.648, and 0.545 mm were used in stratified packed beds. In case of GAC, it was initially sieved into various size fractions, rinsed with deionized water to remove fines and dried in the oven at 105 ^{o}C until it reached constant weight. Based on the largest weight fractions obtained from sieving, five particle sizes with geometric mean diameters of 0.917, 0.771, 0.648, 0.545, and 0.458 mm were used for each layer in the stratified packed beds.

ACS grade acetic acid with > 99.7% purity from VWR (Radnor, PA) was used in this study. Lactic acid (85%) was obtained from Acros Organics (New Jersey, USA). A 20% lactic acid solution was prepared via dilution and was boiled under reflux for 12 hours. This process is needed to hydrolyze lactic acid anhydrides present in lactic acid solutions of concentrations >

20%. The presence of lactic acid anhydride in the 20% solution is monitored by using HPLC. The pH values of the acetic and lactic acid solutions were adjusted to the required value by using HCl and NaOH solutions.

Table 3.1: Properties of activated carbon and weak base anion exchange resins

	GAC	Amberlite IRA67	Amberlite IRA96	Purolite A835	Reillex 425
Functional group	-	Tertiary amine	Tertiary amine	Tertiary amine	4-vinylpyridine
p*K*a	-	8.32 (Lisa A. Tung, 1993)	-	-	4.9/5.2 (Evangelista, 1994)
Matrix	Carbon	Crosslinked acrylic gel	Macroporous styrene divinylbenzene copolymer	Macroporous polyacrylic crosslinked with divinylbenzene	Poly-4-vinylpyridine, crosslinked with divinylbenzene
Particle size (µm)	500-595	500-750	550-750	300-1200	-
Total exchange capacity (eq/L)	-	≥ 1.6	≥ 1.25	1	-
Surface area (m^2/g)	1000-1100	-	-	0.6 (Turku, 2010)	90 (Gusler et al., 1993)
Percentage water retention	-	56-62	59-65	65-73	40-60

3.2 Fermentation broths

The compositions of fermentation broth and synthetic mixture solutions are given in Table 3.2. The fermentation broth was heated at 60 ^oC for 1 hour on a hot plate with constant stirring. After it reached room temperature, the broth was centrifuged at 8000 *rcf in a laboratory centrifuge. The supernatant was collected and used for batch experiments.

Table 3.2: Composition of fermentation broth and synthetic mixture solutions

Component	Concentration in fermentation broth (g/L)		Concentration in synthetic mixture solution (g/L)	
	pH 4.2	pH adjusted to 4.8	pH 2.2	pH adjusted to 4.8
Lactose	21.1	20.8	10.1	10.2
Lactic acid	9.2	9.23	15.33	15.9
Acetic acid	36.7	36.2	28.04	29.3
Propylene glycol	32.9	32.4	30.8	30.3
Ethanol	8.39	8.23	6.4	6.14

3.3 Adsorption equilibrium studies

Batch adsorption isotherm studies were carried out in 120 ml bottles using the bottle point method. These experiments were conducted at a temperature of 21°C. The bottles were shaken in a rotating tumbler for 24 hours until the point of equilibration was reached. After equilibration, the samples were analyzed to determine the equilibrium concentration. The adsorption capacity, q_e (g/g), was calculated based on a mass balance between the solution and solid phase at equilibrium.

$$q_e = \left(\frac{c_0 - c_e}{m}\right) * V \tag{3.1}$$

The Langmuir (Langmuir, 1918), Freundlich (e.g., Foo and Hameed, 2010), linear-Freundlich (Mathews, 2005; Redlich and Peterson, 1959) and Sips (Sips, 1948) isotherm equations were fitted based on an iterative procedure targeted to minimize the average relative error (ARE) between the experimental and predicted adsorbed phase concentration values. The ARE is defined as Equation (3.2) :

$$Average\ relative\ error\ = \sum_{i=1}^{n} \left|\frac{q_{e,e} - q_{e,p}}{q_{e,e}}\right| * \frac{100}{n} \tag{3.2}$$

Nonlinear curve fitting was done using the generalized reduced gradient algorithm in the Solver add-in of Microsoft Excel 2013. The iterative procedure uses different initial estimates of the isotherm constants and finds a solution such that the target error value is minimized.

3.4 Batch adsorption kinetics studies

Adsorption rate experiments were conducted in a 2-litre batch mixer with a diameter (*D*) of 13 cm. These experiments were conducted at a temperature of 21°C. The batch mixer was equipped with four baffles and a lid. The dimensions are shown in Figure 3.1.

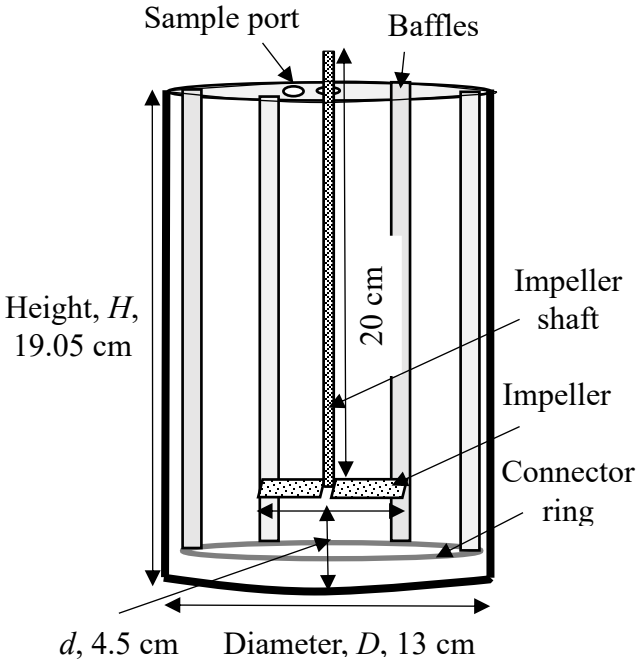

Figure 3.1: Diagram of batch mixer used to study the kinetics of acetic acid adsorption on activated carbon and weak base anion exchange resins

Agitation was provided with a 45° pitched blade turbine impeller of diameter *d* (cm), connected to a stirring motor. The speed of impeller was set at 420 rpm by using a variac and was validated with a digital tachometer. For each experiment, a definite volume of organic acid solution was used in the batch mixer. Once the solution reached equilibrium with the reactor, one initial

sample was withdrawn. A given amount of resin or GAC was added to the reactor, and samples were withdrawn thereafter at specified time intervals until equilibrium was achieved.

3.5 Fixed-bed experiments

Adsorption experiments were conducted in glass columns of conventional cylindrical and tapered configurations. These experiments were conducted at a temperature of 21°C. The details of the tapered bed configuration are given in subsection 3.6. The cylindrical columns had a constant circular cross-sectional area of 5.07 cm^2. Five types of fixed-bed configurations were tested in this study (Figure 3.2).

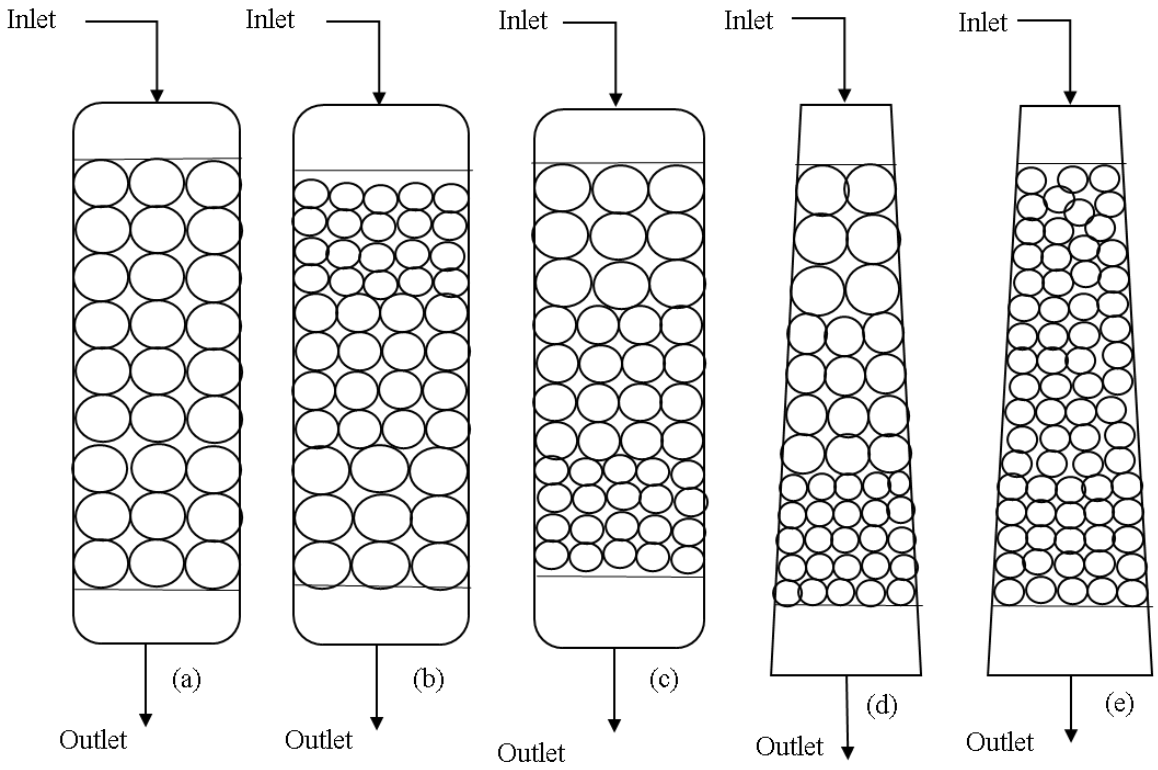

Figure 3.2: Schematic of adsorber configurations: (a) conventional cylindrical adsorber (CCA) with single particle size, (b) cylindrical adsorber with normally stratified adsorbent (SCA), (c) cylindrical adsorber with reverse stratified adsorbent (RSCA), (d) tapered adsorber with reverse stratified adsorbent (RSTA), and (e) tapered adsorber with single particle size

Figure 3.2(a) shows a conventional cylindrical adsorber (CCA) with single adsorbent particle size. In the cylindrical column adsorber with normal stratified particle layering, the adsorbent

particle size increases in the direction of flow similar to the natural stratification expected after backwashing. The adsorber with this configuration is referred to as the normal stratified cylindrical adsorber (SCA) (Figure 3.2(b)), and has adsorbent layers with increasing particle diameters along the depth of the column. In the reverse stratified adsorber, the adsorbent particle size in the layers decreased in the direction of flow in contrast to the normal stratified adsorbers. Cylindrical and tapered adsorbers with such particle layering are referred to as reverse stratified cylindrical adsorber (RSCA) (Figure 3.2(c)) and reverse stratified tapered adsorber (RSTA) (Figure 3.2(d)) respectively. A peristaltic pump was used to discharge the organic acid solution at a given flow rate to the adsorber inlet. Samples from the outlet of the column were collected at specified intervals and analyzed to obtain the breakthrough profiles as a function of time.

3.6 Tapered bed adsorber configuration

The tapered bed adsorber has a cross-sectional area that varies along the length of the bed. This column is conical in shape and had cross-sectional areas of 3.14 cm^2 and 12.57 cm^2 at the top and bottom respectively. The half angle of the taper is 1.15°. The column has a convergent taper in the downflow mode. For the adsorption step, the column was operated in the downflow mode. Fixed-bed adsorption dynamics in the tapered column were studied using two types of adsorber configurations, RSTA (Figure 3.2(d)) and tapered column with single adsorbent particle size (Figure 3.2(e)). In RSTA, once the adsorbent is layered, the particles will tend to remain in that configuration during backwash due to the combined effects of increasing velocity and increasing particles sizes in the upflow direction. The tapered bed adsorber with single adsorbent particle size was used to study the effects of bed geometry on bed capacity utilization.

3.7 Analytical methods

The concentration of organic acids in analytes was measured using Shimadzu high performance liquid chromatography (HPLC) system with a Bio-Rad Aminex HPX87-H column. The samples were eluted with a 0.65 ml/min isocratic 2.5 mM sulfuric acid solution. Organic acids were detected using a Prominence UV detector at 210 nm. Lactose, propylene glycol, and ethanol were detected using an RI detector. They were quantified based on standard curves. The color of the fermentation broth was measured using a UV-Vis spectrophotometer at 400 nm (Cary 60, Agilent, USA). Samples were analyzed in duplicates and the average peak areas were taken for estimating the concentrations.

REFERENCES

Evangelista, R.L., 1994. Recovery and Purification of Lactic Acid from Fermentation Broth by Adsorption. Iowa State University.

Foo, K.Y., Hameed, B.H., 2010. Insights into the modeling of adsorption isotherm systems. Chem. Eng. J. 156, 2–10. https://doi.org/10.1016/j.cej.2009.09.013

Gusler, G.M., Browne, T.E., Cohen, Y., 1993. Sorption of organics from aqueous solution onto polymeric resins. Ind. Eng. Chem. Res. 32, 2727–2735. https://doi.org/10.1021/ie00023a040

Langmuir, I., 1918. The adsorption of gases on plane surfaces of glass, mica, and platinum. J. Am. Chem. Soc. 40, 1361–1403. https://doi.org/10.1021/ja02242a004

Mathews, A.P., 2005. Effect of Adsorbent Particle Layering on Performance of Conventional and Tapered Fixed-Bed Adsorbers. Journal of Environmental Engineering 131, 1488–1494. https://doi.org/10.1061/(ASCE)0733-9372(2005)131:11(1488)

Redlich, O., Peterson, D.L., 1959. A useful adsorption isotherm. J. Phys. Chem. 63, 1024–1024. https://doi.org/10.1021/j150576a611

Sips, R., 1948. On the structure of a catalyst surface. The Journal of Chemical Physics 16, 490–495. https://doi.org/10.1063/1.1746922

Tung, L.A., 1993. Recovery of carboxylic acids at pH greater than pKa (No. LBL--34669, 10125672). https://doi.org/10.2172/10125672

Turku, I., 2010. Adsorptive removal of harmful organic compounds from aqueous solutions. Lappeenranta University of Technology, Lappeenranta, Finland.

Chapter 4
Adsorption Equilibria and Kinetics

4.1 Introduction

Batch adsorption kinetics, and single-, and multicomponent adsorption equilibria of acetic and lactic acid on various sorbents are presented in this chapter. The experimental determination and mathematical characterization of adsorption equilibria and kinetics are important to understand the adsorption mechanisms that are operative. They are also necessary for the effective design of batch and fixed-bed adsorption processes for the recovery of organic acids from multicomponent solutions such as fermentation broths. These studies also give information on the nature of sorbent and are useful for comparative evaluation and selection of sorbents for separation and recovery processes. In addition, simple and rigorous methods for the evaluation of equilibrium and kinetic parameters are also presented. The simplified method for estimating intraparticle diffusivity can be performed using spreadsheet calculations as opposed to the numerical solution of complex diffusion equations required for the rigorous method.

4.2 Single component adsorption equilibria

The experimental equilibrium data for the adsorption of acetic acid on GAC, Amberlite IRA67, Amberlite IRA96, Purolite A835, and Reillex 425 are shown in Figure 4.1. The adsorption isotherm data for the adsorption of lactic acid on Purolite A835 is given in Figure 4.2. In the adsorption of acetic acid, it can be seen that the ion exchange resins have higher equilibrium sorption capacities compared to GAC. The high uptake capacity of resin sorbents is due to the specificity of their tertiary amine and pyridine functional groups to organic acids. Purolite A835 showed the highest sorption capacity compared to other resins. This resin also showed a higher sorption capacity for the adsorption of lactic acid (Figure 4.2) compared to acetic acid.

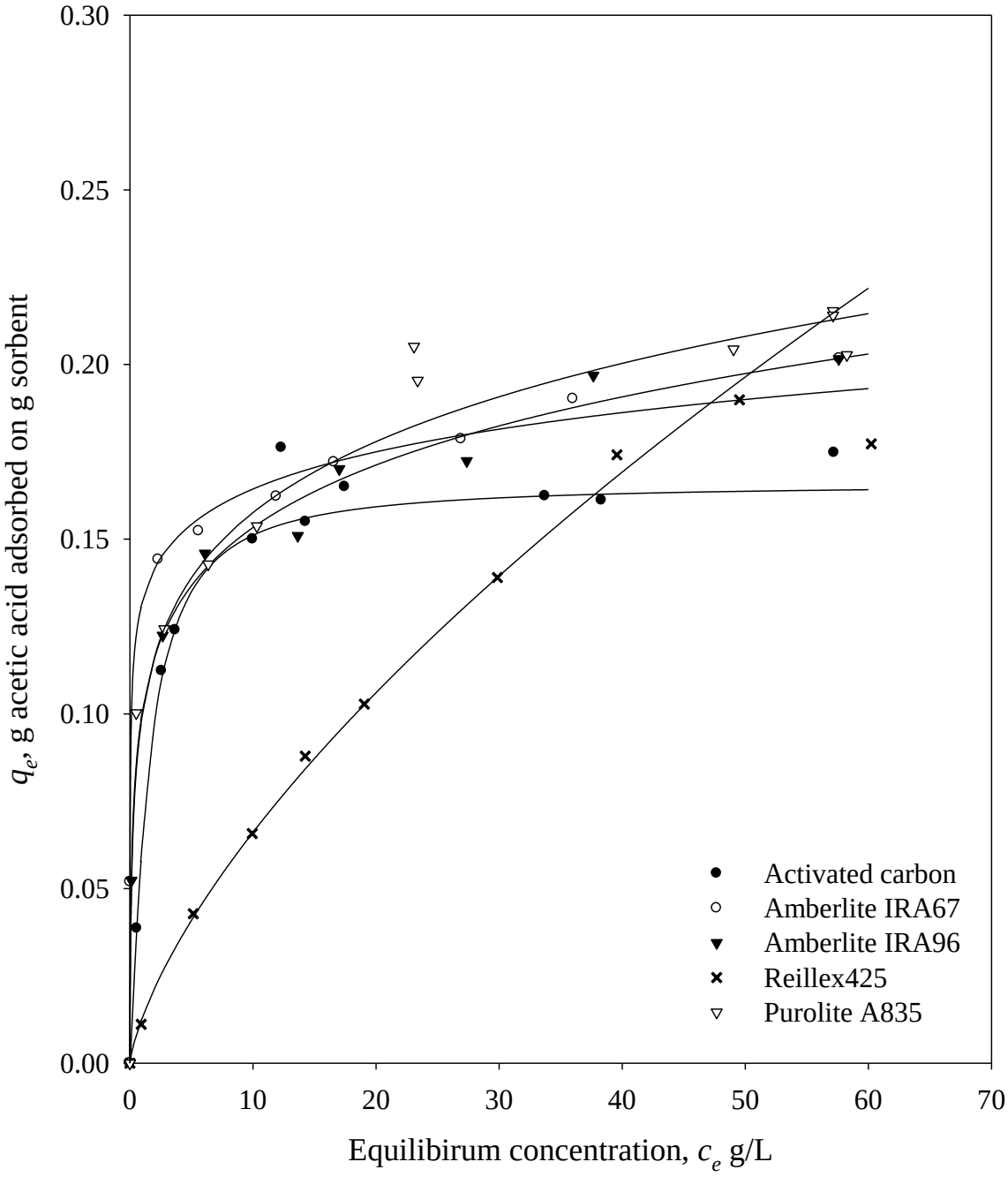

Figure 4.1: Experimental isotherm data for acetic acid adsorption on GAC and weak base anion exchange resins at a pH range of 2.7-2.3, and a temperature of 21^{o}C

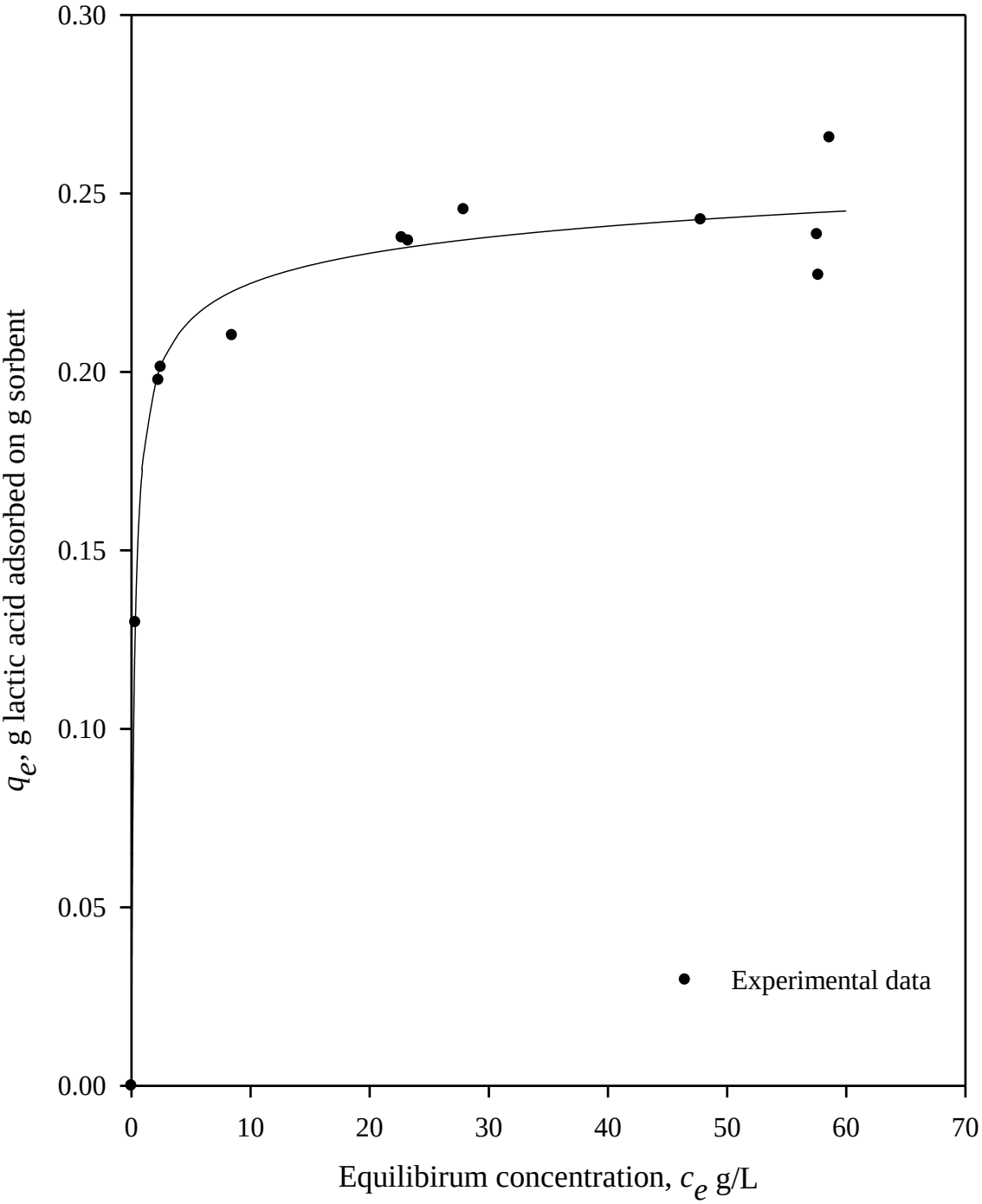

Figure 4.2: Experimental isotherm data for lactic acid adsorption on Purolite A835 at a pH range of 2-2.4, and a temperature of 21°C

The data also shows that the adsorption affinity of lactic acid, as measured by the slope of the isotherm, is also higher compared to acetic acid. Among the Amberlite resins, Amberlite IRA67 showed higher sorption capacities compared to Amberlite IRA96 at different equilibrium experimental concentrations. Amberlite IRA67 and Purolite A835 are acrylic matrix based resins. Acrylic matrix is characterized with a higher inorganic to organic content ratio compared to the styrene divinylbenzene matrix (Matsuda et al., 1996). Thus, Purolite A835 and Amberlite IRA67 are more hydrophilic than Amberlite IRA96. Their hydrophilic matrix enhances the interactions of the functional sites with water to effectively sorb organic acids. In a study on the removal of dyes such as Color Index (C.I.) Acid Orange 7, C.I. Reactive Black 5, and C.I. Direct Blue 71 from textile wastewater, acrylic based resins such as Amberlite IRA958 and Amberlite IRA67 showed higher sorption capacities when compared to the resins with other matrices (Wawrzkiewicz and Hubicki, 2015). On the other hand, resins with styrene matrix such as Amberlite IRA96 have superior bead rigidity and are favorable for use in a fixed bed adsorber operating under a high compression force. The experimental sorption data for Reillex 425 shows a linear trend unlike the other sorbents due to the low basicity of pyridine functional groups compared to other resins.

4.2.1 Equilibrium data analyses using isotherm equations for acetic and lactic acid adsorption

The isotherm constants obtained for the adsorption of acetic acid on various sorbents using a nonlinear estimation method along with the AREs are given in Table 4.1. The best fitting isotherm for the adsorption of acetic acid on each sorbent is determined based on the least ARE obtained from the isotherm model fits (Figure 4.3). The Langmuir isotherm equation fits well to the experimental equilibrium data for adsorption of acetic acid on GAC with minimum

deviations as represented by an ARE of 4.15. The experimental data for resins were well represented by the three parameter isotherms. The linear-Freundlich isotherm gave a good fit to the experimental data for Amberlite IRA67, Amberlite IRA96, and Reillex 425 with AREs of 1.55, 2.25, and 5.28 respectively. The Sips isotherm gave a good fit to the experimental data of Purolite A835 with an ARE of 3.5.

Table 4.1: Isotherm constants obtained for acetic acid adsorption on GAC and weak base anion exchange resins using a nonlinear estimation method at temperature of 21 ^{o}C

	GAC	Amberlite IRA67	Amberlite IRA96	Purolite A835	Reillex 425
Langmuir					
q_m	0.181	0.172	0.173	0.212	0.26
K	0.484	26.769	3.417	0.506	0.037
ARE	4.15	7.08	8.97	9.1	7.25
Freundlich					
K_F	0.094	0.104	0.084	0.109	0.014
n	0.189	0.168	0.227	0.161	0.68
ARE	4.91	3.85	5.01	3.6	6.25
Linear-Freundlich					
a	0.086	7.306	1.181	1.11	0.048
b	0.56	54.436	10.764	10.25	2.73
β	0.95	0.911	0.849	0.83	0.36
ARE	6.86	1.55	2.25	4.3	5.28
Sips					
a	0.101	0.211	0.149	0.104	0.014
b	0.552	0.779	0.546	0.003	0.0056
γ	0.860	0.289	0.405	0.18	0.68
ARE	6.2	1.86	2.45	3.5	5.82

Units: q_m (g/g), K (L/g); K_F (g/g) $(L/g)^n$; linear-Freundlich isotherm constants: a (g/g) (L/g), b $(L/g)^{\beta}$; Sips isotherm constants a (g/g) $(L/g)^{\gamma}$, b $(L/g)^{\gamma}$.

For the adsorption of acetic acid on GAC, the estimated Freundlich isotherm constants K_F and n of 0.094 (g/g) $(L/g)^n$ and 0.189, respectively, are quite close to the values of 0.046 (g/g) $(L/g)^n$ and 0.28, respectively, reported by da Silva and Miranda (2013) for the sorption of acetic

acid from fermentation broth on coconut shell activated carbon. The equilibrium concentration of acetic acid was in the range of 0.11 g/L to 46.34 g/L and the temperature was 20 ^{o}C.

In the adsorption of acetic acid on Amberlite IRA67, at a maximum equilibrium concentration of 57.63 g/L, the q_m value was 0.172 g/g. A similar value was reported in a study using Amberlite IRA67 for the recovery of lactic acid in a fed batch fermentation process operated for a period of 108 days (Garrett et al., 2015). In their study, the experimental isotherms were conducted with a higher sorbent to solute ratio (1 g in 15 ml) than the current study (0.5 g in 50 ml). The maximum monolayer capacity q_m was determined as 0.203 g/g. The recovery of organic acids such as citric and lactic acids from dilute aqueous solutions using Amberlite IRA67 has been studied by several researchers (Arcanjo et al., 2015; Eregowda et al., 2019; Gao et al., 2010; Gluszcz et al., 2004; Moldes et al., 2003; Yousuf et al., 2016). Yousuf et al., (2016) compared the uptake capacities of activated carbon and Amberlite IRA67 for the recovery of organic acids obtained from fermentation of food waste and showed that at pH 3.3, Amberlite IRA67 has somewhat higher maximum acid removal of 74% from batch equilibration compared to 63% for activated carbon. However, no economic analyses were provided comparing the costs of the sorbents and regeneration requirements.

The experimental equilibrium uptake data for acetic acid on Amberlite IRA96 followed the linear- Freundlich isotherm. Several studies have been reported on the use of Amberlite IRA96 resin to recover organic acids from dilute aqueous solutions (Arcanjo et al., 2015; Bishai et al., 2015; Moldes et al., 2003). Arcanjo et al., (2015) compared the adsorption capacities of Amberlite IRA67 and Amberlite IRA96 for the recovery of lactic acid from hydrothermal conversion of glycerol. Amberlite IRA96 showed a high sorption capacity of 544 g/L of resin compared to 341 g/L of resin for Amberlite IRA67.

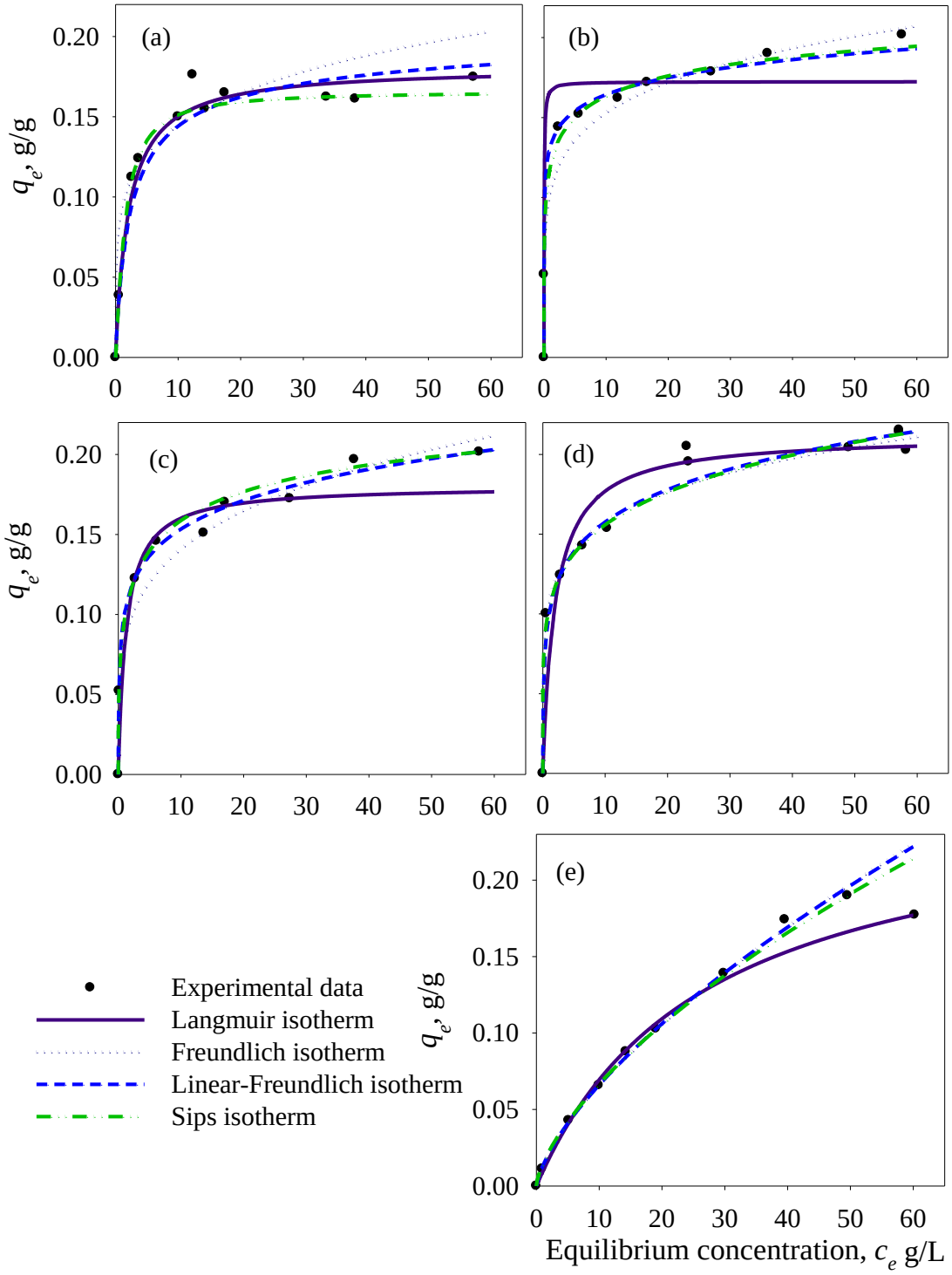

Figure 4.3: Acetic acid isotherm model fit using nonlinear estimation method for (a) GAC, (b) Amberlite IRA67, (c) Amberlite IRA96, (d) Purolite A835, and (e) Reillex 425 at temperature of 21°C

In another study, a maximum adsorption capacity of 0.2 g/g was obtained for lactic acid adsorption on Amberlite IRA 96 resin for equilibrium concentrations of lactic acid > 100 g/L (Bishai et al., 2015). Moldes et al., (2003) used Amberlite IRA96 to recover lactic acid from fermentation broth with the pH adjusted to 4.85. In their study, q_m and K were obtained as 0.27 g/g and 0.0217 L/g respectively for equilibrium concentration of lactic acid up to 125 g/L. The low value of K obtained appears to be due to the interference of ions caused from the addition of alkali.

In the Langmuir isotherm, q_m represents the monolayer capacity of the adsorbate on the adsorbent and K represents the affinity of adsorption. For the adsorption of acetic acid on Reillex 425, q_m and K were obtained as 0.26 g/g and 0.037 L/g respectively. Comparing the K values among the different sorbents, Reillex 425 shows the least affinity for the adsorption of acetic acid. Kaufman et al., (1994) showed that Reillex 425 had the least adsorption capacity of 0.04 g/g at pH 2.5 compared to weak base resins of different basicities. However, Reillex 425 had stable uptake capacities for five sorption and desorption cycles when either hot water or methanol were used as regenerants. Tung et al., (1993) compared the adsorption equilibria of lactic and succinic acids on resins of different basicities and Reillex 425 showed least affinity compared to other resins. Evangelista (1994) studied the adsorption equilibrium of lactic acid on Reillex 425 at pH 2.8 and 4.8 and only Langmuir isotherm was used to fit the experimental data. Reillex 425 showed a linear trend for the sorption of lactic acid and gave the least value for K compared to other resins at both the pH values.

Tung (1993) reported that the Langmuir isotherm parameter, K, is correlated to the pKa of the resin. The greater the basicity of the resin, the greater is the affinity of the sorbent to the organic acid. Hence, Table 4.1 shows that the order of basicity of resins will be Amberlite IRA67

> Amberlite IRA96 > Purolite A835 > Reillex 425. This trend is in order with the p*K*a values reported for Amberlite IRA67 and Reillex 425. The p*K*a of Amberlite IRA96 and Purolite A835 are not reported in the literature.

For Purolite A835, the Langmuir isotherm constants q_m and K were obtained as 0.212 g/g and 0.506 L/g respectively for acetic acid, and 0.24 g/g and 3.57 L/g respectively for lactic acid (Figure 4.4; Table 4.2). There have been no previous studies reported on the adsorption of organic acids on Purolite A835 and this data provides new information that will be useful in the design of adsorption processes for the recovery of organic acids from dilute aqueous solutions. The K value obtained from the Langmuir isotherm constants shows that Purolite A835 has greater affinity for the adsorption of lactic acid compared to acetic acid. This is because lactic acid is a relatively stronger acid (p*K*a = 3.86) compared to acetic acid (p*K*a = 4.76).

4.3 Multicomponent adsorption equilibria

The experimental isotherm data, model fits, and predictions for the multicomponent adsorption equilibria of acetic and lactic acid are shown in Figure 4.5. The isotherm parameters obtained for the multicomponent sorption of acetic and lactic acid are given in Table 4.2. The experimental data shows that lactic acid has high sorption capacity and affinity compared to acetic acid for the adsorption on Purolite A835 resin. The IAST model predictions were obtained by solving Equations (2.32) to (2.35) using the Newton-Raphson method for each binary data point. This model gave reasonable prediction for the adsorption of lactic acid at low concentrations, but at higher concentrations the adsorption affinity and capacity were overestimated. On the other hand, it gave poor predictions for equilibrium adsorption of acetic acid from binary mixtures. In single component adsorption equilibria, lactic acid had higher affinity and capacity for adsorption on Purolite A835 compared to acetic acid. This shows that

IAST gave poor prediction for the adsorption of weakly adsorbed component i.e., acetic acid, compared to lactic acid. The extended Langmuir isotherm model (Equation (2.26)) gave poor predictions for acetic and lactic acid adsorption on Purolite A835. On the other hand, the modified extended Langmuir isotherm model (Equation (2.27)) gave a good fit for the experimental data. The *K* values were obtained as 0.35 and 0.74 for acetic and lactic acids respectively. This shows that in binary mixtures the adsorption affinity for lactic acid on Purolite A835 is higher when compared to acetic acid.

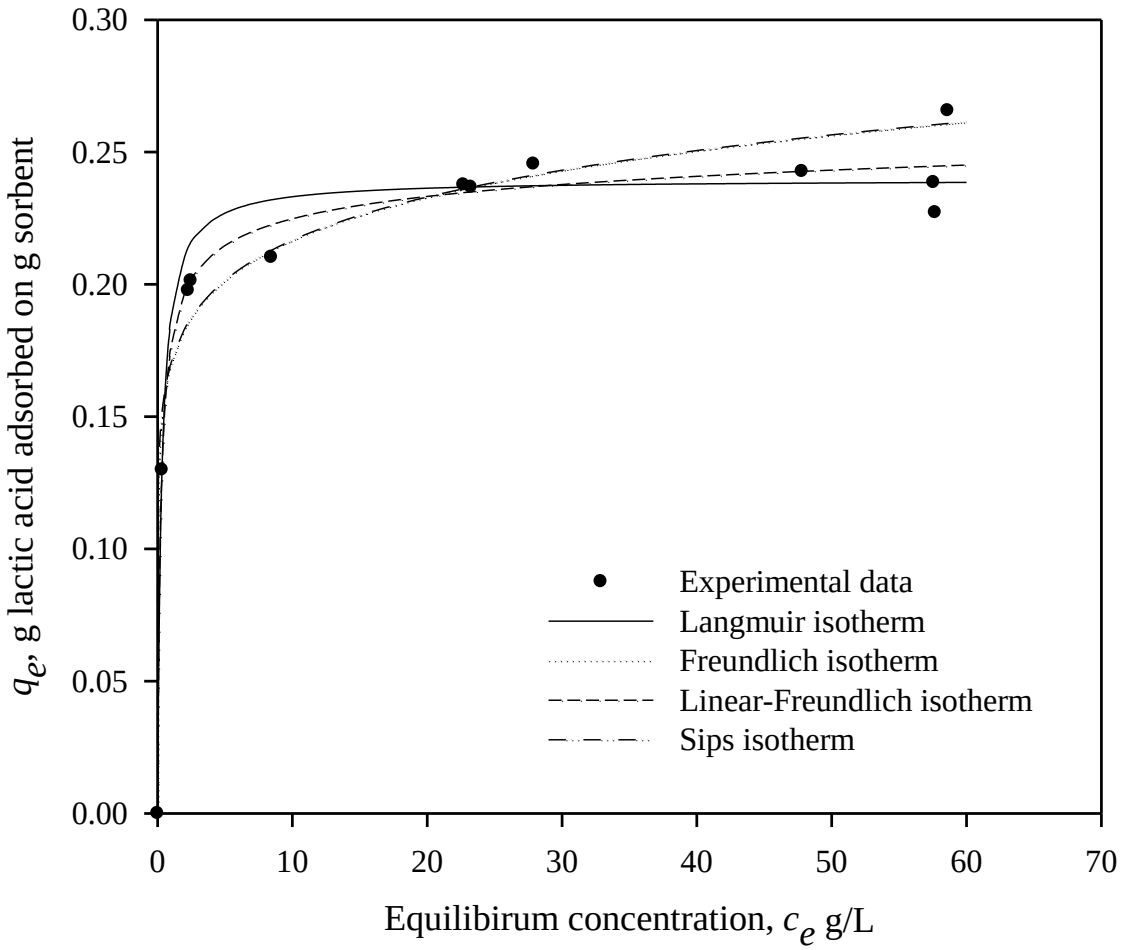

Figure 4.4: Lactic acid isotherm model fit using nonlinear estimation method for Purolite A835 at temperature of 21ºC

Table 4.2: Single component isotherm constants for sorption of acetic and lactic acids on Purolite A835, and multicomponent equilibria constants using modified extended Langmuir isotherm model at pH range of 2-2.8 , and a temperature of 21^{o}C

	Single component		Multicomponent	
	Acetic acid	Lactic acid	Acetic acid	Lactic acid
Langmuir				
q_m	0.212	0.24	0.21	0.24
K	0.506	3.57	0.35	0.74
ARE	9.1	3.9	33.5	23.36
Freundlich				
K_F	0.109	0.17		
n	0.161	0.1		
ARE	3.6	5.4		
Linear-Freundlich				
a	1.11	1.1		
b	10.25	5.24		
β	0.83	0.96		
ARE	4.3	2.5		
Sips				
a	0.104	0.17		
b	0.003	0.003		
γ	0.18	0.105		
ARE	3.5	5.4		

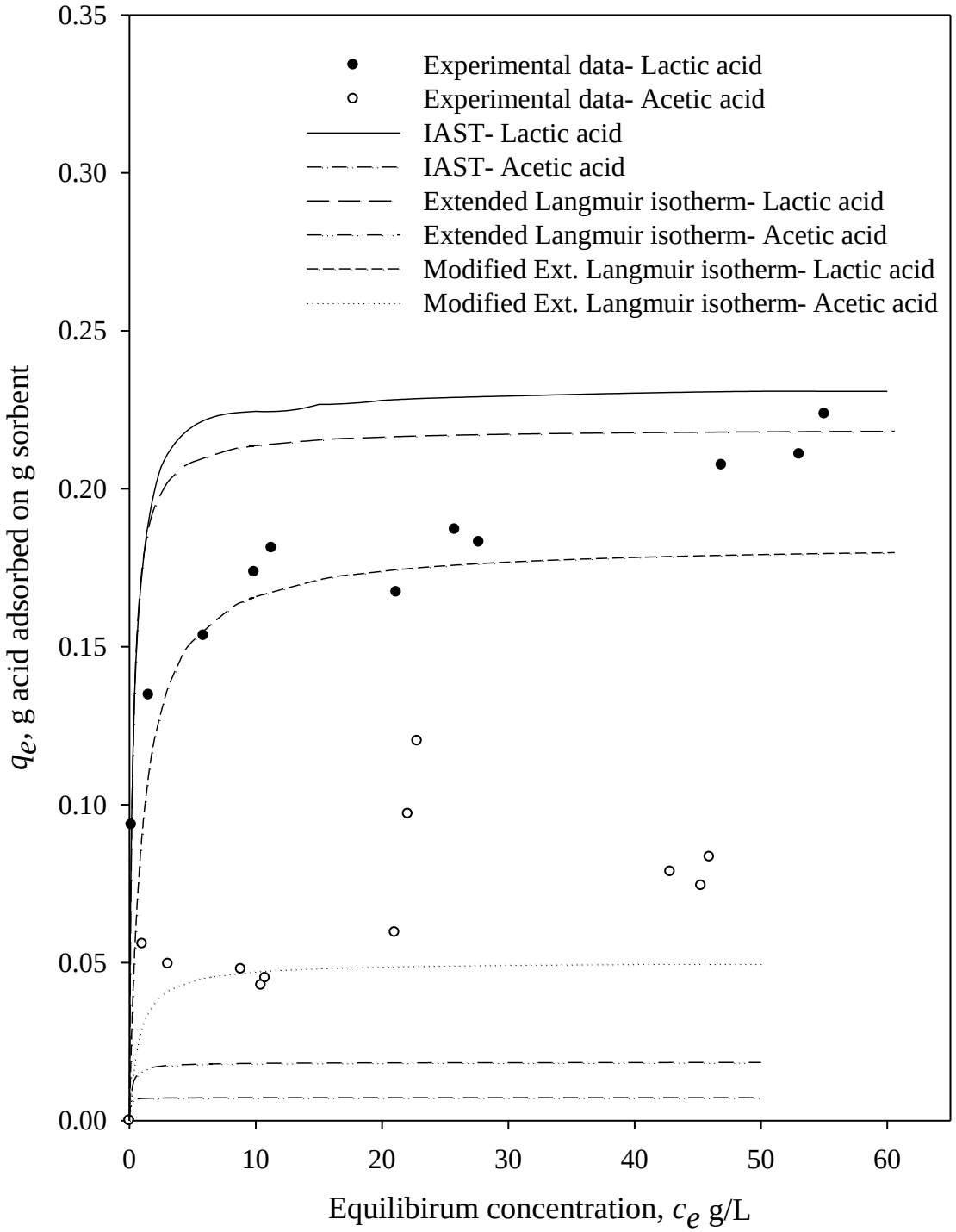

Figure 4.5: Isotherm models for multicomponent solution of acetic and lactic acids on Purolite A835 at pH range of 2-2.8, and a temperature of 21ºC

4.4 Comparative data on adsorption of product acids from fermentation broth and simulated fermentation broth

These studies were conducted in order to determine the effect of functional group of the sorbents on the percentage removal of various fermentation broth components. Amberlite IRA67 and Amberlite IRA96 have same functional groups and percentage water retention (Table 3.1). Hence, Purolite A835, Reillex 425, and GAC were chosen for these studies.

In the adsorption studies using the synthetic mixture solution at an initial pH of 2.2, Purolite A835 showed the following order for the percentage adsorption for the compoents: lactic acid > acetic acid > ethanol > propylene glycol > lactose (Figure 4.6(a)). There was 17.4% adsorption for lactic acid at a dose of 0.5 g and it increased to 37.6% with an increase in dose to 1.5 g. Due to the competitive effect between lactic acid and acetic acid, the percentage adsorption for acetic acid was only 4.92% and 13.19% for 0.5 g and 1.5 g of resin respectively. The order of percentage adsorption for Reillex 425 also follows the same trend as Purolite A835 adsorption of lactic acid > acetic acid > ethanol > propylene glycol > lactose (Figure 4.6(a)), but the percentage adsorption was lower due to its low affinity and sorption capacity. The percentage adsorption for lactic acid was 4.42% and 14.04% at resin doses of 0.5 g and 1.5 g respectively. Unlike Purolite A835, Reillex 425 had higher percentage removal by sorption for propylene glycol and ethanol. This is due to its low selectivity for organic acids and high swelling nature. It was reported that Reillex 425 shows poor selectivity for organic acid over glucose due to its high swelling nature (Dai and King, 1996). However, the percentage water retention is higher for Purolite A835 compared to Reillex 425 (Table 3.1). GAC was nonspecific to organic acids and the order of percentage adsorption was as following: lactose > lactic acid > acetic acid > propylene glycol > ethanol.

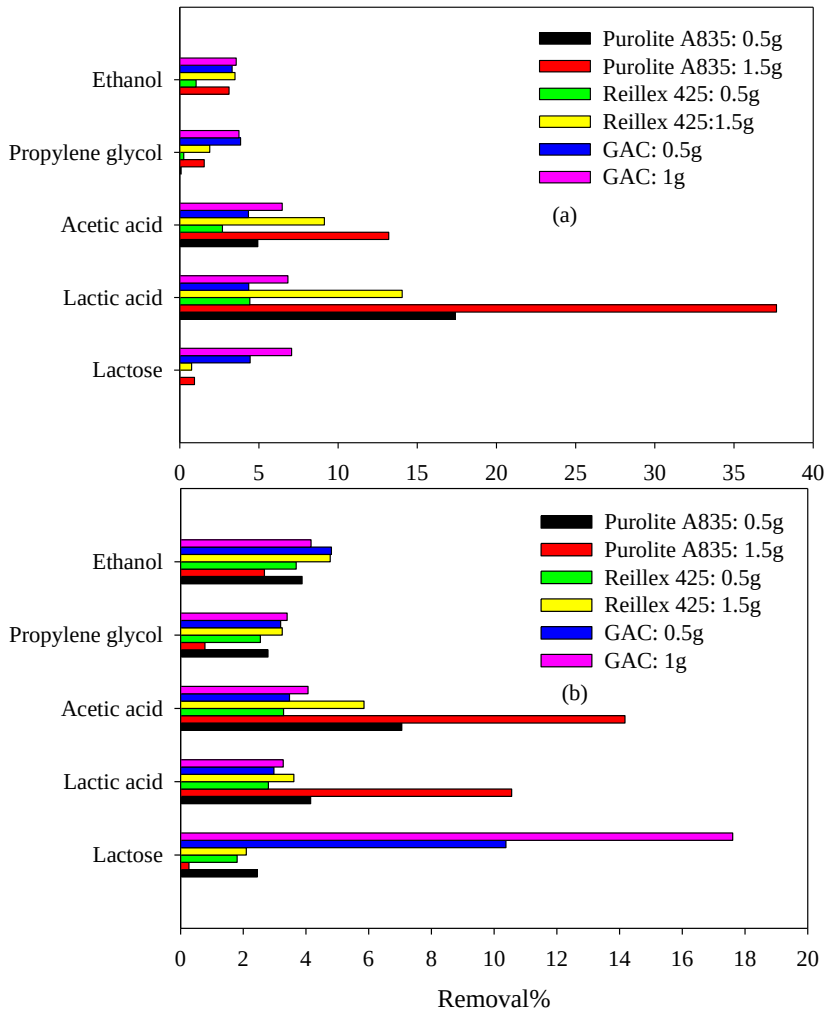

Figure 4.6: Percentage removal of various components in the simulated fermentation broth at pH of (a) 2.2, and (b) 4.8 at temperature of 21 ^{o}C

The pH of the synthetic solution was adjusted to 4.8 to take advantage of the selective adsorption of acetic acid over lactic acid. At this pH, Purolite A835 had higher sorption capacity for acetic acid compared to lactic acid (Figure 4.6(b)). The order of percentage removal for the other components was same as that obtained for solution at pH 2.2 (Figure 4.6(a)). At higher resin dose of 1.5 g, with higher sorption of the organic acids, the percentage adsorption of the rest of the components decreased. Reillex 425 had high specificity to acetic acid when compared to lactic acid at both the resin doses, and the order of percentage adsorption was: acetic acid >

ethanol > lactic acid > propylene glycol > lactose. At pH 4.8, ~50% of acetic acid in the solutions is in the undissociated form, but 90% of the lactic acid is in dissociated from. Since, weak base resins specifically adsorb organic acids in their undissociated form, both resins had higher percentage removal for acetic acid compared to lactic acid. The adsorption on GAC at the solution pH of 4.8 was quite different. There was higher percentage adsorption of lactose compared to all other components. The q_{max} for lactose on activated carbon was found to be 0.24 g/g, which is much higher than that of acetic acid obtained in this study (Lee et al., 2004).

Adsorption studies using fermentation broth at pH 4.2 and with pH adjusted to 4.8 were done. The percentage adsorption in Purolite A835 at a pH of 4.2 was in the following order: acetic acid > lactic acid > lactose > propylene glycol > ethanol (Figure 4.7(a)). The percentage removal was in the same order for Reillex 425, except for the minor components where percentage removal was in the order: propylene glycol > ethanol > lactose. The higher adsorption for acetic acid is due to its dominance in the undissociated acid form over lactic acid at a pH of 4.2. The adsorption of various components of the fermentation broth on GAC was nonspecific to organic acids (Figure 4.7(a)). When the initial pH of fermentation broth was adjusted to pH 4.8 (Figure 4.7(b)), the order of adsorption of the different components in fermentation broth in all the sorbents were similar to that of the adsorption in synthetic mixture solution with pH adjusted to 4.8 (Figure 4.7(b)). But in all the sorbents, the percentage adsorption from fermentation broth decreased when compared to that of the synthetic mixture solution. This is because of the interference from other components like the yeast extract and color compounds present in the broth. However, as Purolite A835 resin shows high sorption capacity and specificity to organic acids in simulated and real fermentation broths, there is a potential of this resin for use in fixed-bed adsorbers to recover and separate these acids.

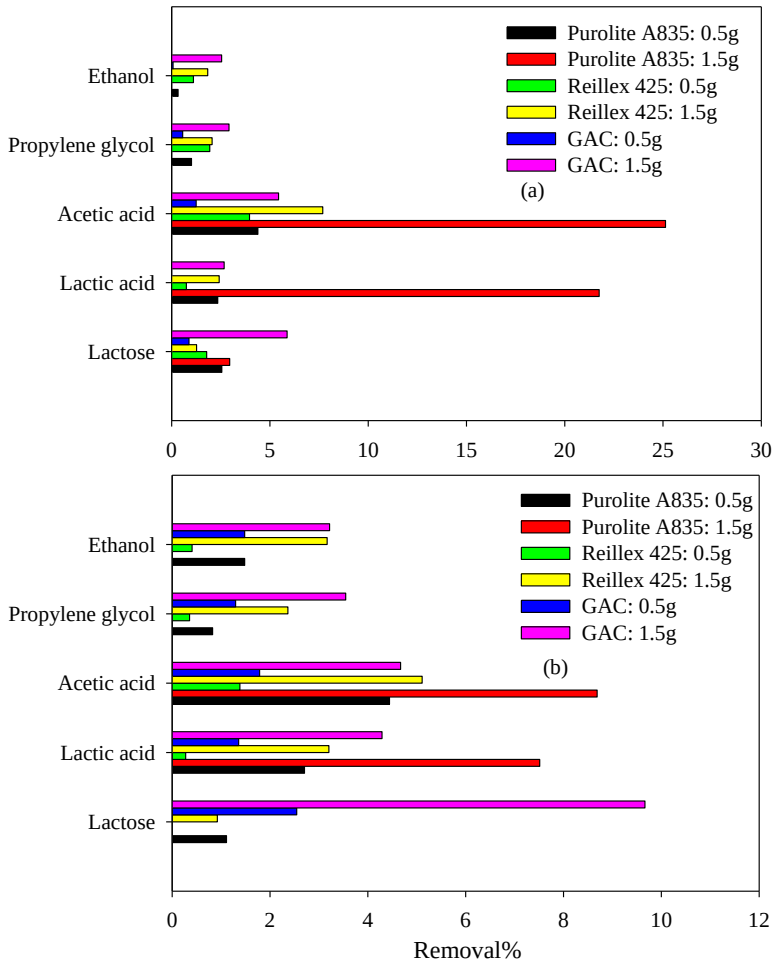

Figure 4.7: Percentage removal of various components in the fermentation broth at pH of (a) 4.2, and (b) 4.8 at temperature of 21 ^{o}C

The final color of fermentation broth after sorption using 1.5 g each of Purolite A835, Reillex 425, and GAC compared to the heat-treated fermentation broth is shown in Figure 4.8. The order for percentage color removal for the different sorbents is as follows: GAC (90%) > Reillex 425 (40%) > Purolite A835 (36%). GAC was very efficient in color removal mainly due to its high surface area and porosity.

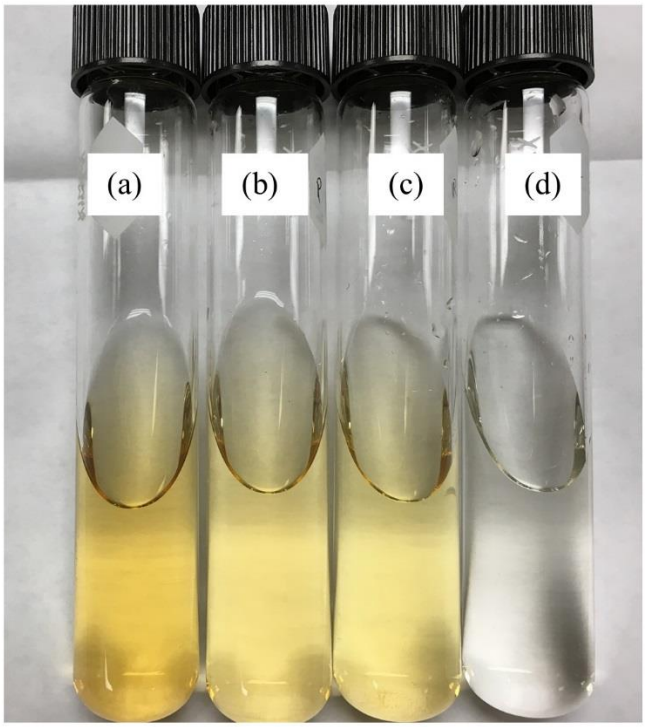

Figure 4.8: Color of 50 ml (a) fermentation broth after adsorption on 1.5 g each of (b) Purolite A835, (c) Reillex 425, and (d) GAC at pH 4.8 at temperature of 21 ºC

4.5 External mass transfer coefficient and intraparticle diffusivity

In batch adsorption kinetics, the rate of solute uptake by the sorbent in the initial time period is controlled essentially by the external mass transfer resistance. The external mass transfer resistance coefficient, k_f, can be determined from the following equation:

$$k_f = \frac{\rho_p r_p}{3W} \frac{ln\left(\frac{C_0}{C}\right)}{t} \tag{4.1}$$

Equation (4.1) is valid only in the initial time period where the surface concentration is negligible and at low mixing intensities. For large values of power input or high intensity mixing, intraparticle diffusion becomes controlling. In a batch reactor with isothermal single component sorption and micropore diffusion control, the transport of adsorbate in the solid phase of a spherical particle and constant intraparticle diffusivity is given by:

$$\frac{\partial q}{\partial t} = D_c \left(\frac{\partial^2 q}{\partial r^2} + \frac{2}{r}\frac{\partial q}{\partial r}\right) \tag{4.2}$$

In the case of an infinite bath system when the sorbate concentration in the bulk phase remains constant, the following initial and boundary conditions apply:

$$q(r,0) = q_0' \tag{4.3}$$

$$q(r_c,t) = q_0 \tag{4.4}$$

$$\left(\frac{\partial q}{\partial r}\right)_{r=0} = 0 \tag{4.5}$$

The solution to the above equations in terms of uptake of solute by the sorbent is given as (Ruthven, 1984):

$$\frac{\bar{q}-q_0'}{q_0-q_0'} = \frac{m_t}{m_\infty} = 1 - \frac{6}{\pi^2}\sum_{n=1}^{\infty}\frac{1}{n^2}exp^{\left(-\frac{n^2\pi^2 D_c t}{r_c^2}\right)} \tag{4.6}$$

In the long-time region, at an uptake of greater than ~ 70%, Equation (4.6) reduces to

$$1 - \frac{m_t}{m_\infty} \approx \frac{6}{\pi^2}exp^{\left(-\frac{\pi^2 D_c t}{r_c^2}\right)} \tag{4.7}$$

A plot of ln (1-m_t/m_∞) versus t will give a straight line with slope $-\pi^2 D_c/r_c^2$ and intercept ln ($6/\pi^2$). In the case of a finite bath system where the surface concentration varies with time, the above equations can be used if the fraction of sorbent ultimately adsorbed by the sorbent, α (Equation (4.8)) is approximately < 0.1.

$$\alpha = \frac{C_0 - C_\infty}{C_0} \tag{4.8}$$

For α > 0.1, the intraparticle diffusivity can be determined from Equations (4.9) and (4.10) proposed by Crank (1975).

$$\frac{m_t}{m_\infty} = 1 - 6\sum_{n=1}^{\infty}\frac{exp^{\left(-\frac{p_n^2 D_c t}{r_c^2}\right)}}{\frac{9\alpha}{(1-\alpha)}+(1-\alpha)p_n^2} \tag{4.9}$$

The value of p_n is given by the nonzero roots of the equation below:

$$tan\, p_n = \frac{3p_n}{3+\left(\frac{1}{\alpha}-1\right)p_n^2} \tag{4.10}$$

Equations (4.9) and (4.10) were solved in Microsoft Excel 2013 software as outlined below:

1. For a given value of α, determine the nonzero roots of the Equation (4.10) using Newton's method with $n\pi$ as starting value.
2. At each experimental data point at time interval t, calculate the m_t/m_∞ values based on an assumed value of D_c.
3. The intraparticle diffusivity was determined by curve fitting using the generalized reduced gradient algorithm, targeted to reduce the ARE between the experimental $m_t/m_{\infty,e}$ and predicted $m_t/m_{\infty,p}$ values, in the Solver add-in of Microsoft Excel 2013.

The ARE is defined as:

$$Average\ relative\ error = \sum_{i=1}^{n} \left| \frac{\frac{m_t}{m_\infty},e - \frac{m_t}{m_\infty},p}{\frac{m_t}{m_\infty},e} \right| * \frac{100}{n} \tag{4.11}$$

4.6 Determination of adsorption kinetic parameters

Adsorption kinetic studies were conducted using a variety of carbonaceous and resin sorbent matrices including GAC, Amberlite IRA67, and Amberlite IRA96. Reillex 425 was not used because the resin disintegrated into fine powder when used in the batch mixer.

Figure 4.9(a) shows the concentration profile of acetic acid with time for the sorbents used in this study. All three sorbents showed a common pattern of rapid decrease in concentration within the first few minutes followed by little or no change in concentration over the remaining time towards saturation. The k_f is estimated using Equation (4.1) and the D_c is obtained using Equation (4.7) and Equation (4.9). The values are given in Table 4.3. When same initial concentrations were used, the k_f of GAC was lower compared to the resins. The low sorption capacity of GAC and the low sorbent to solute ratio of 0.375 g/L used to effectively suspend the denser GAC particles resulted in the lower uptake capacity. In the case of the Amberlite resins, when same sorbent to solute ratio of 5 g/L was used, the k_f of Amberlite IRA67

was higher than that of the Amberlite IRA96. In a study on batch adsorption kinetics of lactic acid on four Amberlite resins, namely Amberlite IRA67, Amberlite IRA96, Amberlite IRA400, and Amberlite IRA900, the overall mass transfer coefficient, K_c, obtained from the linear driving force model was reported to be higher for the Amberlite IRA67 than the other resins (Moldes et al., 2003).

Table 4.3: Mass transfer coefficients and intraparticle diffusivities estimated from uptake rate data for acetic acid sorption on GAC and weak base anion exchange resins at temperature of 21^{o}C

	GAC	Amberlite IRA67	Amberlite IRA96
k_f (cm/sec)	1.98E-3	5.33E-3	2.72E-3
D_c (cm^2/sec) Equation (4.7)	1.59E-7	0.530E-7	0.537E-7
D_c (cm^2/sec) Equation (4.9)	1.94E-7	0.158E-7	0.304E-7
ARE	1.17	11.23	11.08

The plots obtained for determining the D_c values for the linearized equation of infinite bath system (Equation (4.7)) and the nonlinear finite bath system (Equation (4.9)) are shown in Figure 4.9(b) and Figure 4.9(c) respectively. The gel resins such as Amberlite IRA67 show slower diffusion kinetics and have lower D_c values compared to the macroreticular resins such as Amberlite IRA96. The D_c values obtained from Equation (4.7) and (4.9) differ as Equation (4.7) is valid only for infinite volume systems, and when $\alpha < 0.1$. It will lead to erroneous apparent diffusivities when used for finite volume systems (Ruthven, 1984). For GAC, α was 0.15, and the D_c obtained from the finite system equation is 22% higher than that from the infinite volume system equation. But, the values obtained for Amberlite resins are much more different from each other as α values were 0.69 and 0.45 for Amberltie IRA67 and Amberltie IRA96, respectively.

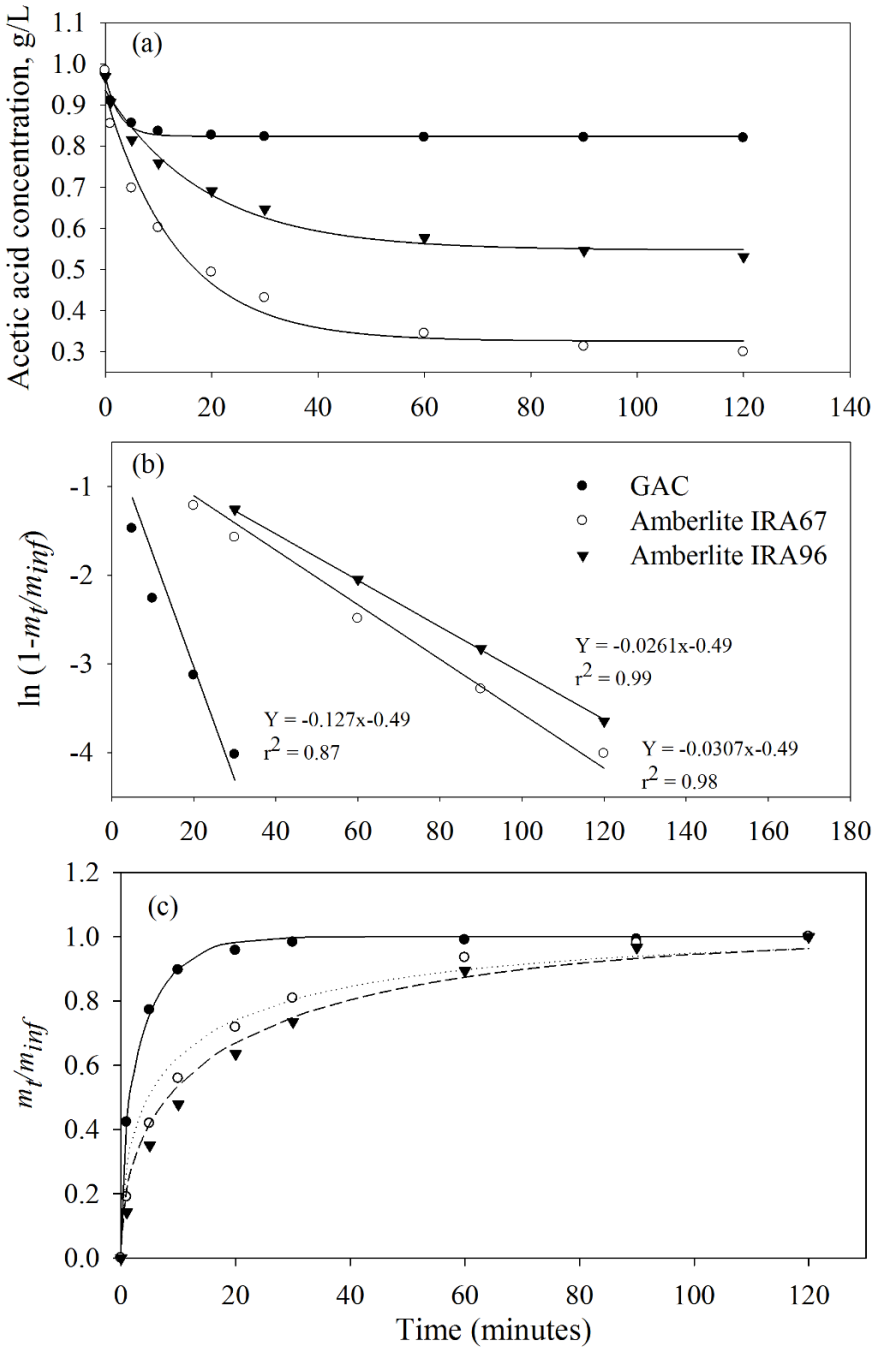

Figure 4.9: Acetic acid adsorption kinetics for GAC and weak base resins (a) experimental data at a pH of 3.28, and a temperature of 21°C, (b) intraparticle diffusivity determination using infinite bath system equation, and (c) intraparticle diffusivity determination using finite bath system equation

The number of roots obtained for Equation (4.10) also determines the goodness of fit. Figure 4.9(c) shows the fit obtained using Equation (4.9) and the experimental data points. At time t = 0, the Equation (4.9) of m_t/m_∞ will tend to zero only when we add infinite number of roots to it. The best possible method is to obtain a good number of roots until the point where the error between the experimental and predicted values is minimum and addition of further roots will not give a significant change in the error.

The Biot numbers estimated with the D_c values obtained from Equation (4.9) were 9.68, 77.53, and 32.43 for GAC, Amberltie IRA67, and Amberlite IRA96, respectively. This shows that the adsorption of acetic acid is controlled by both external mass transfer and intraparticle diffusion in GAC and by intraparticle diffusion alone in the weak base anion exchange resins at an initial concentration of 1 g/L. Jiao et al. (2015) used a Biot number with dimensionless solute and sorbent concentrations to determine the rate controlling mechanism in acetone-butanol-ethanol adsorption on polystyrene diethylbenzene resin with mesopores and micropores. The Biot number for all the components were > 10 and pore diffusion was found to be the controlling mechanism for adsorption.

The estimated values of D_c were validated by developing model predictions using Equation (4.9) for new sets of experimental data with α of 0.18, 0.28, and 0.6 for GAC, Amberlite IRA67, and Amberlite IRA96 respectively. For GAC, using the estimated D_c value of $1.94*10^{-7}$ cm^2/sec for predicting batch kinetic experimental data using Equation (4.9) resulted in a good trend with an ARE of 3.84 as shown in Figure 4.10. For Amberlite resins, the error for prediction is higher as α values are different between the datasets and this shows the effect of isotherm nonlinearity on intraparticle diffusivity.

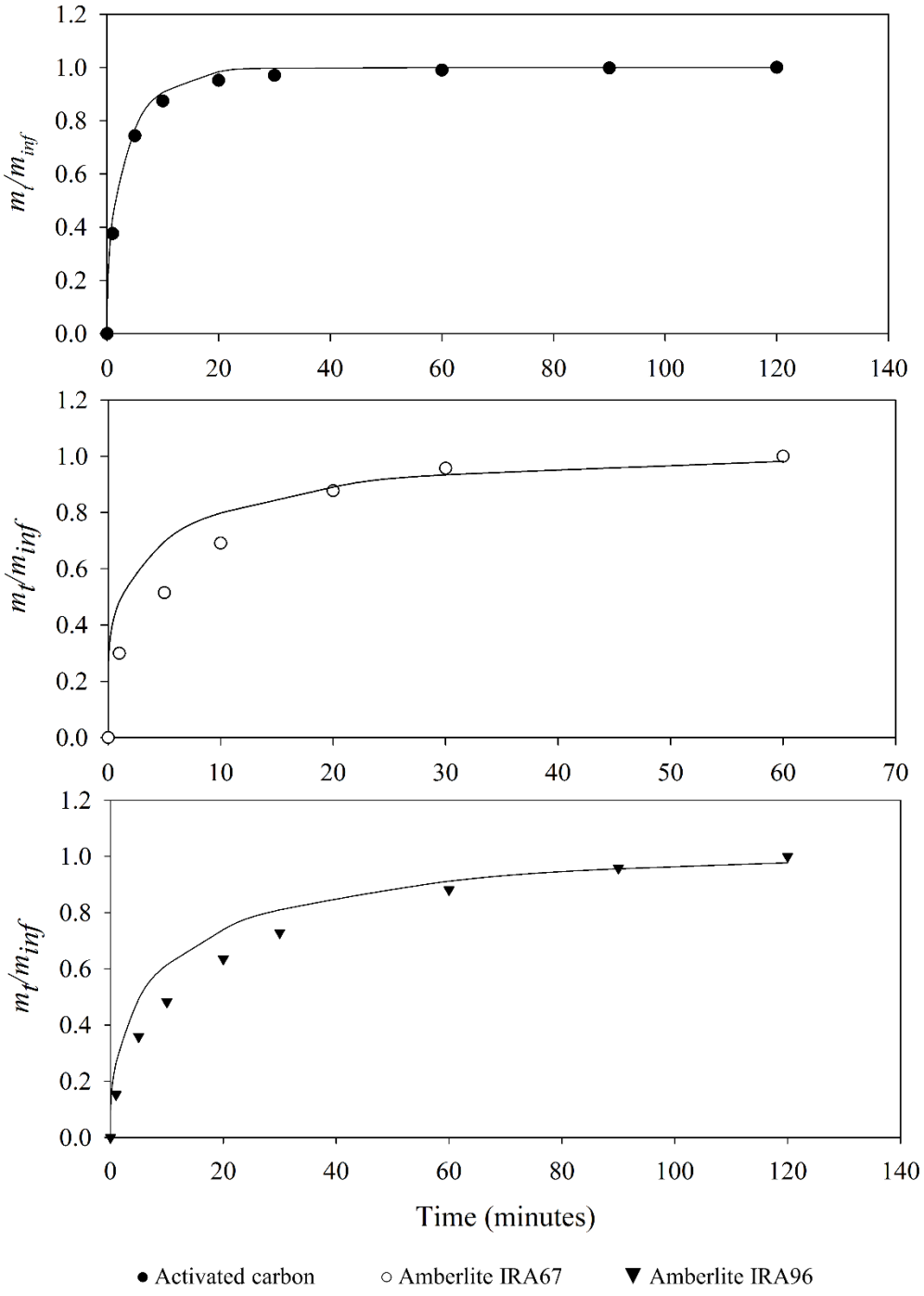

Figure 4.10: Model predictions for acetic acid uptake rate using intraparticle diffusivity obtained from the finite bath model at temperature of 21^{o}C

It is important to note that Equation (4.9) was derived from the PDE in Equation (4.2) based on the assumptions that the uptake curve is measured over a small differential step and that α relates the concentration of solute in the solution to that in the solid phase (Crank, 1975). The diffusion coefficient determined through this method can be used to simulate batch kinetics and fixed-bed breakthrough curves. However, if the uptake curve is measured over a large differential changes in concentration, the effects of isotherm nonlinearity should be accounted for in the model.

The effect of accuracy in the determination of rate parameters was reported by Mathews and Weber (1977), in a study on adsorption of dodecyl benzene sulfonate on activated carbon. A 20% decrease in the k_f value resulted in a 33% decrease in the predicted solute concentration with respect to the actual concentration. This effect is predominant in systems that are controlled by external mass transfer resistance. Also, if intraparticle diffusion is neglected, then the resulting concentration versus time profile will be higher than the actual profile. The accurate determination of k_f and D_c is important in adsorption modeling, especially for scaling up the process for further batch or column studies and inconsistencies in their determination will result in erroneous kinetic or breakthrough curves.

REFERENCES

Arcanjo, M.R.A., Fernandes, F.A.N., Silva, I.J., 2015. Separation of lactic acid produced by hydrothermal conversion of glycerol using ion-exchange chromatography. Adsorption Science & Technology 33, 139–151. https://doi.org/10.1260/0263-6174.33.2.139

Bishai, M., De, S., Adhikari, B., Banerjee, R., 2015. A platform technology of recovery of lactic acid from a fermentation broth of novel substrate *Zizyphus oenophlia*. 3 Biotech 5, 455–463. https://doi.org/10.1007/s13205-014-0240-y

Crank, J., 1975. The Mathematics of Diffusion. Clarendon Press.

da Silva, A.H., Miranda, E.A., 2013. Adsorption/desorption of organic acids onto different adsorbents for their recovery from fermentation broths. J. Chem. Eng. Data 58, 1454–1463. https://doi.org/10.1021/je3008759

Dai, Y.; King, C. J. Selectivity between lactic acid and glucose during recovery of lactic acid with basic extractants and polymeric sorbents. Ind. Eng. Chem. Res. 1996, 35, 1215–1224.

Eregowda, T., Rene, E.R., Rintala, J., Lens, P.N.L., 2019. Volatile fatty acid adsorption on anion exchange resins: Kinetics and selective recovery of acetic acid. Separation Science and Technology 0, 1–13. https://doi.org/10.1080/01496395.2019.1600553

Evangelista, R.L., 1994. Recovery and Purification of Lactic Acid from Fermentation Broth by Adsorption. Iowa State University.

Gao, Q., Liu, F., Zhang, T., Zhang, J., Jia, S., Yu, C., Jiang, K., Gao, N., 2010. The role of lactic acid adsorption by ion exchange chromatography. PLoS One 5. https://doi.org/10.1371/journal.pone.0013948

Garrett, B.G., Srinivas, K., Ahring, B.K., 2015. Performance and stability of Amberlite^{TM} IRA-67 ion exchange resin for product extraction and pH control during homolactic fermentation of corn stover sugars. Biochemical Engineering Journal 94, 1–8. https://doi.org/10.1016/j.bej.2014.11.004

Gluszcz, P., Jamroz, T., Sencio, B., Ledakowicz, S., 2004. Equilibrium and dynamic investigations of organic acids adsorption onto ion-exchange resins. Bioprocess Biosyst Eng 26, 185–190. https://doi.org/10.1007/s00449-003-0348-7

Jiao, P., Wu, J., Zhou, J., Yang, P., Zhuang, W., Chen, Y., Zhu, C., Guo, T., Ying, H., 2015. Mathematical modeling of the competitive sorption dynamics of acetone–butanol–ethanol on KA-I resin in a fixed-bed column. Adsorption 21, 165–176. https://doi.org/10.1007/s10450-015-9659-7

Kaufman, E.N., Cooper, S.P., Davison, B.H., 1994. Screening of resins for use in a biparticle fluidized-bed bioreactor for the continuous fermentation and separation of lactic acid. Appl. Biochem. Biotechnol. 45–46, 545–554. https://doi.org/10.1007/BF02941829

Lee, J.W.; Kwon, T.O.; Moon, I.S. Adsorption of monosaccharides, disaccharides, and maltooligosaccharides on activated carbon for separation of maltopentaose. Carbon 2004, 42, 371–380.

Matsuda, N., Agui, W., Ogino, K., Kawashima, N., Watanabe, T., Sakai, H., Abe, M., 1996. Disinfection of viable *Pseudomonas stutzeri* in ultrapure water with ion exchange resins. Colloids and Surfaces B: Biointerfaces 7, 91–100. https://doi.org/10.1016/0927-7765(96)01285-4

Mathews, A.P., Weber, Jr., W.J., 1977. Effects of external mass transfer and intraparticle diffusion on adsorption rates in slurry reactors. AIChE Symp. Ser. 73, 91–98.

Moldes, A.B., Alonso, J.L., Parajó, J.C., 2003. Recovery of lactic acid from simultaneous saccharification and fermentation media using anion exchange resins. Bioprocess Biosyst Eng 25, 357–363. https://doi.org/10.1007/s00449-002-0316-7

Ruthven, D.M., 1984. Principles of Adsorption and Adsorption Processes. John Wiley & Sons.

Tung, L.A., 1993. Recovery of carboxylic acids at pH greater than p*K*a (No. LBL--34669, 10125672). https://doi.org/10.2172/10125672

Wawrzkiewicz, M., Hubicki, Z., 2015. Anion exchange resins as effective sorbents for removal of acid, reactive, and direct dyes from textile wastewaters. https://doi.org/10.5772/60952

Yousuf, A., Bonk, F., Bastidas-Oyanedel, J.-R., Schmidt, J.E., 2016. Recovery of carboxylic acids produced during dark fermentation of food waste by adsorption on Amberlite IRA-67 and activated carbon. Bioresource Technology 217, 137–140. https://doi.org/10.1016/j.biortech.2016.02.035

Chapter 5
Single Component Adsorption Dynamics in Stratified Beds

5.1 Introduction

The overall rate of adsorption and thus the bed capacity utilization is determined by adsorption equilibrium, kinetics, bed geometry, and sorbent properties. The bed capacity utilization of a fixed-bed adsorber is a major determinant factor in the cycle time for adsorption/regeneration operations and the operating costs. This chapter evaluates the effect of bed geometry and particle stratification on solute front movement and adsorption dynamics in fixed-bed adsorbers. The details of mathematical model used for predicting the adsorption dynamics are also presented in this chapter. In addition, sensitivity analyses of the model are presented. This will enable the prediction of adsorption dynamics and the optimization of process conditions, thus avoiding excessive experimentation costs.

5.2 Mathematical model

A mathematical solution of the general rate model is used to simulate the adsorption dynamics of acetic acid in fixed-bed adsorbers with Purolite A835 and GAC. The general rate model is rigorous and gives a more accurate representation of adsorption dynamics by including axial dispersion, mass transfer resistances, and nonlinear equilibrium isotherm conditions (Gu, 1995). The model equations are given in section 2.6.3.2. The variables in the model equations, c, c_p, and q_p, are converted to dimensionless variables using the initial concentration of solute in the liquid phase, c_0, as the reference as:

$$C = c/c_0 \tag{5.1}$$

$$C_p = c_p/c_0 \tag{5.2}$$

$$Q_p = q_p/c_0 \tag{5.3}$$

The axial and radial coordinates, *x* and *r*, are converted into their dimensionless forms by using length of the column, *L*, and radius of the particle, r_p, respectively as reference as follows:

$$X = x/L \tag{5.4}$$

$$R = r/r_p \tag{5.5}$$

The time variable, *t*, is converted to dimensionless time, τ, by using length of the column, *L*, and interstitial velocity, *v*, as the reference as:

$$\tau = tv/L \tag{5.6}$$

The model equations given in section 2.6.3.2 are then converted to the following dimensionless equations:

$$-\frac{1}{Pe}\frac{\partial^2 C}{\partial X^2} + \frac{\partial C}{\partial X} + \frac{\partial C}{\partial \tau} + \left(\frac{1-\varepsilon_b}{\varepsilon_b}\right) St\left(C - C_{p,R=1}\right) = 0 \tag{5.7}$$

$$\varepsilon_p \frac{\partial C_p}{\partial \tau} + \rho_p \frac{\partial Q_p}{\partial \tau} = \frac{St}{3Bi}\left(\frac{2}{R}\frac{\partial C_p}{\partial R} + \frac{\partial^2 C_p}{\partial R^2}\right) \tag{5.8}$$

The dimensionless parameters obtained from grouping the variables in the dimensionless model equations are defined as:

$$Pe = \frac{vL}{D_L} \tag{5.9}$$

$$St = \frac{3Lk_f}{vr_p} \tag{5.10}$$

$$Bi = \frac{r_p k_f}{\varepsilon_p D_p} \tag{5.11}$$

The corresponding initial and boundary conditions for the dimensionless liquid phase and pore phase mass balance equations are as follows:

$$0 < X < 1, \tau = 0: C = 0 \tag{5.12}$$

$$X = 0, \tau > 0: \frac{1}{Pe}\frac{\partial C}{\partial X} = C_{X=0} - 1 \tag{5.13}$$

$$X = 1, \tau > 0: \frac{\partial C}{\partial X} = 0 \tag{5.14}$$

$$0 < R < 1, \tau = 0: C_p = 0, Q_p = 0 \tag{5.15}$$

$$R = 0, \tau > 0: \frac{\partial C_p}{\partial R} = 0 \tag{5.16}$$

$$R = 1, \tau > 0: \frac{\partial C_p}{\partial R} = Bi\left(C - C_{p,R=1}\right) \tag{5.17}$$

The Langmuir isotherm in its dimensionless form is given by:

$$Q_p = \frac{qmKC_p}{1+KC_pc_0} \tag{5.18}$$

5.3 Correlations used for the determination of model parameters

The axial dispersion coefficient, D_L, is estimated as (Suzuki and Smith, 1972):

$$D_L = 0.44D_m + 0.83Ud_p \tag{5.19}$$

The molecular diffusion coefficient, D_m, of acetic acid in water is estimated using the Wilke-Chang (1955) correlation:

$$D_m = \frac{7.4 \text{ X } 10^{-8}(\varphi M_B)^{1/2}T}{\eta_B V_A^{0.6}} \tag{5.20}$$

The external mass transfer coefficient, k_f, was estimated from Dwivedi and Upadhyay (1977) correlation as:

$$k_f = \frac{v}{Sc^{2/3}}\left\{\frac{0.765}{Re^{0.82}} + \frac{0.365}{Re^{0.386}}\right\} \tag{5.21}$$

The pore diffusion coefficient, D_p, was estimated from the Mackie-Maeres (1955) correlation as follows:

$$D_p = \frac{\varepsilon_p}{(2-\varepsilon_p)^2} D_m \tag{5.22}$$

5.4 COMSOL Multiphysics® software

The mathematical solution to the general rate model was solved using COMSOL Multiphysics® 5.3, a finite element method based software. A detailed procedure of setting up the model in COMSOL is given in the sections below.

5.4.1 Space dimensions

The mathematical solution in the general rate model contains two partial differential equations, liquid phase (Equation (5.7)) and pore phase (Equation (5.8)) mass balances, which are solved in a one-dimensional (1D) and a two-dimensional (2D) domains respectively. In COMSOL a domain is represented by a component. A 1D component with a geometry represented by an interval of dimensionless length of one unit and a 2D component with a geometry represented by a square with dimensionless sides of one unit each were chosen to solve the mathematical model equations. In case of stratified beds, each domain is subdivided into several intervals based on the number of adsorbent layers.

5.4.2 Physics interface

In each component, the partial differential equation was implemented using the coefficient form partial differential equation (PDE) interface in the software given by:

$$e_a \frac{\partial^2 u}{\partial t^2} + d_a \frac{\partial u}{\partial t} + \nabla(-c\nabla u - \alpha u + \gamma) + \beta \nabla u + au = f \tag{5.23}$$

Here, *u* is a vector variable, and the coefficients are replaced with appropriate coefficients from the model equations. Each equation is solved with its respective initial and boundary conditions for the liquid phase and solid phase components. However, in case of stratified beds, the coefficients in the PDEs are different for each layer in the bed. Hence, each interval or sub-domain in the 1D and 2D component is paired with a coefficient PDE equation in the interface.

5.4.3 Extrusion coupling

In the coefficient form PDE interface of 1D component, the dimensionless liquid phase concentration, *C*, is defined as the dependent variable. Similarly, the dimensionless pore phase concentration, C_p, is defined as the dependent variable. Using an operation called extrusion coupling available in COMSOL, the liquid phase and pore phase concentration variables are

defined and shared between the 1D and 2D components. The schematic of the model implementation is shown in Figure 5.1.

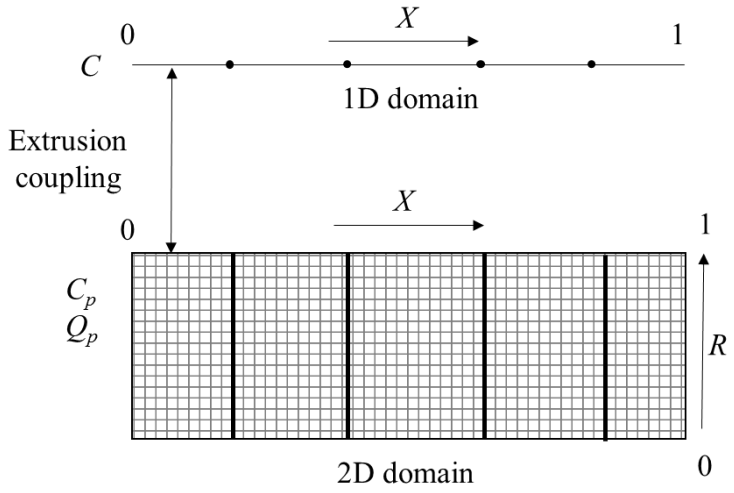

Figure 5.1: Schematic for the general rate model solution using COMSOL Multiphysics® software

5.4.4 Mesh generation

In the finite element method of solution, the mesh refinement determines the accuracy of the computed solution and whether it approaches the true solution or not. There are different methods for mesh refinement, among them changing the element size is the easiest one. COMSOL has 8 options for the element size in a domain, ranging from extremely fine to extra coarse elements. The mathematical model is solved using each element size to confirm that the solution is grid independent. As one can predict, on increasing the element size to an extra coarse element, the computational effort decreases. This also leads to a less accurate solution. On the other hand, decreasing the element size to extremely fine element increases the computational effort. Hence in this study, a fine to normal mesh element size was chosen for obtaining the solution to the mathematical model.

5.4.5 Study type

COMSOL offers a variety of solvers such as stationary, time dependent, and other custom studies, to compute the solution for the model. Since, the equations here are dependent on time, a time dependent study was chosen for solving the equations. The range is defined according to value of the dimensionless time, τ. Most time-dependent problems in COMSOL are solved using adaptive timestepping. The software automatically adjusts the timestep, irrespective of the timestep defined by the user, to maintain the desired relative tolerance value.

5.5 Adsorption dynamics of acetic acid in fixed-bed adsorbers with GAC

In this study, four fixed-bed configurations namely, conventional cylindrical adsorber (CCA) with single adsorbent particle size, RSCA, SCA, and RSTA were used. In the stratified beds, the weight of adsorbent used in each layer in the experiments was 8 g. The total weight of adsorbent used in each experimental study was 40 g. The adsorption isotherm data along with model fits and the isotherm parameters used in this study are given in Figure 5.2 and Table 5.1 respectively. The operational variables and simulation parameters for CCA with single particle size and RSTA are given in Table 5.1. The operating conditions and parameters used for RSCA and SCA are same as for CCA with single particle size.

Table 5.1: Operational and simulation parameter values for different adsorber configurations used for the adsorption of acetic acid on GAC

Parameters	CCA with single particle size	RSTA
Inlet concentration, g/L	17.7	14.7
Flowrate, ml/min	13	13
Bed height, cm	20	14.4
Isotherm parameter, q_m g/g	0.186	0.186
Isotherm parameter, K L/g	0.53	0.53
Pore diffusion coefficient, D_p, cm^2/sec	$4.48*10^{-6}$	$4.48*10^{-6}$

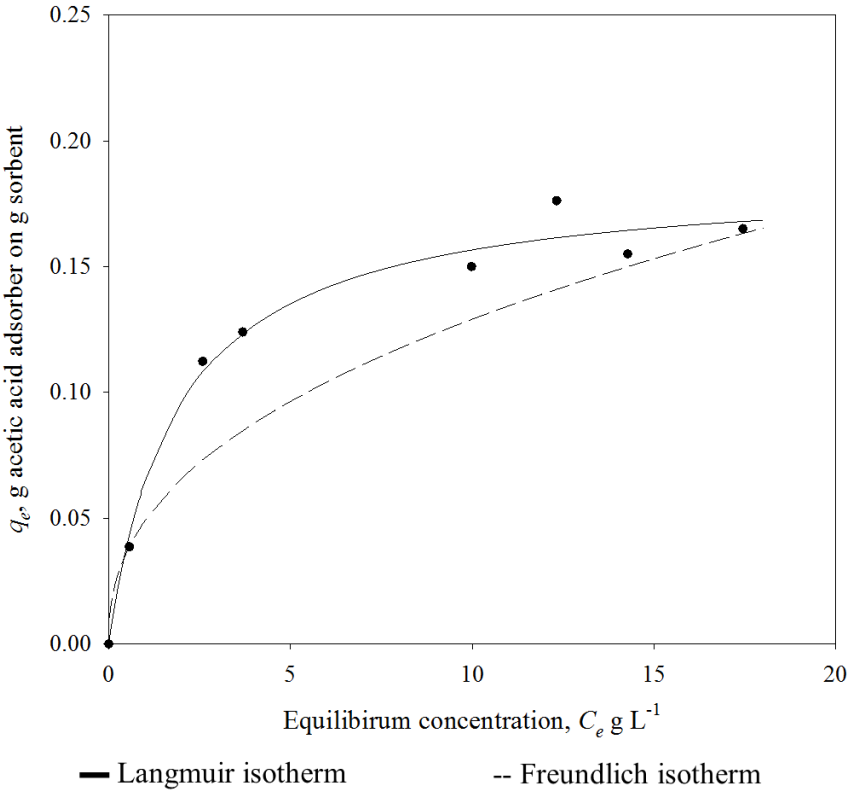

Figure 5.2: Experimental adsorption equilibrium data of acetic acid sorption on GAC at temperature of 21°C, and model fit using nonlinear estimation method

5.5.1 Adsorption dynamics in CCA with single particle size and RSCA

The breakthrough profiles for the adsorption of acetic acid in the CCA with single adsorbent particle size and RSCA are shown in Figure 5.3. The data points in the figure are the experimental points, and the solid line is the output from the general rate model simulations. The model predictions are in good agreement with the experimental data.

The breakthrough time, t_b, and saturation time, t_s, are obtained at $c/c_0 = 0.05$ and $c/c_0 = 0.95$, respectively (Figure 5.3). The difference between these times will give the time for mass transfer zone to travel its own length, t_{MTZ}. The shock front velocity, U_{sh}, can be obtained by two methods. One method uses the experimental data and the time, t_{center}, corresponding to the stoichiometric center of the breakthrough curve and is given as:

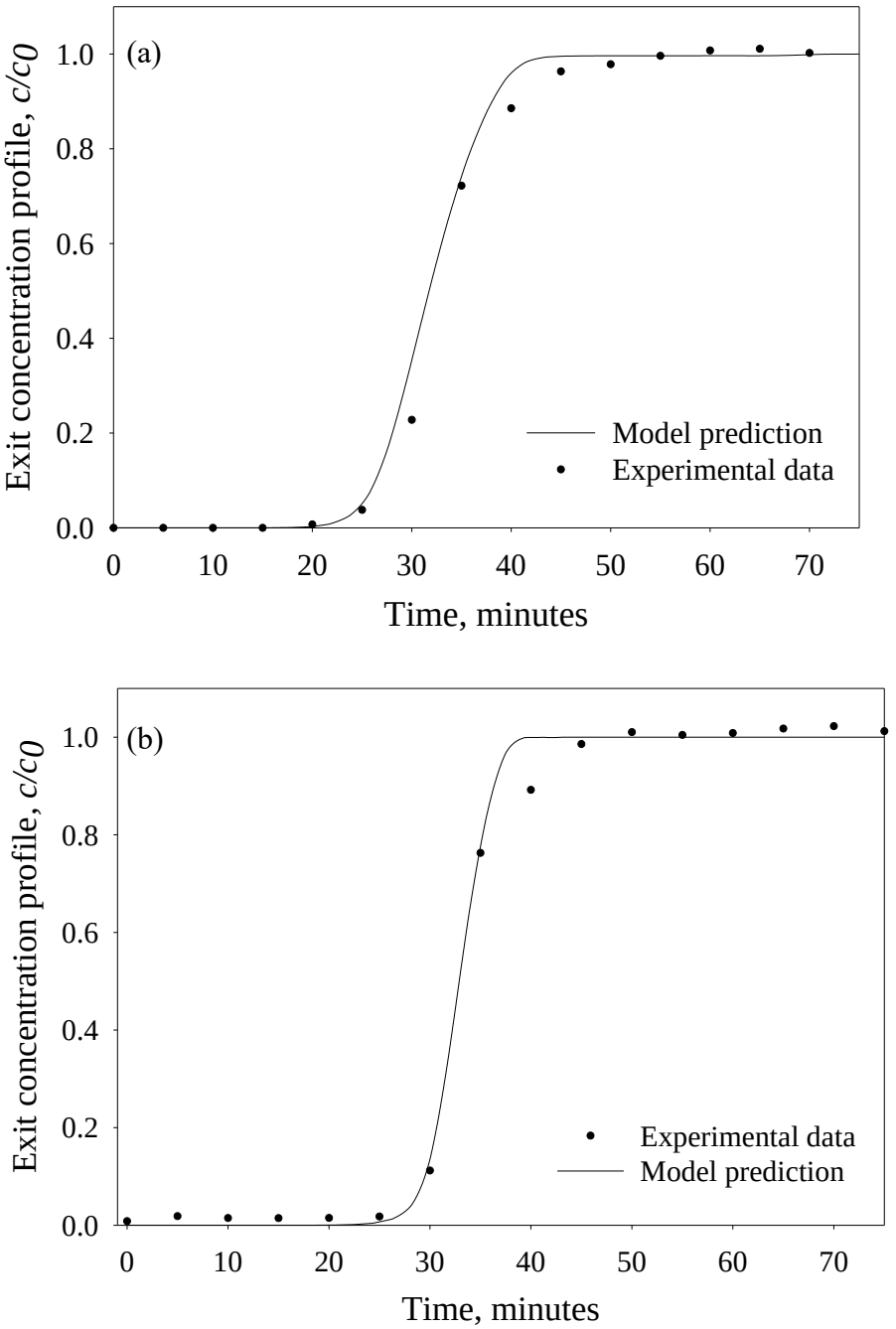

Figure 5.3: Acetic acid breakthrough curves for (a) CCA with single particle size (c_0 = 17.7 g/L) and (b) RSCA (c_0 = 14.7 g/L) with GAC

$$U_{sh} = \frac{L}{t_{center}} \tag{5.24}$$

The second method is based on theoretical analysis, and uses the isotherm, influent velocity, and adsorbent properties, and the equation is given by:

$$U_{sh} = \frac{V}{\left(1+\frac{(1-\varepsilon_b)}{\varepsilon_b}\rho_p\frac{q_0}{c_0}\right)} \tag{5.25}$$

The length of the mass transfer zone, L_{MTZ}, is then obtained from the following equation:

$$L_{MTZ} = U_{sh}t_{MTZ} \tag{5.26}$$

The U_{sh} and L_{MTZ} values obtained for the four fixed-bed adsorber configuration are compared in Table 5.2.

Table 5.2: Comparison of operational and performance parameters for different adsorber configurations used for the adsorption of acetic acid on GAC

Experimental parameters	CCA with single particle size	RSCA	SCA	RSTA
t_b, min	24.8	27.6	23.3	26
t_s, min	39.3	43	42.5	35
t_{MTZ}, min	14.5	15.4	19.2	9
U_{sh}, cm/min	0.612	0.445	0.511	0.308
L_{MTZ}, cm	8.874	6.85	9.81	2.77
Fractional bed capacity utilization	0.78	0.82	0.76	0.90
t_{center}, min (c/c_0 = 0.5)	31.84	32.8	31.5	31.2
U_{sh}, cm/min (from t_{center})	0.628	0.609	0.634	0.461
Fractional bed capacity utilization at double bed length			0.91	0.96

The solute front movement along the bed length at different times is obtained from model simulation and is shown in Figure 5.4.

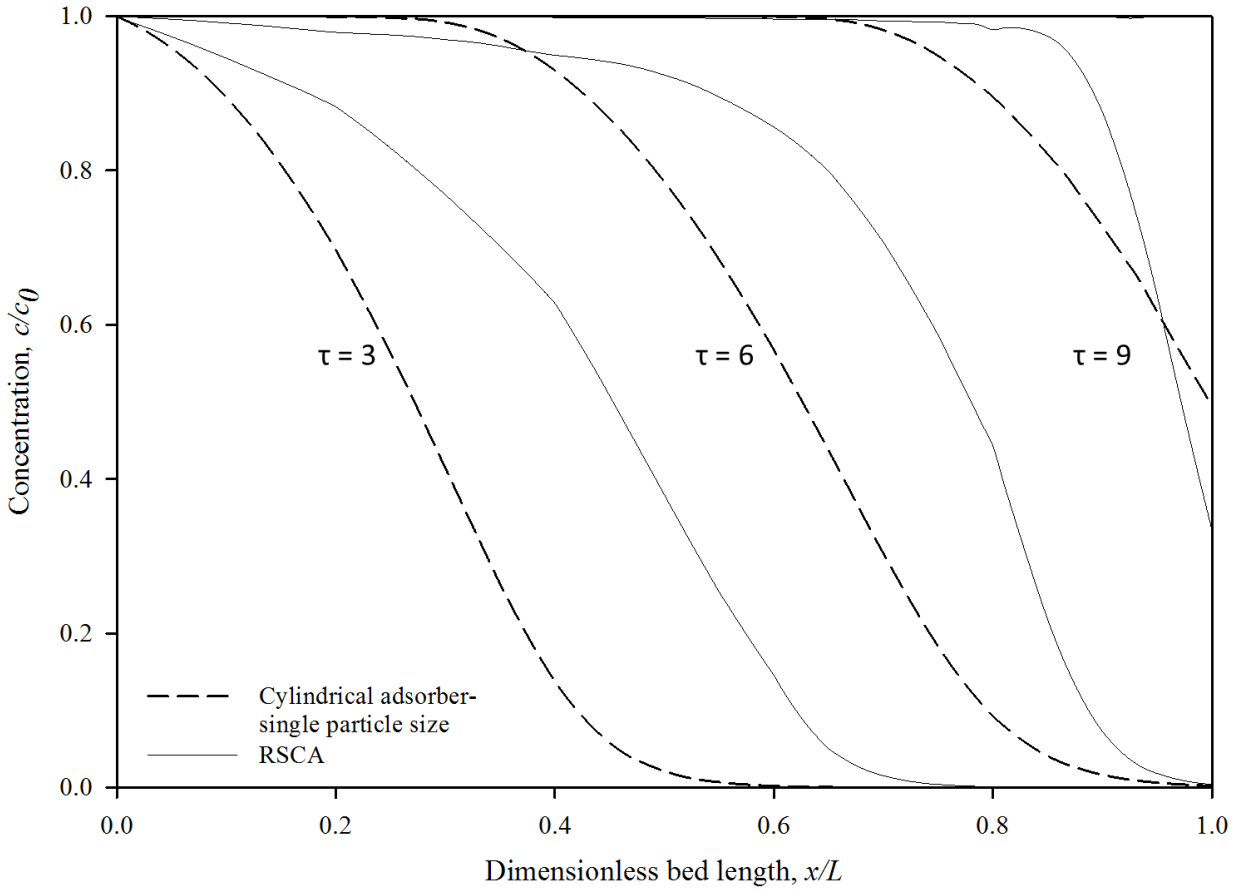

Figure 5.4: Acetic acid concentration profiles along bed length for CCA with single particle size and RSCA with GAC

This figure compares the acetic acid solute front along the bed length for CCA with single particle size and RSCA. For the CCA with single uniformly sized particles, the figure shows a constant pattern shape moving across the length of the column. Constant velocity and uniformly sized particles along the bed length results in uniform mass transfer effects (See Figure 5.5). Hence, the shock front velocity and length of the mass transfer zone are constant along the bed length. Based on the manufacturer specification of pore volume as 0.95 ml/g, the particle density was obtained as 0.701 g/ml and the bed porosity was determined as 0.437. At a flow rate of 13

ml/min and bed height of 20 cm, the shock front velocity calculated with Equation (5.25) was 0.612 cm/min. This is very close and within ~2.6% of the value obtained from the experimental data.

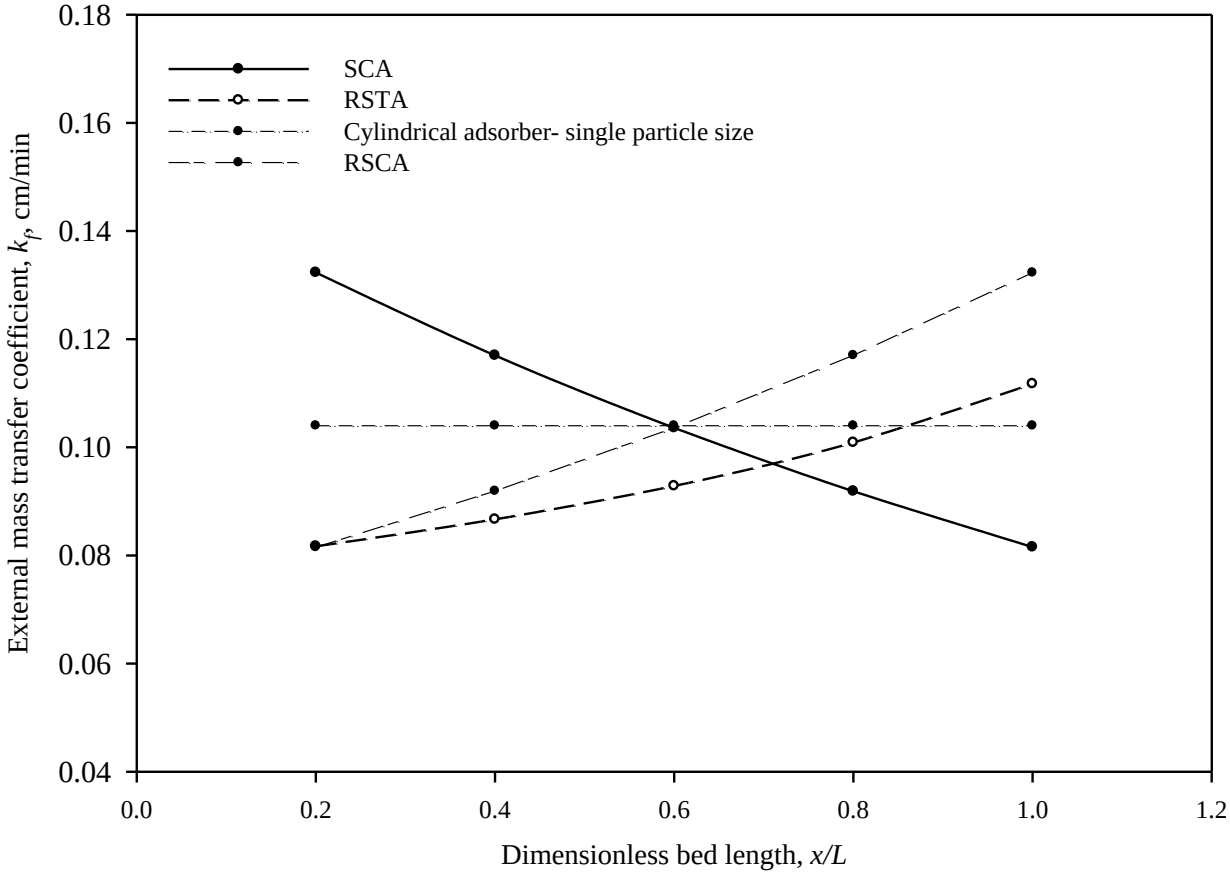

Figure 5.5: Variation of external mass transfer coefficient, k_f, along bed length in GAC adsorbers of different particle stratification and bed geometry

Figure 5.4 shows that the solute front in the RSCA sharpens along the bed length in contrast to the CCA with a single adsorbent particle size. As the particle size decreases along the bed length, the external mass transfer coefficient, k_f, increases along the bed length (See Figure 5.5). This leads to an increase in the uptake rate along the bed length. Though the shock front velocity is constant along the bed length, the increase in k_f leads to a decrease in the length of the mass transfer zone along the bed length. This leads to a sharper breakthrough curve and an

increase in t_b compared to the CCA with single adsorbent particle size (Table 5.2). However, the t_s also increased considerably leading to a minimal improvement in the fractional bed capacity utilization compared to the CCA with a single adsorbent particle size. Also, because of the bed geometry, this reverse stratification is not practicable in industrial processes where the fluid contains particulates and has to be backwashed periodically. Upon backwash, the sorbent particles will restratify with small particles at the inlet of the column and large particles at the outlet of the column as in the SCA configuration.

5.5.2 Adsorption dynamics in SCA and RSTA

The SCA and RSTA configurations have the same empty bed contact time. Figure 5.6 shows the acetic acid breakthrough profiles obtained for adsorption in SCA and RSTA. The data points represent experimental data and the model predictions shown by the solid line show excellent conformance between the two.

Figure 5.7 compares the acetic acid solute fronts along the bed length for SCA and RSTA. The τ_c and τ_t represent dimensionless times in cylindrical and tapered beds respectively. These values are different in SCA and RSTA because the velocity varies along the bed length in the RSTA. Hence, the interstitial velocity at the bottom of the bed is taken as the reference for obtaining the dimensionless time. It is evident from the solute front profile along the bed length shown in Figure 5.7, the solute front is dispersive along the bed length when the particles are normally stratified. In this configuration, as the particle diameter increases along the bed length, the external mass transfer coefficient, k_f, decreases (Figure 5.5). As the solute front becomes increasingly dispersive, the time to breakthrough decreases. Among the different adsorber configurations, SCA has the least t_b of 23.3 minutes (Table 5.2).

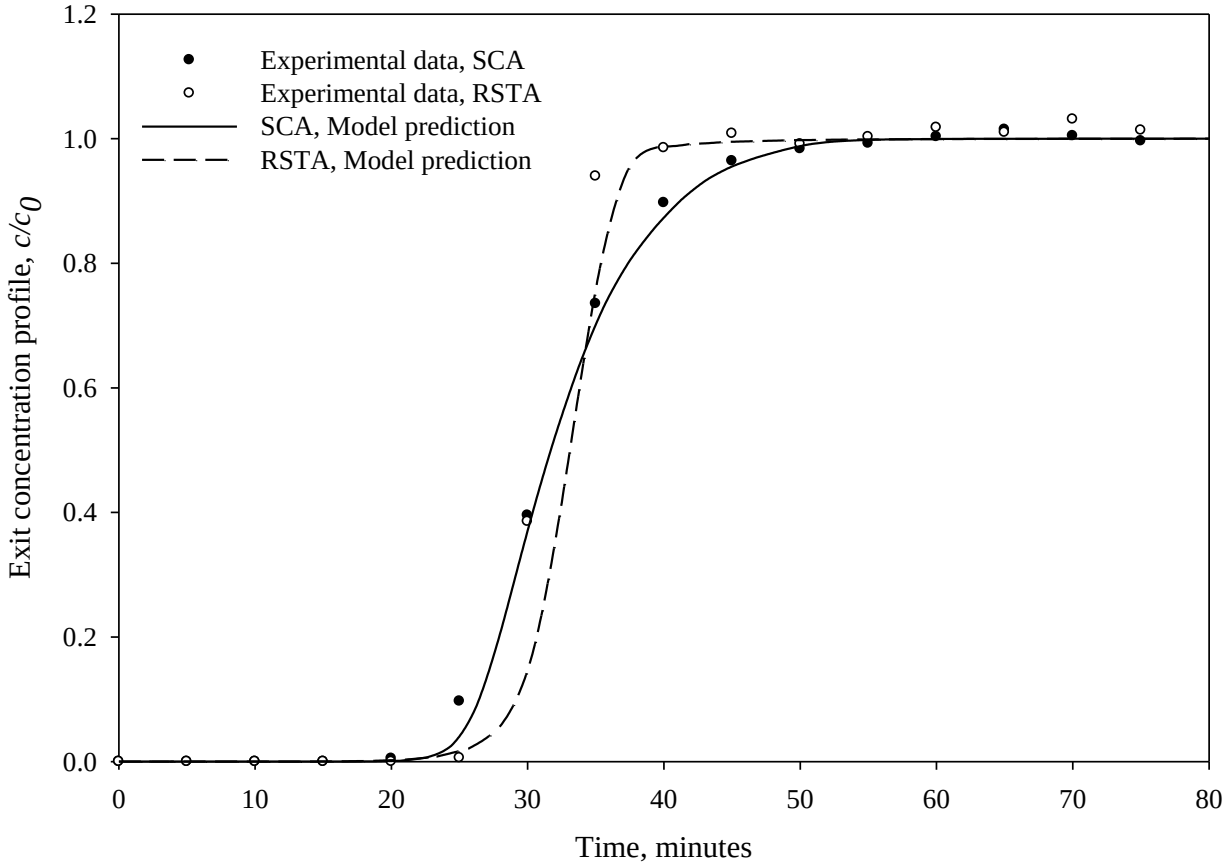

Figure 5.6: Acetic acid breakthrough curves for SCA (c_0 = 14.1 g/L) and RSTA (c_0 = 14.7 g/L) with GAC

However, the t_s increases substantially and its increase is greater than the decrease in time to breakthrough. This leads to longer L_{MTZ}, and poor bed capacity utilization compared to the other configurations. Due to the dispersive nature of the solute front, the breakthrough curve is not symmetric, and this leads to approximate values of U_{sh}. Hence, the values of U_{sh} obtained from the theoretical and experimental methods are somewhat different. At a flow rate of 13 ml/min, the shock front velocity is obtained as 0.511 cm/min and a fractional bed capacity utilization of 0.76 was obtained.

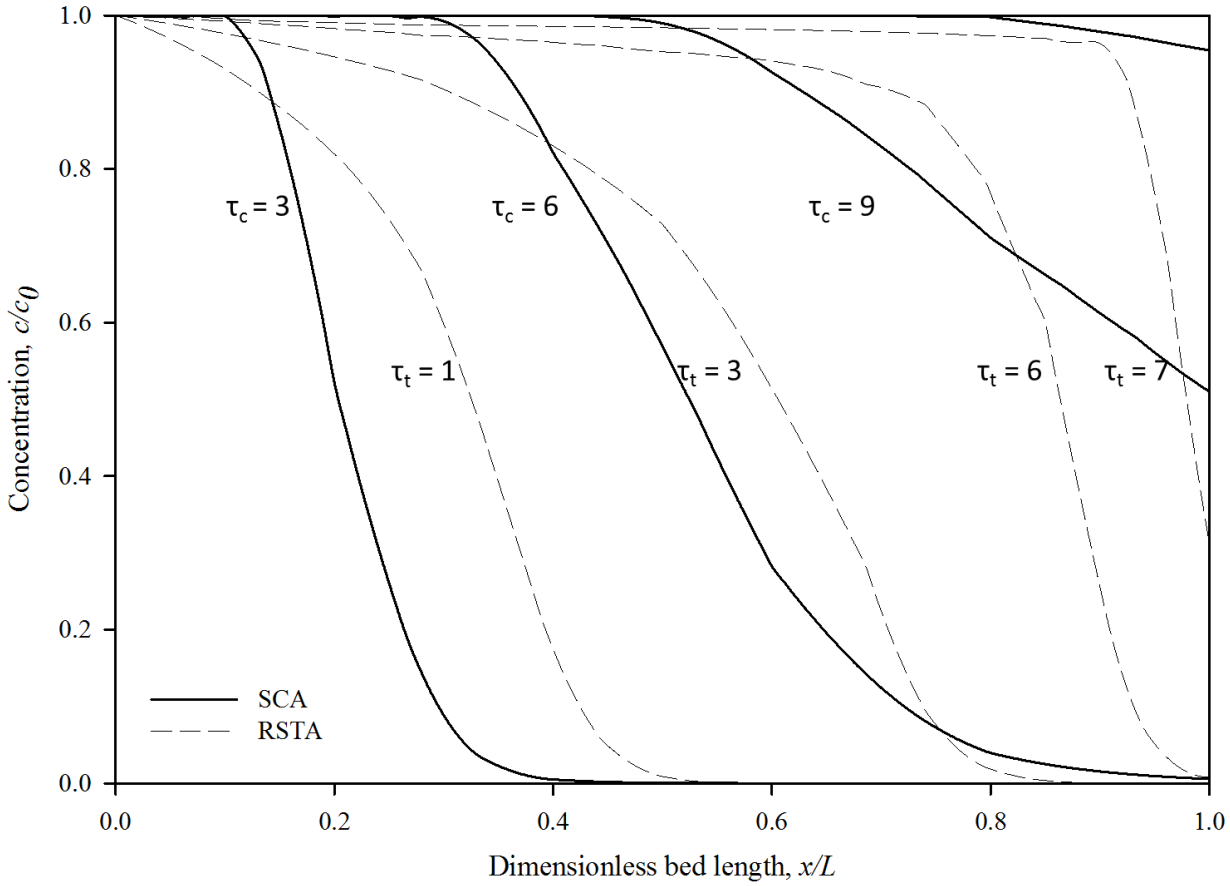

Figure 5.7: Acetic acid concentration profiles along bed length for SCA and RSTA with GAC

For RSTA, the effect of decreasing velocity along the bed length due to the change in cross sectional area results in a solute front that is sharpened to a greater extent compared to RSCA and SCA (Figure 5.4 and Figure 5.7). The k_f values along the bed length in RSTA is compared to other configurations in Figure 5.5. The increase in k_f is higher for RSCA compared to RSTA. This is because of the decrease in the velocity with respect to the geometry in the tapered adsorber. In RSTA, increase in t_b is greater compared to the decrease in t_s and this decreases the length of the mass transfer zone and increases the bed capacity utilization (Figure 5.6; Table 5.2). Mathews and coworkers (Mathews, 2005; Pota and Mathews, 2000) studied the adsorption of phenol and trichloroethylene from aqueous phase onto activated carbon in SCA

and RSTA. It was shown that breakthrough time can be increased by 46% to 75% using tapered beds with adsorbent layered according to kinetic properties compared to SCA. This shows that for the same amount of adsorbent, RSTA provides higher bed capacity utilization than the other configurations studied.

5.6 Adsorption dynamics of acetic acid in fixed-bed adsorbers with Purolite A835

In the fixed-bed adsorption dynamics studies using Purolite A835 resin, four fixed-bed adsorber configurations namely, CCA and tapered bed adsorber with single adsorbent particle size, SCA, and RSTA were used. The operational and simulation parameters are given in Table 5.3. The performance parameters obtained for various configurations are compared in Table 5.4.

In this study, the effect of bed geometry alone on the adsorption dynamics is evaluated using CCA and tapered adsorber with single adsorbent particle size. Figure 5.8 compares the breakthrough curves obtained for the adsorption of acetic acid in these configurations. The data points represent the experimental data and the solid lines are the simulations obtained from the general rate model. In CCA with single adsorbent particle size, the mass transfer kinetics are uniform along the bed length. This is due to the constant velocity and uniformly sized particles along the bed length. Hence, the mass transfer zone travels with a constant U_{sh} and the L_{MTZ} remains constant along the bed length. Whereas, for tapered bed, as the cross-sectional area increases along the bed length, the U_{sh} decreases. This is balanced by the changes in t_{MTZ}. Hence, the L_{MTZ}, remains constant along the bed length. The breakthrough curves for these two configurations are almost similar. The U_{sh} is obtained as 0.21 and 0.26 cm/min for cylindrical and tapered beds respectively. The fractional bed capacity utilization obtained for these configurations are very close. This shows that bed geometry alone does not have much effect on the bed capacity utilization.

Table 5.3: Operational and simulation parameter values for different adsorber configurations used for the adsorption of acetic acid on Purolite A835

Parameters	CCA with single particle size	Tapered bed with single particle size	SCA	RSTA
Inlet concentration, g/L	15.3	15	15	15.3
Flowrate, ml/min	12	12	12	12
Geometric mean particle diameter, d_p, cm	0.065	0.065	0.077, 0.065, 0.055	0.077, 0.065, 0.055
Resin weight, g	60	60	28	28
Bed height, cm	18	13.2	8	5
Isotherm parameter, q_{max}, g/g	0.21	0.21	0.21	0.21
Isotherm parameter, K, L/g	0.51	0.51	0.51	0.51

Table 5.4: Comparison of performance parameters for different adsorber configurations used for the adsorption of acetic acid on Purolite A835

Parameters	CCA with single particle size	Tapered bed with single particle size	SCA	RSTA
t_b, min	33	30.2	12.9	19.8
t_s, min	57	60.6	30.8	29
t_{MTZ}, min	24	30.4	17.9	9.2
U_{sh}, cm/min	0.21	0.26	0.19	0.16
L_{MTZ}, cm	5.13	7.86	3.4	1.5
Fractional bed capacity utilization	0.82	0.8	0.8	0.85

Similar results were obtained by Mathews (2005) in a study on adsorption dynamics of phenol on GAC in tapered adsorber and CCA with single adsorbent particle size. The breakthrough profiles and fractional bed capacity utilization obtained for these configurations were identical to one another. A detailed discussion on single component adsorption dynamics and solute front movement of acetic acid on GAC is given in section 5.5. The pore diffusion

coefficient, D_p, obtained from Mackie- Maeres (1955) correlation (Equation (5.22)) was $1.19*10^{-6}$ cm^2/sec. This correlation did not give good prediction in this model. Hence in this study, D_p of $8.3*10^{-8}$ cm^2/sec was obtained by fitting the experimental data of CCA with single particle size to the model. This value gave good predictions for the adsorption dynamics in RSTA.

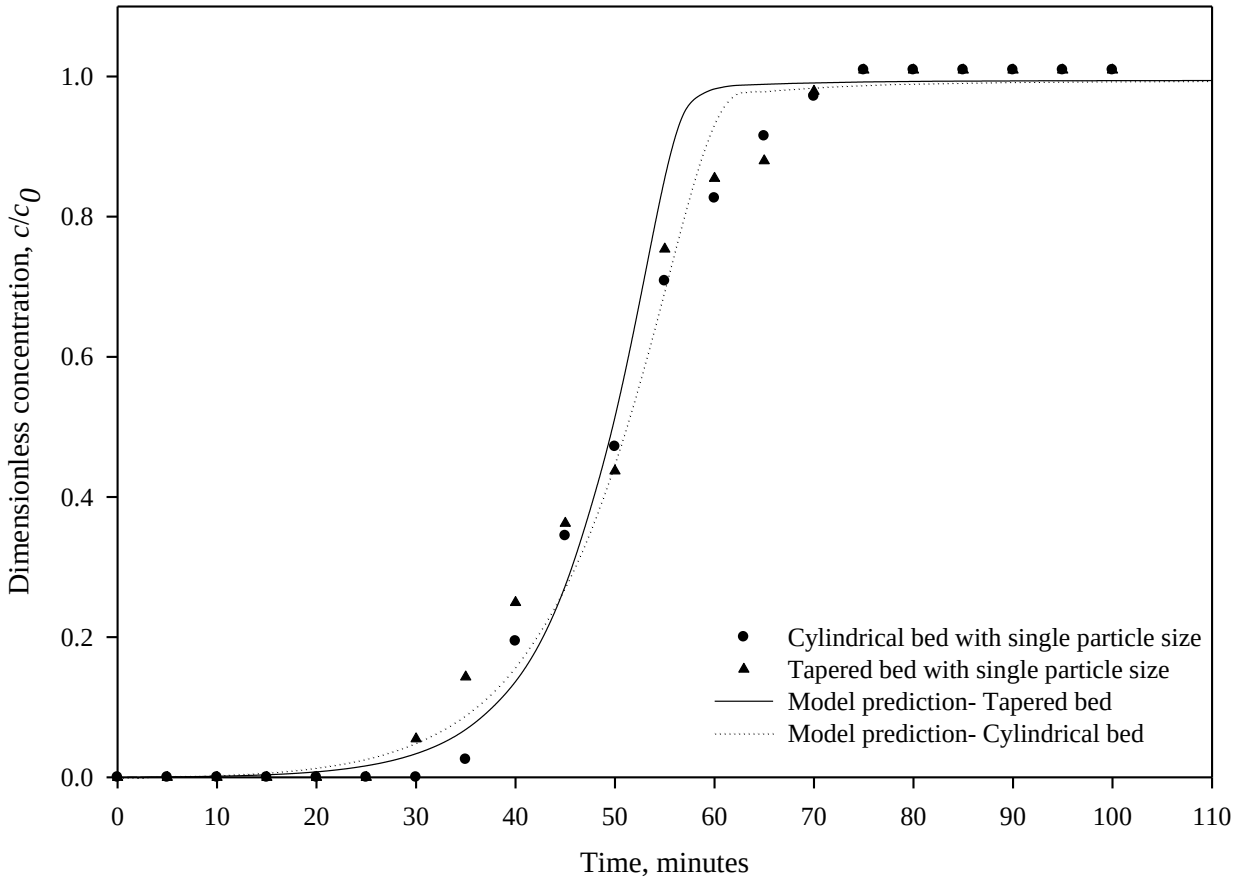

Figure 5.8: Acetic acid breakthrough curves for CCA (c_0 = 15.3 g/L) and tapered (c_0 = 15 g/L) adsorber with single particle size with Purolite A835

The effect of bed geometry and adsorbent particle stratification on adsorption dynamics is studied using SCA and RSTA. Figure 5.9 compares the breakthrough curves of acetic acid obtained using SCA and RSTA. The D_p obtained from fitting the experimental data to general rate model gave good prediction for RSTA. However, for SCA, the model prediction did not

match the experimental data well. The experimental data shows more dispersion compared to the prediction.

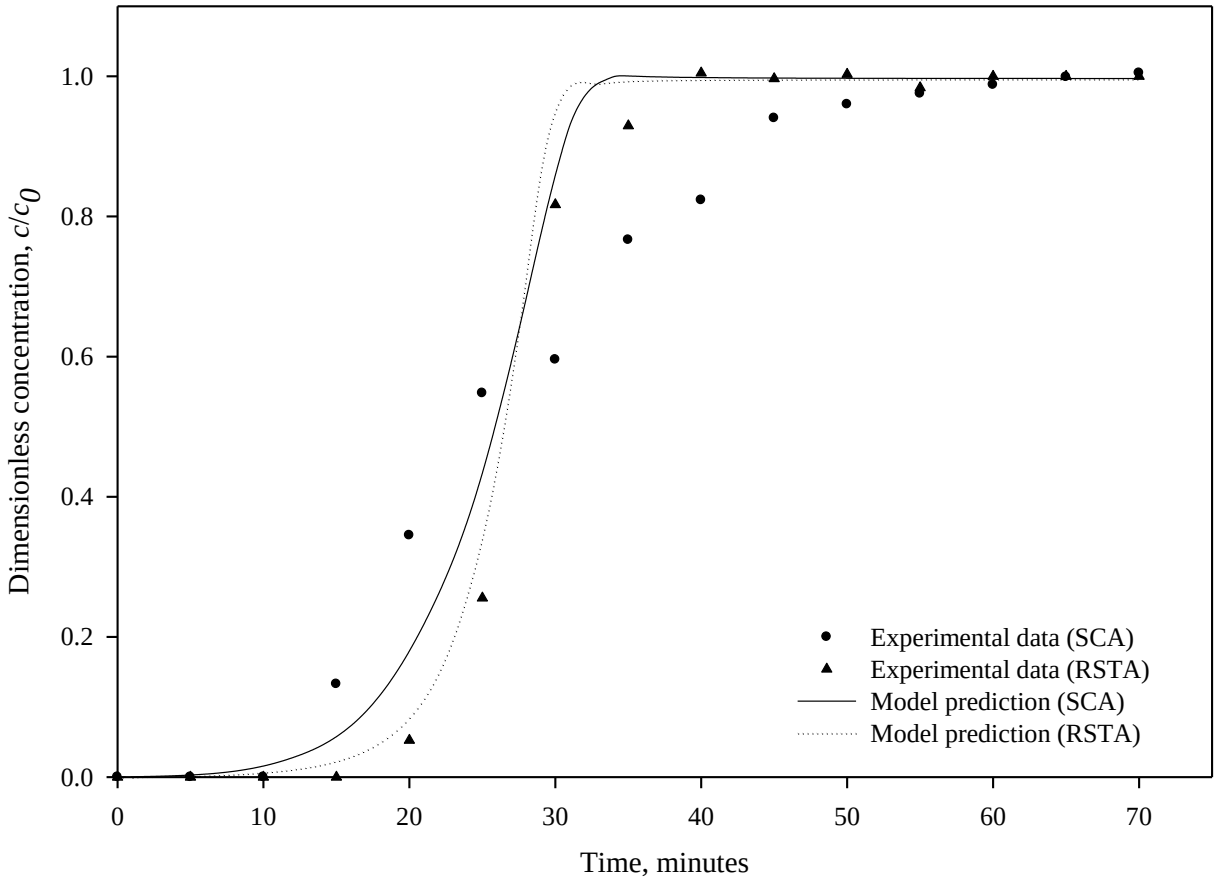

Figure 5.9: Acetic acid breakthrough curves for SCA (c_0 = 15 g/L) and RSTA (c_0 = 15.3 g/L) with Purolite A835

In SCA, as the adsorbent particle size increases along the bed length, k_f decreases along the bed length. The mass transfer zone disperses along the bed length. Whereas in RSTA, the dual effect of decrease in the particle size and U_{sh} along bed length led to the sharpening of solute front. For the same inlet flowrate and concentration, t_b, is 53% greater in RSTA compared to SCA. The values of t_s did not show much difference. This led to a substantial difference in the L_{MTZ} and bed capacity utilization. The bed capacity utilization of RSTA is greater by 6.3% than for SCA. This difference in the bed capacity utilization can be increased when the number of

particle layers are increased. The bed capacity utilization was increased by 14 and 23% in RSTA compared to SCA when 5 and 8 layers respectively were used (Mathews, 2005; Naidu and Mathews, 2019).

5.7 Sensitivity analyses

Sensitivity analyses will help in understanding the effect of operating variables on the dynamics of adsorption in the fixed-beds. This will reduce the cost of running multiple experiments to optimize the process conditions. In the literature, several operational and design variables such as bed length, flow rate, particle diameter, bed diameter, and inlet solution concentration are individually varied to study the effects of each parameter one at a time. In this study, the effects of various parameters on the exit concentration profiles of acetic acid in SCA and RSTA with GAC were determined. This study will also aid in determining the effect of uncertainty in the determination of mass transfer parameters on the simulation accuracy of concentration profiles.

Figure 5.10 shows the comparison of exit concentration profiles for SCA and RSTA for different bed lengths. RSTA shows a longer time to breakthrough compared to SCA. The difference between their breakthrough times is even greater when the column length is doubled. Table 5.2 shows that the fractional bed capacity utilization in SCA increases to 0.91 when the bed length is doubled. However, the same fractional bed capacity utilization of ~ 0.9 was achieved with a single bed length in the case of the RSTA. Increasing the bed length to improve bed capacity utilization will increase adsorbent inventory costs, and also increase operating costs due to increased pressure drop. Lin et al. (2017a) studied the effect of bed length on bed capacity utilization in CCA with single adsorbent particle sizes. L/L_{MTZ} values of 1.45, 1.72, and 4.23 were obtained in three separate fixed-bed experiments increasing the bed capacity utilization

only by ~ 13% overall. As evident from Equation (2.16), an increase in L/L_{MTZ} beyond a factor of three will not result in significant improvements in bed capacity utilization. This indicates that RSTA is effective in achieving the highest fractional bed capacity utilization compared to other configurations.

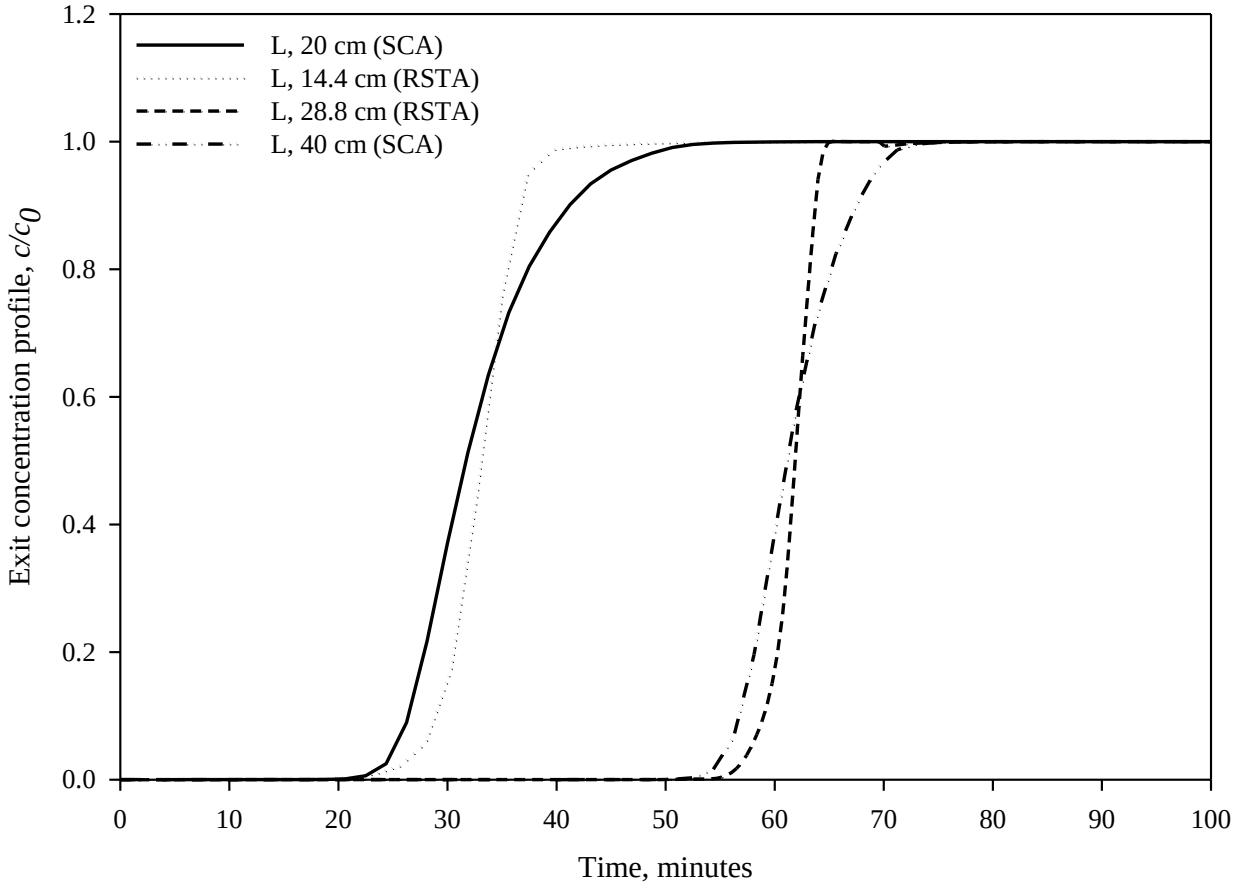

Figure 5.10: Comparison of breakthrough profiles for different bed lengths for SCA and RSTA with GAC

Sensitivity analysis for inlet flow rate was carried for ±50% of the base value for SCA and RSTA (Figure 5.11). In the SCA, with a 50% increase in the inlet flow rate, the incipient breakthrough throughput is reduced by ~ 30% whereas with a 50% decrease in the inlet flow rate, the corresponding throughput is increased by about ~ 10%. The solute front is spreading more as the flow rate is increased while the opposite is true with a decreased flow rate.

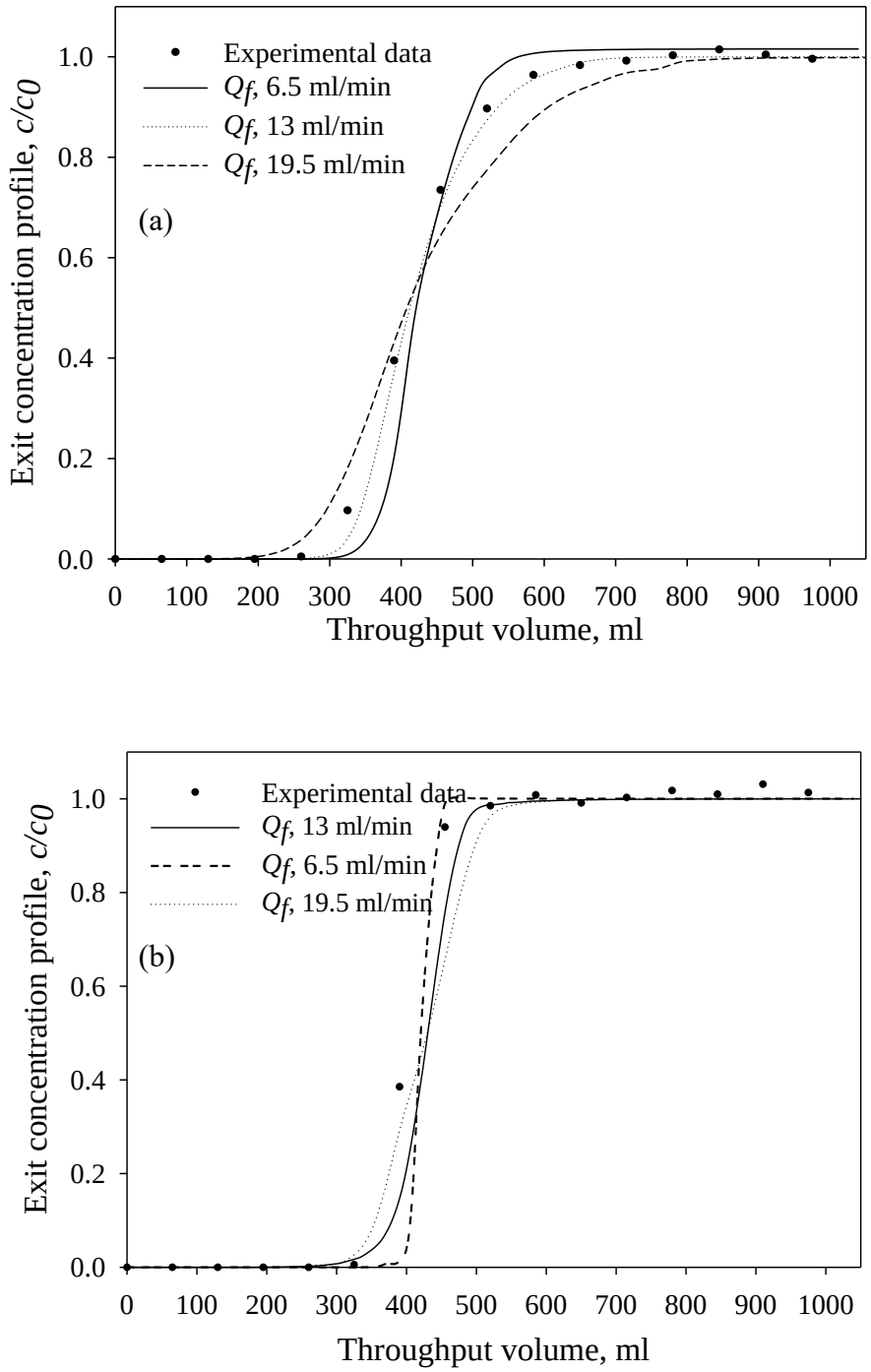

Figure 5.11: Sensitivity of exit concentration profile to inlet flow rate, Q_f, in (a) SCA and (b) RSTA with GAC

In the case of RSTA, the decrease in flow rate by 50% increased the incipient breakthrough throughput by ~ 50% from the base case, while an increase in flow rate by 50%

showed marginal decrease in incipient throughput. The throughput at 5% breakthrough increased by ~ 23% from the base case when flow rate was decreased by 50%, and showed marginal decrease of ~ 8% from the base case for a 50% increase in flow. In this case, simulations show that a smaller flow rate tends to provide a much higher throughput. Flow rate also affects the dispersion of solute in the column. At higher flow rates, the axial dispersion in the fixed-bed adsorber increases leading to a dispersive solute front. This effect is prominent in the case of SCA compared to the case of RSTA. As the velocity decreases along the bed length in RSTA, the effect of change in flow rate on axial dispersion is also minimal.

Sensitivity analysis for D_p was carried out for ±50% change from the base value (Figure 5.12). In the case of SCA, a 50% increase in D_p, resulted in slight increase in the incipient breakthrough time, and a sharper solute front than the base case. This is due to the faster solute uptake rate with the higher D_p value. The t_b increased by about 8% and t_s decreased by ~ 12% compared to the base case thereby reducing the mass transfer zone length. With a 50% decrease in D_p value, t_b decreased by about 20%, and t_s increased by ~25% resulting in a more diffuse mass transfer zone. On the other hand, with RSTA, a 50% decrease in D_p value resulted in a decrease in t_b of 11%, and a 50% increase in D_p resulted in a 10% increase in t_b. Whereas, a 50% decrease in D_p value resulted in an increase in t_s of 23% and a 50% increase in D_p value resulted in a decrease of 3% in t_s value. For all cases, the incipient breakthrough time and t_b were higher for the RSTA than the SCA. Also, the change in incipient breakthrough time was much higher for the RSTA than the SCA. The sensitivity analysis results for k_f show interesting results in that the effects of change of 50% from the base value had opposite results in RSTA to that of SCA. When k_f is increased by 50%, there is marginal change in the incipient breakthrough time for SCA, whereas this time increased by about 20% from the base case for the RSTA. When k_f value

was decreased by 50%, the incipient breakthrough time decreased from the base case by 30% for the SCA and there was very little change for RSTA. Thus, it is clear that adsorbent geometry, particle sizes, and stratification play an important role in how the mass transfer coefficient changes throughout the column (Figure 5.5), affecting the sharpening or dispersion of the solute front. This could be explained in part from the fact that the magnitude of increase of k_f in the case of RSTA is much larger relative to the base case compared to that for SCA. On the other hand, when k_f is decreased the change in magnitude in the bottom layer is smaller for SCA compared to that for RSTA. These dynamics play out in the breakthrough profiles shown in Figure 5.13.

Sensitivity analyses using the developed model will allow the evaluation of different operating scenarios to select the best operating conditions to maximize bed capacity utilization. Thus, the adsorption of acetic acid in fixed-bed adsorbers with GAC was found to be sensitive to variations in the pore diffusion coefficient when compared to those in the external mass transfer coefficient. Under the present experimental conditions, the uptake rate of acetic acid on GAC is more controlled by intraparticle diffusion than external mass transfer. However, since each play a role in the series transfer of mass from the fluid phase to the solid phase, an accurate estimation or determination of both transport coefficients would be necessary to describe adsorption dynamics in stratified adsorbers well.

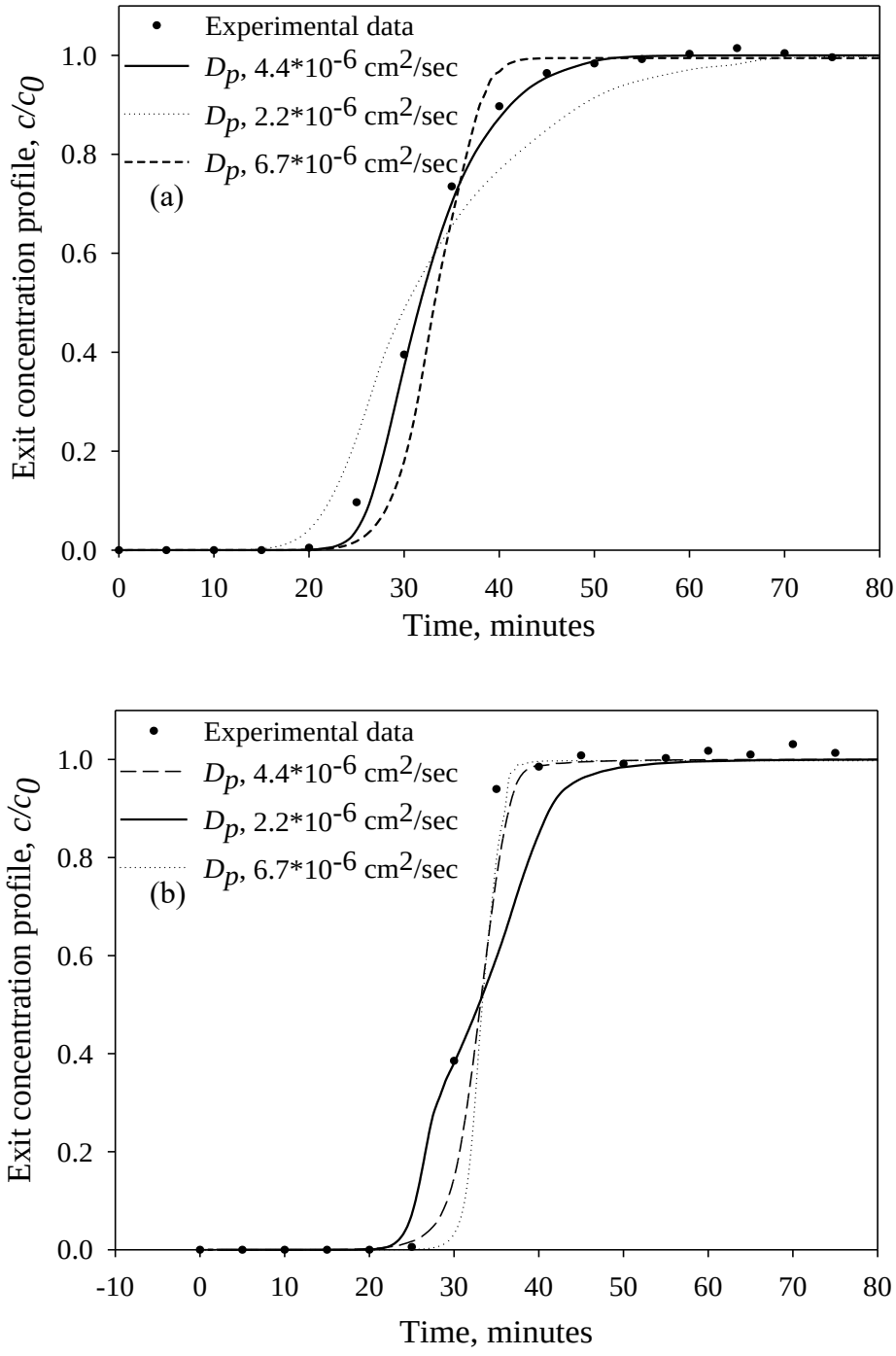

Figure 5.12: Sensitivity of exit concentration profile to pore diffusion coefficient, D_p, in (a) SCA and (b) RSTA with GAC

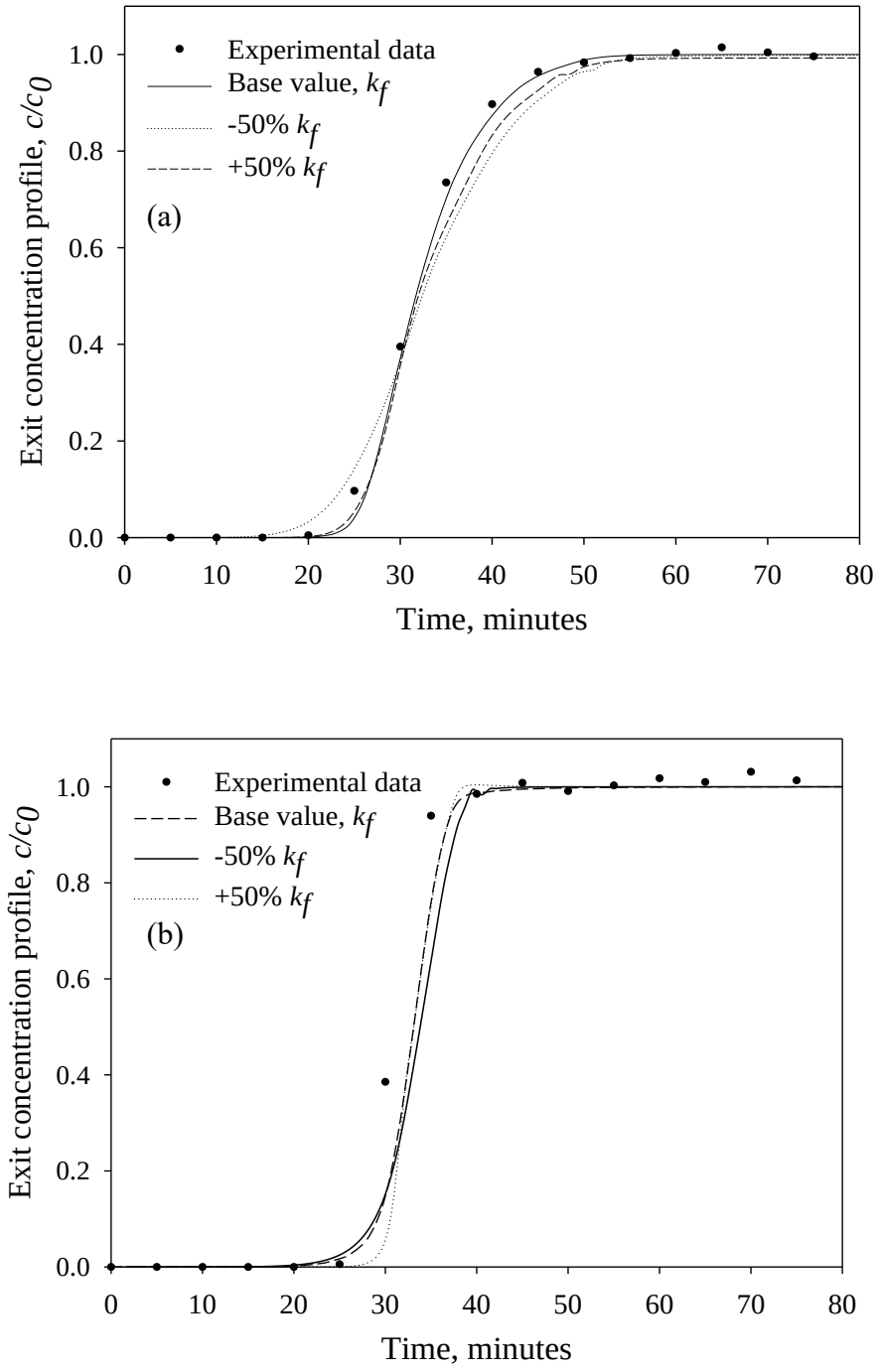

Figure 5.13: Sensitivity of exit concentration profile to external mass transfer coefficient, k_f, in (a) SCA and (b) RSTA with GAC

REFERENCES

Dwivedi, P.N., Upadhyay, S.N., 1977. Particle-Fluid Mass Transfer in Fixed and Fluidized Beds. Ind. Eng. Chem. Proc. Des. Dev. 16, 157–165. https://doi.org/10.1021/i260062a001

Gu, T., 1995. Scale-Up of Liquid Chromatography using General Rate Models, in: Gu, T. (Ed.), Mathematical Modeling and Scale-up of Liquid Chromatography. Springer Berlin Heidelberg, Berlin, Heidelberg, pp. 111–120. https://doi.org/10.1007/978-3-642-79541-1_11

Lin, X., Huang, Q., Qi, G., Shi, S., Xiong, L., Huang, C., Chen, Xuefang, Li, H., Chen, Xinde, 2017. Estimation of fixed-bed column parameters and mathematical modeling of breakthrough behaviors for adsorption of levulinic acid from aqueous solution using SY-01 resin. Separation and Purification Technology 174, 222–231. https://doi.org/10.1016/j.seppur.2016.10.016

Mackie, J.S., Meares, P., 1955. The diffusion of electrolytes in a cation-exchange resin membrane I. Theoretical. Proc. R. Soc. Lond. A 232, 498–509. https://doi.org/10.1098/rspa.1955.0234

Mathews, A.P., 2005. Effect of Adsorbent Particle Layering on Performance of Conventional and Tapered Fixed-Bed Adsorbers. Journal of Environmental Engineering 131, 1488–1494. https://doi.org/10.1061/(ASCE)0733-9372(2005)131:11(1488)

Naidu, H., Mathews, A.P., 2019. Acetic acid adsorption dynamics in stratified tapered beds. Chemical Engineering Journal 371, 337–347. https://doi.org/10.1016/j.cej.2019.04.034

Pota, A.A., Mathews, A.P., 2000. Adsorption dynamics in a stratified convergent tapered bed. Chemical Engineering Science 55, 1399–1409. https://doi.org/10.1016/S0009-2509(99)00032-9

Suzuki, M., Smith, J.M., 1972. Axial dispersion in beds of small particles. The Chemical Engineering Journal 3, 256–264. https://doi.org/10.1016/0300-9467(72)85029-9

Wilke, C.R., Chang, P., 1955. Correlation of diffusion coefficients in dilute solutions. AIChE J. 1, 264–270. https://doi.org/10.1002/aic.690010222

Chapter 6
Multicomponent Adsorption Dynamics in Stratified Fixed-beds

6.1 Introduction

In this chapter, multicomponent adsorption dynamics of acetic and lactic acids in RSTA configuration are presented. These studies were conducted at different pH values to understand the effect of pH on adsorption dynamics and breakthrough curves of mixtures. Since lactic acid and acetic acid are weak acids, their percentage dissociation depends on the pH of the solution. The pH of the broth obtained from xylose fermentation by *Lactobacillus buchneri* is ~4.2. Hence, two pH values of 2.8 and 4.8, which are one pH unit greater and lower than the p*K*a of lactic acid were selected. Hence this study will give insights into the effects of organic acid dissociation on the adsorption dynamics in fixed-beds. The operational parameters for RSTA are presented in Table 6.1.

Table 6.1: Operational and simulation parameter values for RSTA with Purolite A835

Parameters	RSTA (multicomponent system)			
	pH 2.8		pH 4.8	
	Acetic acid	Lactic acid	Acetic acid	Lactic acid
Inlet concentration, g/L	6.7	15.5	4	9.5
Flowrate, ml/min	12		12	
Geometric mean particle diameter, d_p, cm	0.065, 0.055		0.065, 0.055	
Resin weight, g	30		30	
Bed height, cm	5.13		5.13	
Isotherm parameter, *a*, (g/g)(L/g)	0.107	0.251	0.09	0.03
Isotherm parameter, *b*, L/g	0.502	0.55	0.3	0.25

6.2 Multicomponent adsorption dynamics in RSTA

Figure 6.1 shows the breakthrough curves obtained for the adsorption of multicomponent mixture of acetic and lactic acids in the RSTA at different pH values. When a solution mixture with a pH of 2.8 was used, lactic acid shows a higher sorption capacity and affinity compared to acetic acid. At pH 2.8, the adsorption equilibrium of acetic and lactic acids is similar to that for the pH range of 2-2.8 used in the batch isotherm studies. The t_b for acetic and lactic acid were 13 and 24 minutes respectively. A roll-over effect is observed for acetic acid as it is being displaced by lactic acid, the more strongly adsorbed component. The outlet concentration of acetic acid at the peak is ~1.5 times that of the inlet concentration. When the pH of inlet solution is maintained at 4.8, the order of breakthrough is reversed. Acetic acid shows a higher sorption affinity and capacity compared to lactic acid. This is due to the effect of pH on the dissociation of organic acids. Since the p*K*a of acetic acid is 4.76 at 25 ^{o}C, ~50% of the acetic acid will be in its undissociated form. On the other hand, the p*K*a of lactic acid is 3.86 at 20 ^{o}C and > 90% of this acid exists in its dissociated form. When a mixture of dissociated and undissociated acid forms are present, weak base resins favor the adsorption of undissociated acid forms. Lactic acid elutes almost instantly whereas the t_b for acetic acid was 17.5 minutes. The experimental data shows sharpening effect with an increase in t_b and decrease in t_s. The model simulation for lactic acid shows a roll-over effect. In a study on separation of lactic and succinic (pKa$_1$ = 4.16, pKa$_2$ = 5.6) acids, a similar approach was used by Husson and King (1999). At pH 2, when a 3:1 molar ratio mixture of lactic-succinic acids was used, the exit concentration profiles of acids do not show much separation. When the pH of the solution was adjusted to 4, i.e., greater than the p*K*a of lactic acid and lower than the pKa$_1$ of succinic acid, there was more separation. It was estimated

that 3.83 mmol of lactic acid/g of dry sorbent or ~15 bed volumes of lactic acid that is free of succinic acid can be recovered (Husson and King, 1999).

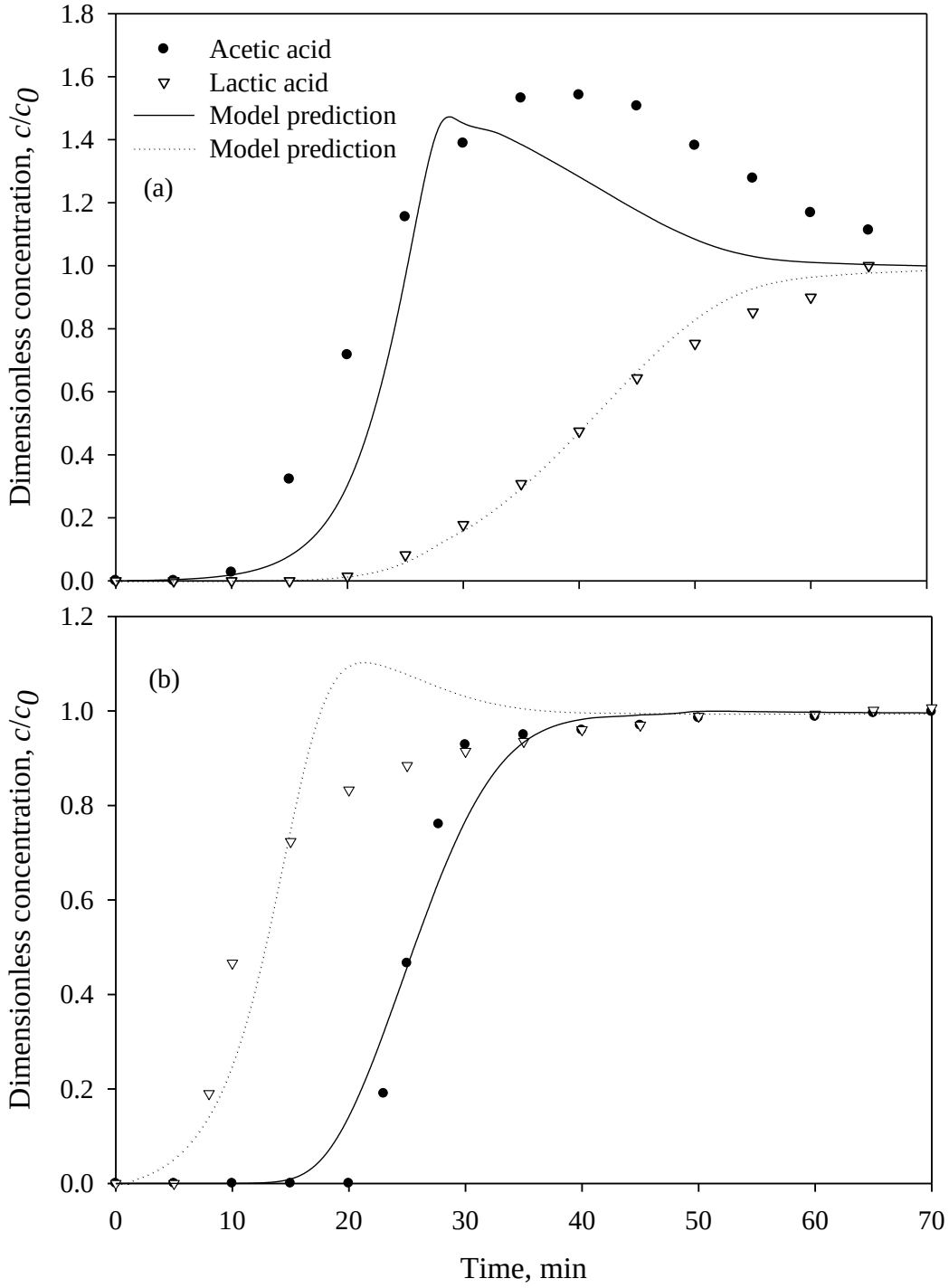

Figure 6.1: Acetic and lactic acid breakthrough curves for the multicomponent adsorption in RSTA with Purolite A835 at pH (a) 2.8, and (b) 4.8

Figure 6.2 shows the concentration profile along bed length for acetic and lactic acids at pH 2.8. This shows that at time, *t*, of 10 minutes, acetic acid and lactic acid are separated by 0.2 units of dimensionless bed length.

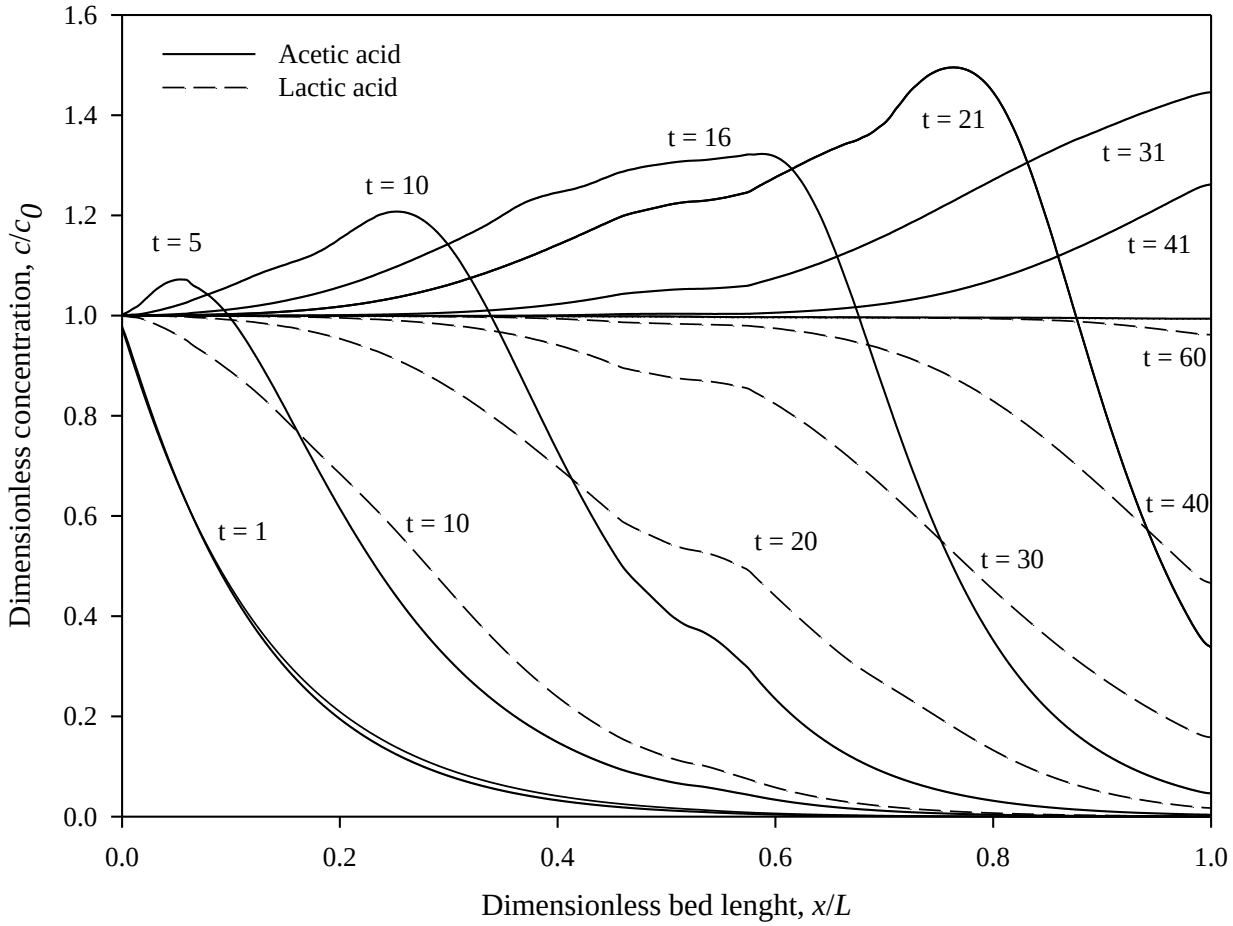

Figure 6.2: Concentration profile of multicomponent acid solution along bed length in RSTA with Purolite A835 at pH 2.8

Acetic acid starts to breakthrough at that time while the mass transfer zone of lactic acid is still in the column. This shows that acetic acid is displaced by lactic acid along the bed length. At this pH, pure acetic acid can be recovered by operating the fixed-bed till the t_b of lactic acid. However, due to the roll-over effect, higher concentrations of acetic acid will be left in the bed. This can be recovered using steam regeneration and subsequently lactic acid can be recovered

using base/solvent regeneration. These acids can also be separated at pH 4.8. At this pH, lactic acid can be recovered first and then acetic acid can be separated from the resin. However, at this pH the adsorption capacity of the resin decreases as the acids are majorly present in their dissociated forms. This will lead to low cycle times and increases overall costs. Husson and King (1999) reported that it is economically feasible to separate acetic acid from a high-value nonvolatile acid such as lactic or succinic acid when they are coadsorbed on a weak base resin. Batch sorption using 1 g of Dowex MWA-1 resins and equimolar (0.23 M) mixture of acetic and lactic acid, regeneration using air stripping, and solvent leaching using sodium hydroxide were conducted. The sorption capacities were reported as 0.2 g/g and 0.11 g/g of lactic and acetic acids respectively. Thermal regeneration using air stripping was shown to remove the acetic acid completely without much effect on the adsorbed lactic acid. Thus, this is a feasible regeneration technique for the resin in the fixed-bed adsorber to separate and recover acetic and lactic acids.

6.3 Sensitivity analyses

In this study, sensitivity analyses of adsorption dynamics in multicomponent mixtures is conducted. This study will enable to optimize the operational parameters for maximum separation and recovery of organic acids using RSTA.

Figure 6.3 shows the sensitivity of breakthrough profiles of acetic and lactic acids to changes in flowrate, Q_f. With a +50% change in Q_f, the throughput for acetic acid decreased by 3.2%. Whereas with a -50% change in Q_f, its throughput increased by 40.5%. On the other hand, for lactic acid, the throughput decreased by 6.5% and increased by 13% for changes of +50% and -50% of Q_f, respectively. The breakthrough curve for acetic acid at +50% Q_f shows sharpening effect and thus increased bed capacity utilization.

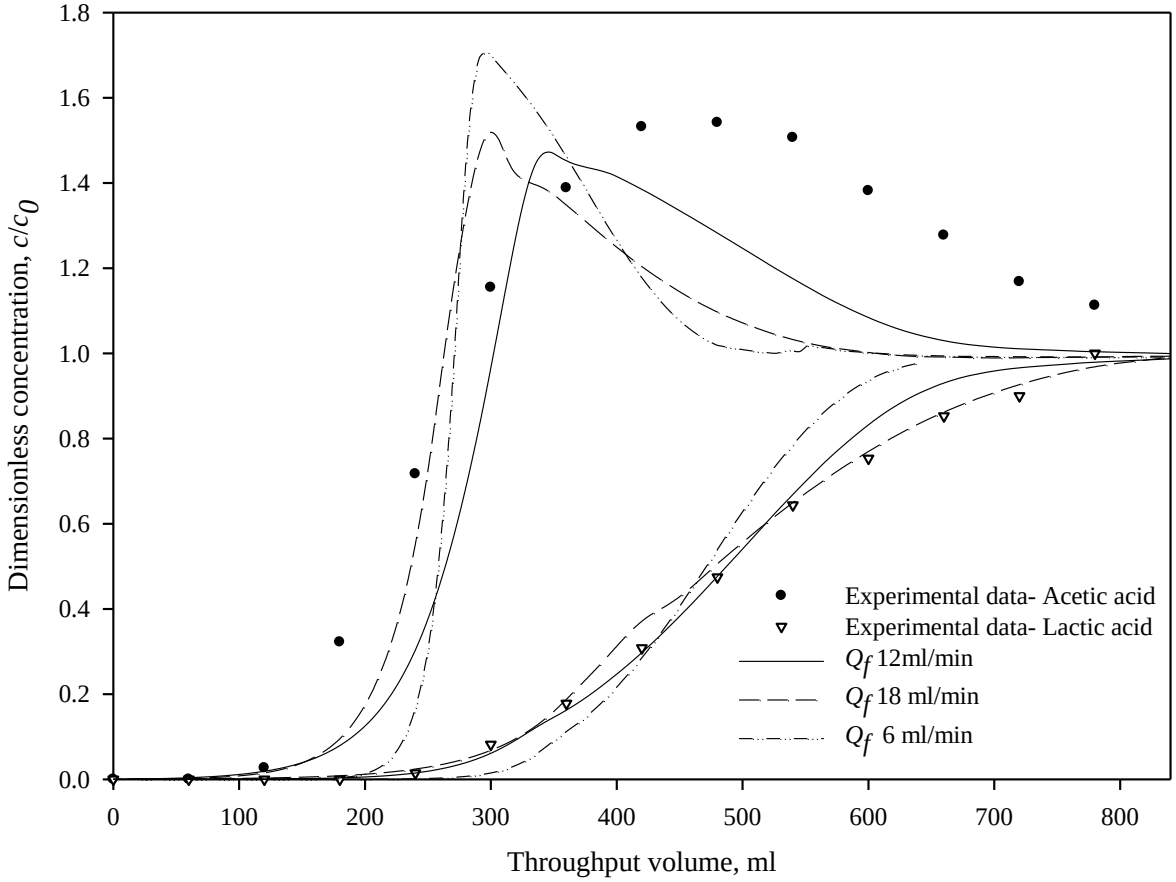

Figure 6.3: Sensitivity of exit concentration profile of multicomponent solution to inlet flow rate, Q_f, in RSTA with Purolite A835

Figure 6.4 shows the sensitivity of breakthrough profiles of acetic and lactic acids number of particle layers and particle size. Two particle sizes of 0.077 and 0.045 cm were selected. In RSTA configuration and in different simulations, adsorbent layers with particles sizes of 0.077 and 0.045 cm were added at the top and bottom respectively. When an adsorbent layer with particle size of 0.077 cm is added, the t_b for acetic and lactic acid decreased by 10 and 5% respectively. On the other hand, when a layer with particle size of 0.045 cm is added, the t_b for acetic and lactic acids increased by 37 and 15.1% respectively. This shows that the addition of a larger particle size leads to dispersion, whereas the addition of smaller particle size leads to

sharpening effect. This is because with the decrease in particle size, the k_f increases and leads to an overall increase in the uptake of organic acids.

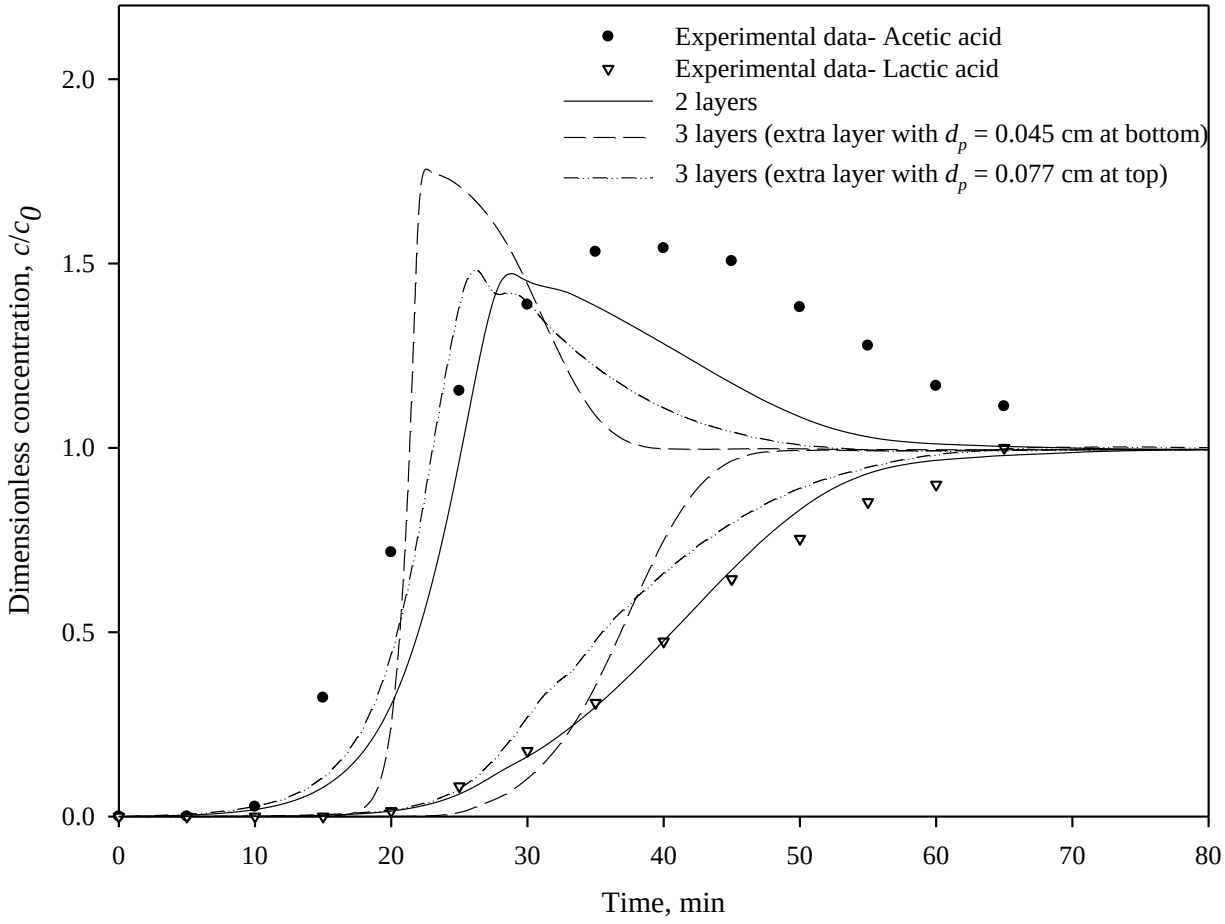

Figure 6.4: Sensitivity of exit concentration profile of multicomponent solution to number of particle layers in RSTA with Purolite A835

Figure 6.5 shows the sensitivity of breakthrough profiles of acetic and lactic acids to bed length. The breakthrough profile of lactic acid remains unchanged. However for acetic acid, the roll-over peak concentration increased by 20.5% with double the bed length. In a study on modeling of adsorption dynamics of acetic acid, butanol, and ethanol, with an increase in bed length, the peak concentration in the roll-over increased by similar percentages (Jiao et al., 2015). This is because with an increase in bed length, the competitive displacement of weakly

adsorbed component by the strongly adsorbed component increases. In addition, with increase in bed length, there will be an increase in the adsorbent and the adsorption sites which results in more separation between the components. The difference between the t_{center} of acetic and lactic acids increased by 23% when the bed length is doubled. This shows that separation and recovery of organic acids can be enhanced at these process conditions.

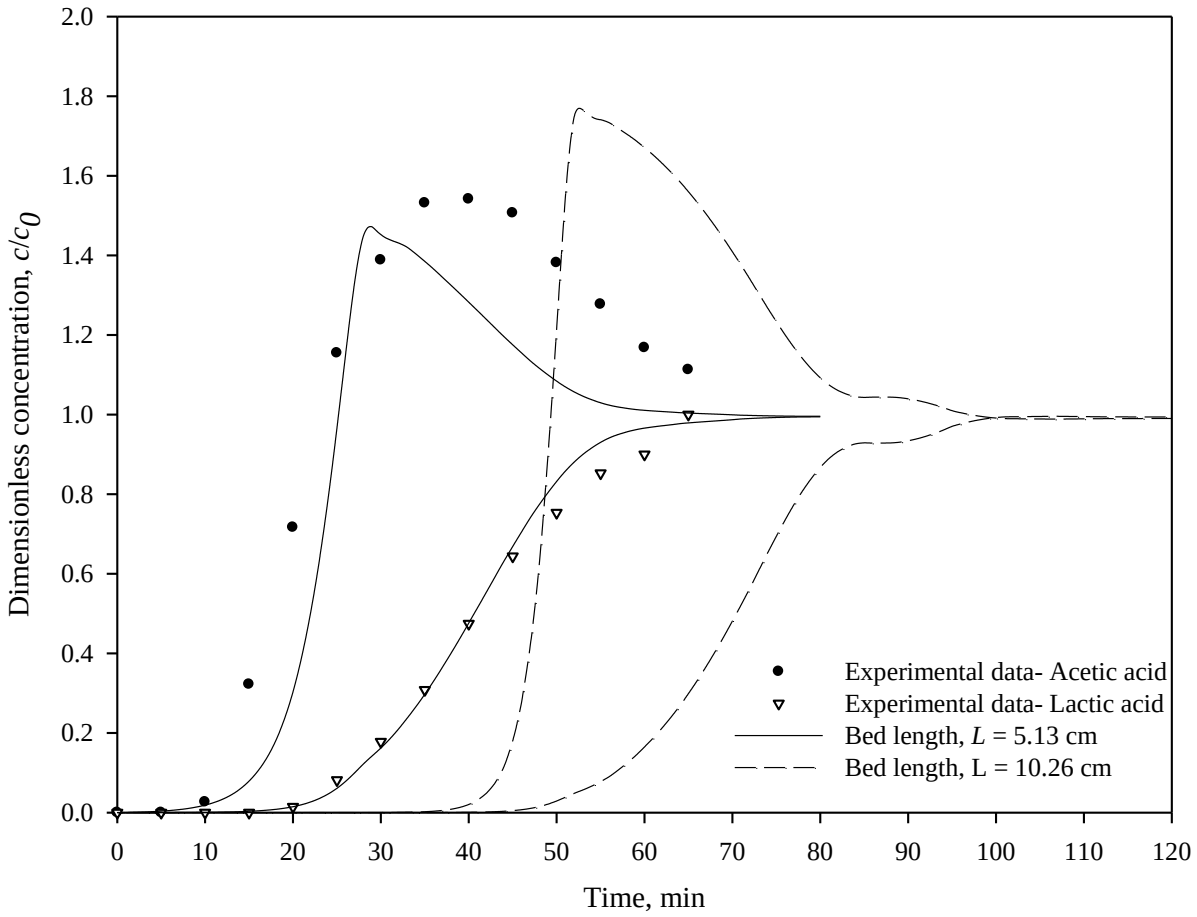

Figure 6.5: Sensitivity of exit concentration profile of multicomponent solution to bed length in RSTA with Purolite A835

REFERENCES

Husson, S.M., King, C.J., 1999. Multiple-acid equilibria in adsorption of carboxylic acids from dilute aqueous solution. Ind. Eng. Chem. Res. 38, 502–511. https://doi.org/10.1021/ie9804430

Jiao, P., Wu, J., Zhou, J., Yang, P., Zhuang, W., Chen, Y., Zhu, C., Guo, T., Ying, H., 2015. Mathematical modeling of the competitive sorption dynamics of acetone–butanol–ethanol on KA-I resin in a fixed-bed column. Adsorption 21, 165–176. https://doi.org/10.1007/s10450-015-9659-7

Chapter 7
Summary, Conclusions, and Recommendations

The production of chemicals through bioconversion processes using biomass and biomass wastes will promote sustainability and reduce dependence on fossil fuels. Due to their high demand and an array of applications in several industries, the bioproduction of acetic and lactic acids has been gaining a lot of attention in recent years. While ~90% of the worldwide demand of lactic acid is met through bioprocesses, about 90% of acetic acid production is via synthetic chemical processes. This is mainly because bioprocesses for acetic acid production operate under neutral pH and anaerobic conditions, and the product concentrations are quite low. Hence, conventional downstream separation processes are not suitable for efficient separation and recovery of acetic acid.

7.1 Summary

Separation efficiencies for organic acids using synthetic resins and activated carbon are quite low at neutral pH values. In this research, equilibria, kinetics, and dynamics of acetic acid adsorption on weak base resins and granular activated carbon (GAC) were studied at low pH conditions. Single and multicomponent adsorption equilibrium studies were conducted to determine adsorption equilibria of acetic and lactic acids on resins and GAC. Multicomponent sorption equilibria of acetic and lactic acids were determined using the Ideal Adsorbed Solution Theory (IAST) model, and extended Langmuir and modified extended Langmuir isotherm equations. Adsorption kinetic studies were conducted using carbonaceous and resin sorbent matrices including GAC, Amberlite IRA67, and Amberlite IRA96. A relatively simple spreadsheet method to estimate intraparticle diffusivity using the analytical solution of diffusion equation is presented in this research.

In fixed-bed adsorbers, a high overall rate of adsorption is needed for improving the bed capacity utilization and the overall efficiency of the recovery process. In this research, five different adsorber configurations were chosen to examine the effect of sorbent size, particle stratification, and bed geometry on solute front movement and bed capacity utilization. Multicomponent adsorption studies using solutions of acetic and lactic acids were conducted in fixed-beds to determine the sorption dynamics and solute front movement. These studies were conducted at pH 2.8 and 4.8.

A general rate model that considers axial dispersion, external film transfer resistance, intraparticle diffusion resistance, and nonlinear isotherm was used to model adsorption dynamics. The resulting equations were solved using COMSOL Multiphysics® software. This model was used to predict breakthrough curves from fixed-beds of different configurations using correlations and independently determined adsorption equilibrium and kinetic parameters.

7.2 Conclusions

Based on the objectives of the research and experimental results, the conclusions of this research are given below:

- A comparison of the equilibrium isotherm data show that weak base resins have higher adsorption capacities and affinities for the adsorption of acetic acid from dilute aqueous solutions compared to GAC. Among the resins studied, Purolite A835 had relatively higher affinity and capacity for adsorption of acetic acid from aqueous solutions including fermentation broths. Purolite A835 was found to have little affinity for lactose substrates. GAC was found to adsorb lactose in the broth preferentially to acetic and lactic acids.

- A simplified method for fitting the equilibrium sorption data via nonlinear estimation method is used in this work. This method provides better fit and lead to consistent and accurate estimates of isotherm parameters compared to the use of linearized equations. Three parameter isotherms namely, Sips and linear-Freundlich isotherms gave better fits to the adsorption data for acetic acid and lactic acid on Purolite A835, respectively.
- Batch sorption kinetic studies show that Amberlite IRA67 had higher external mass transfer coefficient compared to the other resins and GAC sorbents. However, due to the gel nature of its matrix, the intraparticle diffusion coefficient is lower compared to the other sorbents.
- The single component sorption dynamic studies using a divergent tapered and a conventional cylindrical adsorbers (CCA), gave constant pattern solute fronts in each case. These configurations were shown to have similar bed capacity utilizations. A dispersive solute front is seen to be formed in the normally stratified cylindrical adsorber (SCA). In this case, the mass transfer zone length increased as the front moved through the column. On the other hand, a sharpening solute front was observed with the reverse stratified tapered bed adsorber (RSTA). The reverse stratified cylindrical adsorber (RSCA) is also shown to produce a sharpening solute front, but this system is not feasible in practice as the bed will restratify when backwashed.
- The mathematical solution to the general rate model was solved using COMSOL Multiphysics® 5.3, a finite element method based software. Model simulations for acetic acid adsorption for five different adsorber configurations were presented.

The model predictions match the experimental data well in each case. It was determined from the analyses that bed capacity utilization is maximum with the RSTA. For acetic acid, the bed capacity utilization of RSTA is higher by 18.4% relative to SCA in relatively short beds with 40 g of GAC as the sorbent. Sensitivity analyses for have shown that to achieve 90% bed capacity utilization with GAC as the sorbent, two column lengths or double the quantity of adsorbent will be required in the case of SCA when compared to RSTA.

- Multicomponent adsorption breakthrough curves show that the adsorption dynamics of organic acids are affected by the pH of the inlet solution. At a pH of 2.8, lactic acid showed higher sorption capacity and affinity compared to acetic acid, resulting in the preferential displacement of acetic acid from the bed. But, at pH of 4.8, the elution order reversed with acetic acid showing higher affinity and higher capacity compared to lactic acid. Sensitivity analyses indicate that by increasing the bed length, greater separation can be achieved between acetic acid and lactic acid.
- The model developed will be useful in the examination of different operating conditions and enable the selection of optimum process conditions for enhancing bed capacity utilization to minimize adsorbent inventory in the separation of organic acids. The acetic acid adsorption data presented in this research will facilitate the development of cost-effective sorption processes for its recovery from low pH fermentations. The methodology can also be adaptable for the recovery of lactic acid from bacterial or yeast fermentations at low pH values (Carlson and Peters, Jr., 2002; Rush, 2012).

7.3 Recommendations

Based on the experimental results from this work and literature, the following recommendations are proposed for further research:

- Multicomponent adsorption equilibrium models for the adsorption of various fermentation broth components and products on resins and GAC are needed for the efficient design of fixed-bed processes. It is recommended that additional research be conducted to develop simple models to address adsorbed phase nonidealities to improve IAST predictions of multicomponent adsorption equilibria.
- In fixed-bed adsorption, the bed capacity utilization determines the economic viability of the sorption process. Fixed-bed adsorber configurations with novel bed geometries, layering based on different sorbents with different adsorption characteristics, and particle size distributions need to be investigated to obtain further enhancements to this technology.
- In the case of multicomponent adsorption, the pH of the inlet solution and the nature of resin determine the sorption dynamics and elution behavior of acetic and lactic acids. Further studies need to be conducted at different influent pH values, resins of different basicities, and different resin matrices to determine the effect of these parameters on the efficient separation of the acids.
- Weak base resins and GAC can be regenerated using thermal regeneration, chemicals such as sodium hydroxide, calcium hydroxide, and solvents such as methanol. Further studies need to be conducted to evaluate these regeneration schemes to determine the separation and recovery efficiencies of acetic and lactic

acids in fixed-bed adsorbers. This will enable the design of cyclic operation scheme and determination of elution time and product concentrations obtained.

- When a constant pattern solute front is formed in adsorption, desorption step leads to the formation of a diffuse front. This leads to poor regeneration efficiencies. There have been no studies conducted on desorption dynamics in RSTA. Hence, further studies are recommended to examine the effect of bed geometry, particle size, and particle size distribution on desorption efficiency.
- RSTA technology is relatively new and pilot testing under field conditions are recommended. The results presented herein can be expected to stimulate pilot and full-scale tests leading to the adoption of this technology in industrial separation applications.

REFERENCES

Carlson, T.L., Peters, Jr., E.M., 2002. Low pH lactic acid fermentation. US6475759B1.

Rush, B., 2012. Turning a Novel Yeast into a Platform Host for Industrial Production of Fuels and Chemicals. Metabolic Engineering IX.